

THESIS

ANALYSIS OF RIPRAP DESIGN METHODS USING PREDICTIVE EQUATIONS FOR
MAXIMUM AND AVERAGE VELOCITIES AT THE TIPS OF TRANSVERSE IN-STREAM
STRUCTURES

Submitted by

Thomas Richard Parker

Department of Civil and Environmental Engineering

In partial fulfillment of the requirements

For the Degree of Master of Science

Colorado State University

Fort Collins, Colorado

Spring 2014

Master's Committee:

Advisor: Christopher Thornton

Steven Abt

John Williams

ABSTRACT

ANALYSIS OF RIPRAP DESIGN METHODS USING PREDICTIVE EQUATIONS FOR MAXIMUM AND AVERAGE VELOCITIES AT THE TIPS OF TRANSVERSE IN-STREAM STRUCTURES

Transverse in-stream structures are used to enhance navigation, improve flood control, and reduce stream bank erosion. These structures are defined as elongated obstructions having one end along the bank of a channel and the other projecting into the channel center and offer protection of erodible banks by deflecting flow from the bank to the channel center. Redirection of the flow moves erosive forces away from the bank, which enhances bank stability. The design, effectiveness, and performance of transverse in-stream structures have not been well documented, but recent efforts have begun to study the flow fields and profiles around and over transverse in-stream structures. It is essential for channel flow characteristics to be quantified and correlated to geometric structure parameters in order for proposed in-stream structure designs to perform effectively. Areas adjacent to the tips of in-stream transverse structures are particularly susceptible to strong approach flows, and an increase in shear stress can cause instability in the in-stream structure. As a result, the tips of the structures are a major focus in design and must be protected. Riprap size is a significant component of the design and stability of transverse in-stream structures, and guidance is needed to select the appropriate size such that the structure remains stable throughout its design life.

The U.S. Bureau of Reclamation contracted the Engineering Research Center at Colorado State University to construct an undistorted 1:12 Froude scale, fixed bed, physical model of

two channel bend geometries that are characteristic of a reach of the Rio Grande River south of the Cochiti Dam in central New Mexico. A series of factors including the construction of the Cochiti Dam and control levees has caused the historically braided river to meander and become more sinuous. Bank erosion threatens farmlands, irrigation systems, levee function, aquatic habitat, and riparian vegetation. The purpose of the model was to determine the effectiveness of in-stream structures in diffusing the magnitude of forces related to bank erosion. Multiple configurations of transverse in-stream structures with varying x, y, and z parameters were installed in the model, and velocity and shear stress data were collected. A series of twenty-two different configurations of transverse in-stream structures were tested.

An analysis of the average and maximum velocities at the tips of the transverse in-stream structures was performed. Utilizing a channel bend approach velocity, average and maximum velocity ratios were calculated using physical model data. A set of dimensionless parameters consisting of influential structure design parameters was organized and arranged for regression analysis. Predictive equations were developed that describe the ratios of maximum and average velocity at the tips of the in-stream structures to bend-averaged velocities. The predictive equations for maximum and average velocity ratios function as a first approximation of in-stream structure riprap design for configurations that are within the range of tested data. Velocity data were used to assess the suitability of current riprap sizing techniques for transverse in-stream structures.

Bank revetment design methodologies were found to be dependable methods for in-stream structure riprap design. Methodologies developed by the United States Army Corps (USACE) and the United States Bureau of Reclamation (USBR) were recommended for the sizing of riprap for in-stream structures. Velocity adjustment procedures were created for

use in the USACE and USBR methods. The velocity adjustment procedures include a velocity factor for the determination of a riprap sizing design velocity. The riprap sizing design velocity produces a conservative riprap size for bank revetment, but an appropriate riprap size for in-stream transverse structures. Two velocity factors are provided: one for natural channels and the one for uniform, trapezoidal channels. Limitations and recommendations of the proposed tip velocity ratios and riprap sizing techniques are provided.

ACKNOWLEDGEMENTS

First, I would like to thank my parents and brother for their continual and unyielding support with everything I do. Next, I would like to thank Dr. Abt for providing me guidance throughout my graduate study and in my thesis research and writing. I would like to thank the rest of my committee members (Dr. Christopher Thornton and Dr. John Williams) for their guidance and feedback during the completion of my thesis. The research for the thesis could not have been done without the tremendous help and support of my Ph.D. mentors: Michael Scurlock and Natalie Youngblood.

The Engineering Research Center staff was essential in making this all possible including: Patrick Noonan, Janice Barman, Ryan Zilly, Molly Sullivan, Shane Ritchie, Ryne Pearce, and Tyler Sobieck. Lastly, I would like to thank all of my friends and colleagues for their advice and support over the last few years. In particular, Ami Cobb has been one of the most inspirational and helpful people I have ever had the honor of working with. My graduate school studies and research could not have been completed without her continuous support and encouragement.

This thesis is typeset in \LaTeX using a document class designed by Leif Anderson.

TABLE OF CONTENTS

Abstract	ii
Acknowledgements	v
List of Tables	ix
List of Figures	xii
Chapter 1. Introduction	1
1.1. General Background	1
1.2. Project Background.....	2
1.3. Research Objectives.....	4
Chapter 2. Literature Review	5
2.1. Rock Riprap Sizing	5
2.2. Description of Riprap Sizing Methods	6
2.3. Types of In-Stream Structures	35
Chapter 3. Physical Model Description.....	43
3.1. Introduction	43
3.2. Model Geometry and Flow Conditions	43
3.3. Model Construction, Components and Startup	46
3.4. Instrumentation and Measurements	50
Chapter 4. Data Collection	56
4.1. Baseline Data Collection	56
4.2. In-Stream Structure Test Program	56

Chapter 5. Data Analysis	74
5.1. Terms for Analysis	74
5.2. Maximum and Average Velocity Ratios (MVR & AVR)	76
5.3. Regression Analysis	79
5.4. MVR_{tip} & AVR_{tip} Results	81
Chapter 6. Bernalillo Priority Site Case Study	91
6.1. Introduction	91
6.2. Bernalillo Priority Site Background	91
6.3. HEC-RAS® Model	94
6.4. USBR Velocity Data and Observed MVR_{tip} 's	96
6.5. Design Velocity Calculation from MVR_{tip} 's	100
6.6. Summary	101
Chapter 7. Analysis of Riprap Sizing Relationships	103
7.1. Introduction	103
7.2. Median Riprap Size Results	103
7.3. Comparison of Methods	110
7.4. Discussion of Results	112
7.5. Average Velocity Adjustment Procedures for the USACE EM-1601 (1991) and USBR EM-25 (1984) Methods	114
7.6. Example Procedures for In-stream Structure Riprap Design	117
Chapter 8. Conclusion and Recommendations	123
8.1. Overview	123
8.2. Conclusion	124

8.3. Recommendations for Further Research	125
Bibliography	128
Appendix A. Velocity and Weir Data for Regression Analyses	134
Appendix B. Regression Analyses Results	152
Appendix C. Velocities for Riprap Design Analysis	160
Appendix D. Median Riprap Results for Agency Methodologies	167

LIST OF TABLES

2.1	Agency, publication title, and abbreviated title of various rock riprap design procedures.....	19
2.2	Guide for selecting stability factors	21
2.3	Guidelines for selection of Shields parameter and safety factor.....	25
3.1	Similitude Scaling Used for the Physical Model (1:12 Froude Scale).....	44
3.2	Geometric characteristics of Type 1 and 3 bends in the field.....	44
3.3	Geometric characteristics of Type 1 and 3 bends in the model.....	44
4.1	In-stream Structure Design Program.....	59
4.2	Velocity Results from Data Collection.....	67
5.1	Material Properties	75
5.2	Channel Properties	75
5.3	Flow Properties.....	75
5.4	Weir Properties.....	75
5.5	Parameters used for analysis.....	78
5.6	MVR_{tip} Regression Results.....	82
5.7	AVR_{tip} Regression Results.....	82
5.8	Observed vs. Predicted MVR_{tip} Percent Errors.....	87
5.9	Observed vs. Predicted AVR_{tip} Percent Errors.....	87
6.1	Design parameters of bendway weir design [1].....	93

6.2	Cox (2012) Observed Field $MV R_{tip}$'s (Natural Channel)	99
6.3	CSU Physical Model Data $MV R_{tip}$'s (Trapezoidal Channel).....	100
7.1	USACE EM-1601 (1991) Median Riprap Size Results	105
7.2	FHWA HEC-11 (1989) Median Riprap Size Results	106
7.3	CALTRANS Cal-B&SP (2000) Median Riprap Size Results	107
7.4	ASCE Man-110 (2006) Median Riprap Size Results	108
7.5	USBR EM-25 (1984) Median Riprap Size Results	108
7.6	USGS Vol. 2 (1986) Median Riprap Size Results	109
7.7	Isbash Median Riprap Size Results.....	110
7.8	Extrapolated Median Riprap Size Results for a Design Velocity of 10 ft/s	110
7.9	Methodology Groups for Analysis	113
7.10	Hydraulic Parameters of San Ildefonso Priority Site [2].....	118
A.1	Weir Data for Regression Analysis	134
A.2	Velocity Data for Regression Analysis.....	142
B.1	Regression Statistics Results for $MV R_{tip,total}$	152
B.2	Regression Line Results for $MV R_{tip,total}$	152
B.3	Regression Statistics Results for $AV R_{tip,total}$	153
B.4	Regression Line Results for $AV R_{tip,total}$	153
B.5	Regression Statistics Results for $MV R_{tip,spur}$	154
B.6	Regression Line Results for $MV R_{tip,spur}$	154

B.7	Regression Statistics Results for $AVR_{tip,spur}$	155
B.8	Regression Line Results for $AVR_{tip,spur}$	155
B.9	Regression Statistics Results for $MVR_{tip,BW}$	156
B.10	Regression Line Results for $MVR_{tip,BW}$	156
B.11	Regression Statistics Results for $AVR_{tip,BW}$	157
B.12	Regression Line Results for $AVR_{tip,BW}$	157
B.13	Regression Statistics Results for $MVR_{tip,vanes}$	158
B.14	Regression Line Results for $MVR_{tip,vanes}$	158
B.15	Regression Statistics Results for $AVR_{tip,vanes}$	159
B.16	Regression Line Results for $AVR_{tip,vanes}$	159
C.1	Weir Data for Regression Analysis	160
D.1	USACE EM-1601 (1991) Median Riprap Size Results	167
D.2	FHWA HEC-11 (1989) Median Riprap Size Results	174
D.3	CALTRANS Cal-B&SP (2000) Median Riprap Size Results	176
D.4	ASCE Man-110 (2006) Median Riprap Size Results	178
D.5	USBR EM-25 (1984) Median Riprap Size Results	180
D.6	USGS Vol. 2 (1986) Median Riprap Size Results	182
D.7	Isbash (1936) Median Riprap Size Results	184

LIST OF FIGURES

1.1	Planview of Middle Rio Grande River [3]	2
2.1	Design curves to size riprap protection on embankments of various slopes (no safety factor included)	11
2.2	Curve to determine maximum stone size in riprap mixture	33
2.3	Series of bendway weirs in the field during low flow conditions [4]	36
2.4	Planview of Bendway Weir Parameters [5]	40
2.5	Cross-Section View of Bendway Weir Parameters [5]	40
2.6	Schematic of a Spur Dike [5]	41
2.7	Schematic of a Vane [5]	41
3.1	Planview of Model Layout of Type 1 and 3 Bends [4]	45
3.2	Physical Model Headbox for Flow Delivery [4]	46
3.3	Finishing of Concrete for Desired Channel Roughness [4]	47
3.4	Constructed Benway Weir during Testing [4]	49
3.5	Bendway Weir Series in Model [4]	49
3.6	Planview of model with labeled cross-sections [4]	50
3.7	SIGNET Meters	51
3.8	Electronic Display Boxes	52
3.9	Piezometer locations for upstream and downstream bends [4]	53
3.10	Stilling wells to measure water surface elevations [4]	53
3.11	ADV Probe [4]	54

3.12	ADV Setup [4].....	55
4.1	Upstream bend of model during baseline testing [4]	57
4.2	Data collection locations [4].....	66
5.1	Observed vs. predicted $MV R_{tip}$ and $AV R_{tip}$ for all in-stream structure types.....	84
5.2	Observed vs. predicted $MV R_{tip}$ and $AV R_{tip}$ for spur dikes.....	85
5.3	Observed vs. predicted $MV R_{tip}$ and $AV R_{tip}$ for bendway weirs	85
5.4	Observed vs. predicted $MV R_{tip}$ and $AV R_{tip}$ for vanes	86
6.1	Map of Bernalillo Site [1]	92
6.2	Pre-construction aerial photograph date March 31, 2006 (left) and post-construction aerial photograph dated February 25, 2007 (right).....	92
6.3	Planview of Bernalillo Site Weir Configuration [1].....	93
6.4	Planview sketch of bendway weir field design [?]	94
6.5	Bendway weir design planview [?].....	94
6.6	Bendway weir design cross-section view [?].....	95
6.7	Middle Rio Grande cross-section surveyed for HEC-RAS model [1]	97
6.8	Structure Tip Velocity Measurement Area	99
7.1	Extrapolated Results for Design Velocity vs. Median Riprap Size.....	111

CHAPTER 1

INTRODUCTION

1.1. GENERAL BACKGROUND

As the United States population continues to grow, the demand for water continues to increase for such things as municipal supply, power production, irrigation, and recreation [6]. The demand for water in the United States has affected the balance of natural river systems and caused channel stability to be the subject of extensive research efforts. Channel stability can include protecting the property and land along the river banks, maintaining water quality, protecting aquatic habitats, and improving the aesthetics of areas near rivers. Two natural effects that may occur when altering the flow of water and sediment in rivers are bank erosion and channel migration [7]. The magnitude of damage caused by these two mechanisms may be catastrophic if not managed; therefore, techniques such as armored revetment, in-stream structure placement, and bioengineering have traditionally been used to stabilize stream banks and river channels. In particular, transverse in-stream structures have been used to protect rivers from the harmful erosive effects of high velocity flows and the subsequent high shear stresses. In theory, a transverse in-stream structure redirects high velocity flows away from the outer bank of a channel, decreases bank erosion, and enhances aquatic habitats for native species when designed properly.

Despite the effectiveness of these structures, complete reliable design criteria for transverse in-stream structures have not been developed. Many of the past designs are site specific and dependent upon site specific conditions. The applicability of site specific criteria to other channel sites is questionable. A comprehensive riprap design method applicable to in-stream structures would allow for consistency in transverse in-stream structure design.

1.2. PROJECT BACKGROUND

The United States Bureau of Reclamation (USBR) commissioned Colorado State University Engineering Research Center to construct a physical model to investigate structure-induced hydraulic conditions in two representative channel bends of the Middle Rio Grande River. The Middle Rio Grande is a 29-mi reach of the Rio Grande River in central New Mexico that extends from the Cochiti Dam downstream to Bernalillo, New Mexico. Figure 1.1 presents a map of the Middle Rio Grande reach.

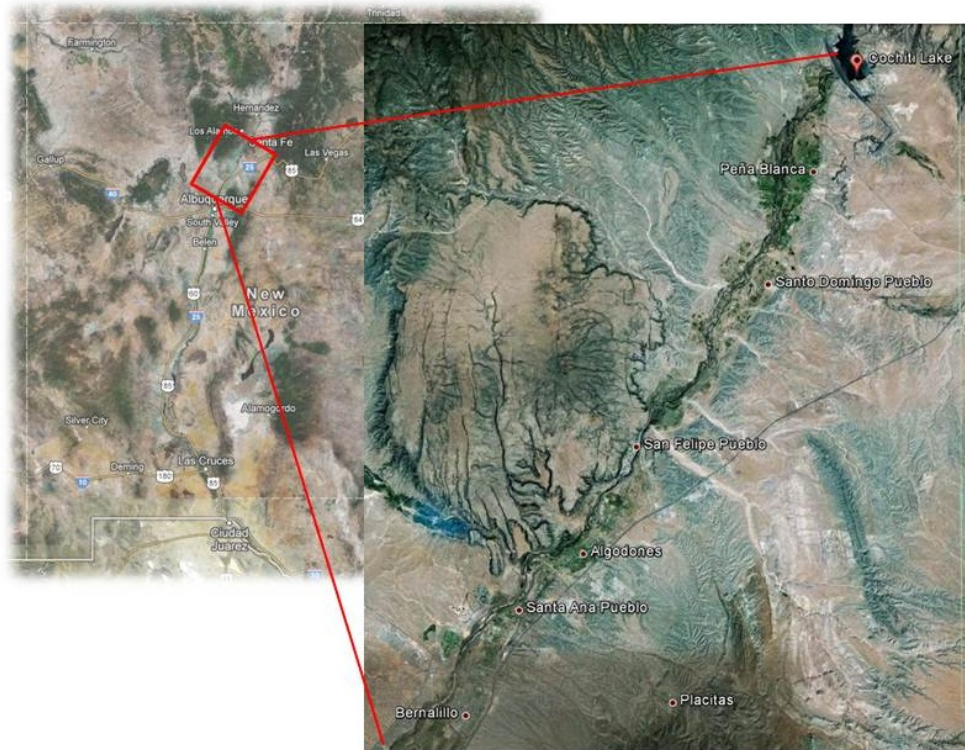


FIGURE 1.1. Planview of Middle Rio Grande River [3]

In 1973, the Cochiti Dam was installed upstream of Albuquerque, New Mexico for flood and sediment control. The dam was installed in a portion of the river that was classified as braiding, which is typical of channel systems with its characteristic slope, vegetation, and sediment gradation properties. The dam effectively controlled the sediment supply

available to the downstream reach of the channel and resulted in a geomorphic alteration of the channel from braided to meandering. The meandering nature of the stream resulted in natural changes such as bank erosion and channel migration. In turn, this placed valuable land properties and infrastructure in the path of the newly meandering river [3].

Numerous methods have been developed to combat the unwanted bank instability and channel migration. For example, the use of rock riprap blankets and rigid armor structures have been popular methods used to stabilize banks and prevent channel migration; however, these methods are not effective at enhancing the habitat for vegetation and fish alike. The use of riprap as a blanket along the outer bank of a stream subdues the growth of riparian vegetation and advantageous aquatic habitat features such as pools [7]. To combat the potential for undesired channel migration while possibly enhancing the habitat, the USBR in Albuquerque, NM identified a set of in-stream structures that could be implemented along the outside banks of the meanders.

In recent years, the Middle Rio Grande has continued to be the focus of channel-restoration techniques including the use of native material and rock weir structures in the attempt to control bank-erosion rates, channel-migration rates, and habitat degradation [6]. The construction and testing of a physical model will help to alleviate the general lack of knowledge of flow properties around in-stream structures and aid in the development of design criteria for rock and native weir structures. In response, an undistorted 1:12 Froude scale hard boundary model with two characteristic bends was designed and built for the development of appropriate design guidelines for in-stream structures.

1.3. RESEARCH OBJECTIVES

The application of stone-sizing criteria is subjective and generally non-applicable to traditional bendway weir and spur dike design. For this study, stone-sizing criteria were evaluated for in-stream transverse structure design applicability. Specifically, the research objectives for this particular project are as follows:

- (1) Observe and collect flow depth and time-averaged velocity data from twenty-two structure configurations including bendway weirs, spur-dikes, and vanes
- (2) Determine bend-averaged and maximum velocity values for each structure configuration
- (3) Identify influential structure design parameters for all structure configurations
- (4) Develop predictive bend-averaged and maximum velocity ratio equations for all structure configurations
- (5) Identify existing riprap sizing relationships, as well as, design criteria for in-stream transverse structure design, and
- (6) Provide recommendations for modifying applicable existing equation(s) for specific use in in-stream transverse structure design

To address these objectives, a literature review of stone-sizing relationships for bank revetments, overtopping, and in-stream structure design and types of in-stream structures was conducted. An existing 1:12 Froude scale hard boundary model was used to test and collect flow depth and velocity data for twenty-two structure configurations. Channel sites currently utilizing in-stream structures for bank protection along the Middle Rio Grande were analyzed, and velocity and riprap size data were collected and analyzed.

CHAPTER 2

LITERATURE REVIEW

2.1. ROCK RIPRAP SIZING

Rock riprap is one of the most commonly used methods to prevent the erosion and degradation of channel banks, embankments, levees, spillways, and in-stream structures that are subjected to high-velocity flow conditions [8]. Channel protection practices address the use of rock as individual stones or part of an integrated system. Many federal and state agencies have developed methods and approaches for the sizing of riprap. Most of the stone sizing methods are developed for specific applications and caution must be given in their application [9]. The majority of rock sizing methods are based on empirical data and can be considered empirical techniques; therefore, physical models, field data, and theoretical data have contributed to the variety of approaches used to determine stable riprap design [9]. Currently, empirically derived equations offer the best approach to design in-stream structures.

Most rock sizing methods have been developed for either high-energy or low-energy environments. Low-energy conditions are characterized by mild slopes, low turbulence, subcritical flow, and uniform or gradually varied steady flows. High energy conditions are characterized by steep slopes, high turbulence, supercritical flow, and rapidly varied unsteady flow. There are many techniques that can be used with advantages and disadvantages depending on site specific conditions. A literature review was conducted to identify current stone-sizing relationships used for riprap design and how the relationships were developed.

2.2. DESCRIPTION OF RIPRAP SIZING METHODS

Twenty eight stone-sizing relationships were identified for the design of a protective riprap layer. The applications of these stone-sizing criteria were flow overtopping and bank stabilization and revetment. Of the twenty-eight relationships identified, twenty-one relationships were developed for use in flow overtopping conditions. Eleven of the twenty-one flow overtopping relationships will be reviewed. The remaining seven relationships were developed by United State's agencies for bank stabilization and revetment.

- Overtopping flow methods
 - (1) Isbash (1936)
 - (2) Knauss (1979)
 - (3) Wittler and Abt (1997)
 - (4) Mishra (1998)
 - (5) Frizell et al. (1998)
 - (6) Chang (1998)
 - (7) Robinson et al. (1998)
 - (8) Siebel (2007)
 - (9) Peirson et al. (2008)
 - (10) Khan and Ahmad (2011)
 - (11) Thornton et al. (2013)

- Agency methodologies for bank stabilization
 - (1) Federal Highway Administration techniques
 - (a) HEC-11 (1989)
 - (b) HEC-15 (2005)
 - (2) California Department of Transportation (CALTRANS) Cal-B&SP (2000) method
 - (3) USACE EM-1601 (1991) method
 - (4) American Society of Civil Engineers (ASCE) Man-110 (2006) method
 - (5) U.S. Bureau of Reclamation (USBR) EM-25 (1984) method
 - (6) U.S. Geological Survey (USGS) Vol. 2 (1986) method

A brief summary of each methodology and subsequent relationships are presented.

2.2.1. OVERTOPPING FLOW METHODS.

2.2.1.1. *Isbash (1936)*. Isbash (1936) developed a riprap sizing relationship for the construction of dams by studying the ability of water to flow over rocks in a river channel. A series of in-channel experiments was undertaken to develop the rock sizing relationship. The experiments consisted of depositing rock of known size and weight into a flowing channel. The shape of the cross-section was described, and a relationship between the rock size and the minimum velocity necessary for movement was developed. His efforts focused on sizing individual stones to resist displacement due to overtopping flow and percolation through the rock mass. Isbash developed his relationship on principle hydraulic variables such as stone size, bed slope, and unit discharge. The results of his studies have become the foundation of many other riprap sizing studies including Olivier (1967), Hartung and Scheurelein (1970), Knauss (1979), and Stephenson (1979) [8]. A coefficient is utilized such that high and low turbulence conditions are both applicable. Information required for sizing riprap includes the channel velocity, specific gravity of the stone, and choice of turbulence coefficients. The Isbash equation is provided in Equation 1.

$$(1) \quad V_c = C * \left(2 * g * \frac{\gamma_s - \gamma_w}{\gamma_w} \right)^{0.5} * (D_{50})^{0.5}$$

Where:

V_c = critical velocity (ft/s);

C = 0.86 for high turbulence, or 1.20 for low turbulence;

g = 32.2 ft/s^2 ;

γ_s = stone density (lb/ft^3);

γ_w = water density (lb/ft^3); and

D_{50} = median stone diameter (ft)

2.2.1.2. *Knauss (1979)*. Knauss (1979) compared the Olivier (1967) equation and the Hartung and Scheuerlein (1970) equation which are both used to determine the maximum admissible discharge capacity for the overspilling of rockfill dams. Using flume studies, Olivier developed his rock stability theory through the overtopping of rock dams. An empirical equation for crushed and rough stones was derived that related the overtopping flow to the following parameters: unit flow, slope, and median rock size. Hartung and Scheuerlein (1970) presented a set of rock stability equations for angular stones on steep slopes that included consideration of aerated flow. The stone stability relationship relates maximum unit discharge, roughness height, specific weight of water and stone, and slope. The Hartung and Scheuerlein (1970) equation was derived from the previously developed Isbash equation and extensive observations of aerated flow over fixed rock beds. Knauss determined that both empirical relationships were valid for crushed stones with angular shapes with a specific mass density around $2.7 t/m^3$. Equation 2 provides the Knauss relationship developed from work by Olivier (1967), and Equation 3 provides the Knauss relationship developed from work by Hartung and Scheuerlein (1970).

$$(2) \quad \frac{q_{max}}{\sqrt{g} * d_s^{3/2}} = 0.18 \left(\frac{1.2}{p} \right)^{5/3} * J^{-7/6}$$

$$(3) \quad \frac{q_{max}}{\sqrt{g} * d_s^{3/2}} = 1.9 + 0.8 * \phi - 3 \sin \theta$$

Where:

q_{max} = max unit discharge (m^2/s);

$g = 9.81 \text{ m/s}^2$;
 $d_s =$ equivalent diameter of the stone in the rock fill layer (m);
 $p =$ porosity (0-1);
 $J =$ slope of downstream face (for example, 1V:2H equals 0.5) (m/m);
 $\phi =$ packing factor of stones $= 0.0575 G_s N^{3/2}$;
 $G_s =$ weight of the average stone (kN);
 $N =$ number of stones per unit area ($stones/m^2$); and
 $\theta =$ angle of slope ($^\circ$)

2.2.1.3. *Wittler and Abt (1997)*. A study by Wittler and Abt (1990) investigated the influence of material gradation on the stability of a riprap layer during overtopping flow conditions. In general, uniformly graded riprap displays a greater stability for overtopping flows but fails suddenly, while well-graded riprap resists sudden failure as voids are filled with smaller material from upstream. Additional studies at CSU from 1994 to 1997 provided more details on the different types of failure for different gradations. Failure of the riprap slope was defined as removal or dislodgement of enough material to expose the bedding material. It was observed during testing that the failure of the riprap layer occurred when the measured water depth was within the thickness of the rock layer. Using failure observations, an empirical relationship was developed for the sizing of rock riprap, which is provided in Equation 4.

$$(4) \quad D_{50} = 0.6q^{0.56}C_s^{-0.67}(\tan\alpha)^{-0.683} \left[\frac{\sin\alpha}{(2.65\cos\alpha - 1)(\cos\alpha * \tan\phi - \sin\alpha)} \right]^{1.11}$$

$$(5) \quad C_s = 0.75 + (\log C_u^6)^{-2}$$

Where:

$D_{50} =$ median stone diameter (in);

q = flow discharge per unit width (ft^3/ft);
 C_s = stability coefficient;
 α = angle of the embankment with the horizontal;
 ϕ = angle of repose of riprap (42° for all angular rocks with diameter ≥ 5 cm); and
 C_u = coefficient of uniformity

2.2.1.4. *Mishra (1998)*. Through a cooperative agreement between the U.S. Bureau of Reclamation (USBR) and Colorado State University (CSU), Mishra (1998) experimented with rock stability by subjecting angular stones 10" to 25" in diameter to overtopping flows on a 50% slope. He considered failure to be movement of rock riprap by erosion or high flows until the bed was exposed. Mishra found that the void sizes inside the riprap layer play a significant role in the interstitial velocity of water. In turn, the void sizes of the riprap layer are strongly influenced by the gradation of the rock. He applied a coefficient of uniformity C_u to his resulting equation to account for these relationships and found that it provided a good representation of the rock gradation and its effects on the prediction of the interstitial velocity. He combined his results with the datasets of Abt and Johnson (1991) and Robinson *et al.* (1998) yielding an expression that sizes the stable rock size as a function of the stone coefficient of uniformity, unit discharge, and embankment slope. The relationship developed by Mishra is provided in Equation 6.

$$(6) \quad D_{50}C_u^{0.25} = 0.55q_f^{0.52}S^{-0.75} \left[\frac{\sin\alpha}{(2.65\cos\alpha - 1)(\cos\alpha * \tan\phi - \sin\alpha)} \right]^{1.11}$$

Where:

D_{50} = median stone diameter (m);
 C_u = coefficient of uniformity;
 q_f = unit discharge at failure (m^2/s);
 S = channel slope (m/m);

α = angle of the embankment with the horizontal; and
 ϕ = angle of repose of riprap material (42° for all angular rocks with diameter ≥ 5 cm)

2.2.1.5. *Frizell et al. (1998)*. Frizell et al. (1998) addressed the need for a reliable riprap sizing method during flow conditions associated with dam overtopping. The objectives of the study were to perform large scale testing of riprap on steep slopes and determine criteria for riprap size and layer thickness necessary to protect an embankment dam during overtopping flows. A design procedure to predict median stone size for a protective riprap layer was developed. The curves in Figure 2.1 shows Frizell's relationship that relates the properties of the rock riprap, flow discharge, and embankment slope. Additionally, velocity data obtained from the test program were used to develop an analytical approach to determine the required riprap thickness. Equation 7 presents the non-dimensional relationship between interstitial velocity, median stone size, slope, and the coefficient of uniformity.

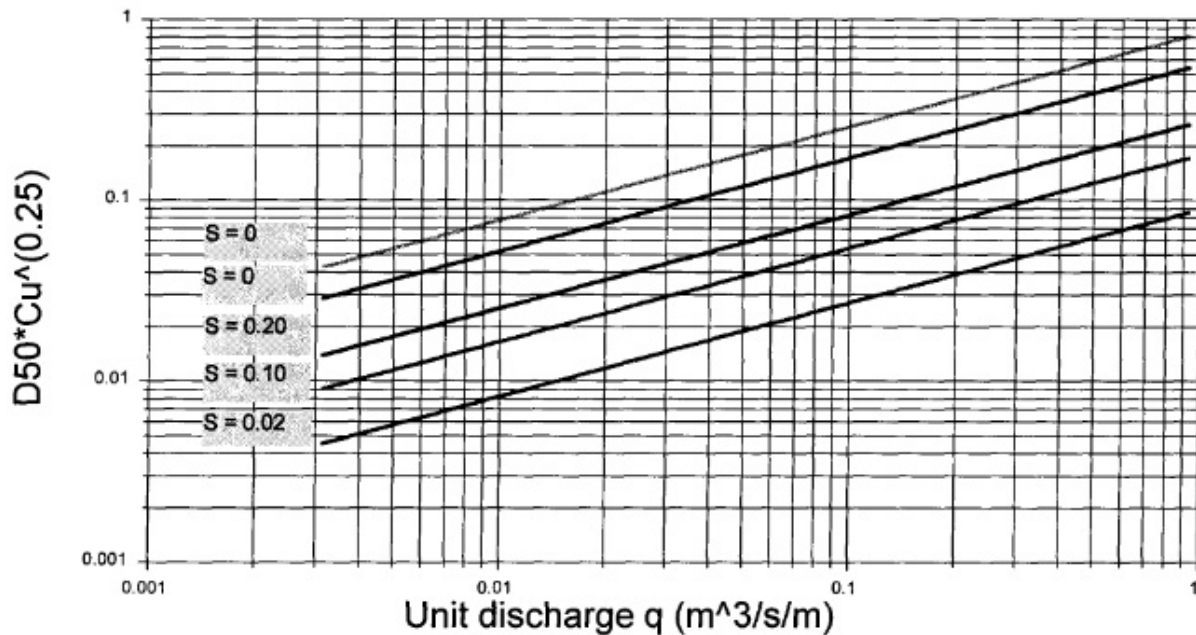


FIGURE 2.1. Design curves to size riprap protection on embankments of various slopes (no safety factor included)

$$(7) \quad \frac{v_i}{\sqrt{gD_{50}}} = 2.48S^{0.58}C_u^{-2.22}$$

Where:

- v_i = interstitial velocity (m/s);
- D_{50} = median stone size (m);
- g = gravitational constant ($9.81 m/s^2$);
- S = embankment slope (m/m); and
- C_u = coefficient of uniformity = D_{60}/D_{10}

2.2.1.6. *Chang (1998)*. Chang (1998) observed that rock slope failure occurred in two different stages. During the first stage, he found that individual stones initiated movement. The initial movement lead to the riprap layer becoming settled and interlocked. Thus, higher discharges were required to observe catastrophic failure. The two stages were termed the motion stage and failure stage by Abt and Johnson (1991). Chang developed a new design method for angular riprap with consideration to the two stages of rock slope failure. Interlocking effects were included in his analysis through the implementation of an internal angle of friction. The Chang (1998) relationship relates the size of angular riprap to the slope and discharge at slope failure and is provided in Equation 8.

$$(8) \quad D_{50} = \frac{0.887 * q^{5/9}}{S^{5/18} \left[\frac{1}{S} - \frac{1}{\tan(1+5S)\phi} \right]^{25/27}}$$

Where:

- D_{50} = median rock riprap diameter (m);
- q = discharge at slope failure per unit width ($m^3/s/m$);
- S = slope (m/m); and

ϕ = angle of repose of riprap material or the internal angle of friction ($^{\circ}$)

2.2.1.7. *Robinson et al. (1998)*. Robinson *et al.* (1998) evaluated multiple rock chute design techniques in an attempt to provide a comprehensive rock chute design tool. Angular riprap with median stone sizes ranging from 15 to 278 *mm* were tested on rock chutes with slopes ranging from 2 to 40%. The loose riprap was installed in a $2 * D_{50}$ blanket layer consisting of uniform, angular riprap and tested to overtopping failure. An empirical relationship was developed that predicts the highest stable discharge on a rock chute as a function of median stone size and bed slope. It is important to note that a factor of safety should be applied to the predicted rock size where appropriate. The predictive equations are provided in Equations 9 and 10. Both equations have not been verified for slopes lower than 2% or greater than 40%, and were developed for a rock specific gravity range of 2.54 to 2.82.

for $S < 0.1$

$$(9) \quad D_{50} = 12(1.923qS^{1.5})^{0.529}$$

for $0.1 < S < 0.40$

$$(10) \quad D_{50} = 12(0.233qS^{0.58})^{0.529}$$

Where:

D_{50} = median stone size (*in*);

q = highest stable unit discharge ($ft^3/s/ft$); and

S = channel slope (ft/ft)

2.2.1.8. *Siebel (2007)*. Siebel (2007) performed a series of dam overtopping tests to observe the performance of individual rock elements within a protection layer. He tested slope protection layers by individually placing stones on the slope of a large scale physical model in the hydraulics laboratory at Universtat Stuttgart. Experiments were completed for failure scenarios such as erosion of single stones, sliding of the protection layer, and disruption of the protection layer. Specifically, the experiments for the erosion of single stone elements were conducted on a flume with an adjustable slope from 1:26 to 1:3. A thin layer of concrete was placed on the bottom of the experiment's flume and single stones were placed into the concrete before the drying process was complete. Multiple configurations of flow discharge and bed slope were tested to observe single stones within protection layer. A relationship for the design of multi-layer riprap protection layers was developed with an included factor of safety of 1.6. The relationship is provided in Equation 11.

$$(11) \quad d_{50,req} = 1.71 S_0^{0.68} q_0^{2/3} \left(\frac{\rho_w}{\rho_s - \rho_w} \right)^{1/3}$$

Where:

- $d_{50,req}$ = average stone diameter (m);
- S_0 = bed slope (m/m);
- q_0 = highest stable unit discharge ($m^3/s/m$);
- ρ_s = stone density (kg/m^3); and
- ρ_w = water density (kg/m^3)

2.2.1.9. *Peirson et al. (2008)*. In 2008, Peirson *et al.* quantified the additional resistance to erosion that can be accomplished by the individual placement of stones instead of the typical dumping construction process. A large-scale flume investigation for slopes of 0.2, 0.3, and 0.4 was performed. Two sizes of sandstone and basalt were installed such that

a maximum bulk density was reached. During experimentation, Peirson found that the failure flow rate for placed riprap was more than 30% higher than the failure flow rate of the same type of randomly dumped material. The total armor mass per unit surface area was increased by 35% for placed riprap. The relationships developed by Peirson *et al.* are provided in Equations 12, 13, 14, and 15.

$$(12) \quad q_{over} = \sigma * y_e * v_e$$

Where:

q_{over} = total overflow discharge per unit width;

σ = mean volumetric proportion of water in the air-water mixture;

y_e = representative flow depth; and

v_e = representative mean velocity of the air-water mixture

and

$$(13) \quad y_e = y_0 + d_{50}/3$$

Where:

y_0 = flow depth above the armor; and

$d_{50}/3$ = characteristic hydraulic roughness

and

$$(14) \quad \sigma = 1 - 1.3 * \sin\theta + 0.24 \frac{y_e}{d_{50}}$$

Where:

θ = channel slope

and

$$(15) \quad v_e = 0.88 \sqrt{2g(\rho_s - \rho)/\sigma\rho} \sqrt{d_{50} \cos\theta} \sqrt{\tan\phi - \tan\theta}$$

Where:

g = acceleration of gravity (9.81 m/s^2);

ρ_s = density of rock (kg/m^3);

ρ_w = density of water (kg/m^3); and

ϕ = angle of friction of the rock ($^\circ$)

2.2.1.10. *Khan and Ahmad (2011)*. Khan and Ahmad (2011) used a series of 53 stability tests for angular riprap with a median stone size ranging from 15 to 278 mm and slope ranging from 1 to 40% to analyze rock stability in overtopping flows. Data were obtained from Abt and Johnson (1991) and Robinson et al. (1998) and used to evaluate the accuracy of the existing riprap sizing equations. The collaborative dataset had unit discharges of rock failure from 0.003 to 0.752 m^2/s for rock sizes of 15 to 278 mm , respectively. Khan and Ahmad used the dataset from the 53 stability tests to evaluate different stone sizing equations that are published including: Abt et al. (2008), Mishra (1998), Hartung and Scheuerlein (1970), Eli and Gray (2008), Robinson et al. (1998), and Abt et al. (1991). A multivariable power regression was performed with the dataset that included such parameters as median stone size, coefficient of uniformity, slope, layer thickness, and unit discharge at rock failure. The Khan and Ahmad relationship that was developed is provided in Equation 16. Equation 16 accurately predicted the desired angular stone size within an error of plus or minus 20% of the observed stone size.

$$(16) \quad D_{50} = 0.66t^{0.58}S^{0.22}C_u^{-0.45}q_f^{0.22}$$

Where:

- D_{50} = median stone size (mm);
- t = rock layer thickness ($n * D_{50}$)(mm);
- S = channel slope (m/m);
- C_u = coefficient of uniformity = D_{60}/D_{10} ; and
- q_f = unit discharge at rock failure (m^2/s)

2.2.1.11. *Thornton et al. (2013)*. Thornton *et al.* (2013) conducted a similar analysis to that of Khan and Ahmad (2011). Data were obtained from ten relevant studies that contained 102 discrete observations related to riprap failure under flow overtopping conditions. Variables within the overtopping flow dataset included stone size, discharge at movement/failure, bed/embankment slope, coefficient of uniformity, stone specific gravity, and riprap layer thickness. Median riprap sizes ranged from 0.59” to 25.76” and bed/embankment slopes from 0.2 to 50%. The unit discharges at riprap layer movement/failure for these types of channel/flow conditions ranged from 0.46 to 17.5 $ft^3/s/ft$. Using the comprehensive dataset, a multivariate power regression analysis was performed in a manner similar to Khan and Ahmad (2011). The independent variables were defined as unit discharge at riprap failure, thickness, slope, coefficient of uniformity, and specific gravity, and the dependent variable was defined as the median rock riprap size. The predictive relation that was developed as a result of the analysis is provided in Equation 17.

$$(17) \quad D_{50} = 0.57S^{0.20}C_u^{-0.28}q_f^{0.21}t^{0.62} [1.16/(SG - 1)^{0.30}]$$

Where:

D_{50} = median rock riprap size (*in*);

S = channel/embankment slope (*ft/ft*);

C_u = coefficient of uniformity = D_{60}/D_{10} ;

q_f = unit discharge at riprap layer movement/failure ($ft^3/s/ft$);

t = rock layer thickness (*in*); and

SG = specific gravity

2.2.1.12. *Summary of Overtopping Flow Methods.* The stone-sizing relationships in Section 2.2.1 were developed to design revetment for dams, chutes, and spillways subjected to overtopping flows. Stone-sizing criteria for overtopping flows are remotely applicable for the sizing of riprap in in-stream structures. Riprap protection for overtopping flows consists of installing a layer of riprap on the slope of a dam or spillway to prevent undercutting. Overtopping methods routinely apply to slopes greater than or equal to 10%, where as channels with in-stream structures usually have channel bed slopes much less than 2%. The hydraulic forces and stresses applied to riprap on large slopes (i.e. dams or spillways) are significantly higher than forces impacting in-stream structures. Therefore, overtopping methods provide a highly conservative approach to stone-sizing for in-stream structure design. However, the Isbash (1936) method will be analyzed for in-stream structure riprap sizing because of its longevity in the hydraulic design field and the significant number of procedures that are derived from the principles the Isbash method.

2.2.2. AGENCY METHODOLOGIES FOR BANK STABILIZATION. A number of agencies have developed procedures for the design of protective rock riprap layers for bank revetment including the Federal Highway Administration (FHWA), California Department of Transportation (CALTRANS), United States Army Corps of Engineers (USACE), American Society of Civil Engineers (ASCE), United States Bureau of Reclamation (USBR), and United State Geological Survey (USGS). Table 2.1 summarizes each technique. A brief overview

of each procedure, how it was developed, and resultant design relationships is provided in Sections 2.2.2.1 through 2.2.2.6.

TABLE 2.1. Agency, publication title, and abbreviated title of various rock riprap design procedures

Agency	Title and Date of Riprap Design Procedure	Procedure Abbreviation
FHWA	Hydraulic Engineering Circulars: Design of Riprap Revetment (1989), Design of Roadside Channels with Flexible Linings (2005)	HEC-11/HEC-15
CALTRANS	California Bank and Shore Rock Slope Protection Design (2000)	Cal-B&SP
USACE	Hydraulic Design of Flood Control Channels, EM 1110-2-1601 (1991)	EM-1601
ASCE	Sedimentation Engineering: Processes, Measurements, Modelling, and Practice, Manual No. 110 (Garcia, 2006)	Man-110
USBR	Hydraulic Design of Stilling Basins and Energy Dissipators (Peterka, 1984, Engineering monograph No. 25)	USBR EM-25
USGS	Rock Riprap Design for Protection of Stream Channels near Highway Structures (1986)	USGS Vol. 2

2.2.2.1. *Federal Highway Administration Techniques.* The Federal Highway Administration (FHWA) developed multiple techniques that discuss the use of riprap for a wide range of channel protection applications. Two of the techniques involving bridge scour, slope protection, and maximum permissible depth of flow were reviewed and evaluated for applicability with in-stream structure riprap design. The two applicable methods reviewed were HEC-11 (1989) and HEC-15 (2005). HEC-11 (1989) presents a series of design procedures for bank revetments and channel linings on large rivers. HEC-15 (2005) presents a set of design procedures for flexible linings on small channels.

HEC-11 HEC-11 (1989) provides a methodology for the design of riprap revetments for channel bank protection and channel linings on large streams and rivers. The technique is primarily applicable to rivers where the average discharge exceeds 50 *cfs* (HEC-15 should be

used for smaller channels). In addition to the design procedure, the circular discusses many erosion and riprap topics including: erosion potential, erosion mechanisms, riprap failure modes, and common riprap types.

A boundary shear stress based riprap relationship is presented with the flow velocity remaining as the primary design parameter. Equation 18 assumes uniform, gradually varying flow as expressed:

$$(18) \quad D_{50} = C * 0.001 * V_a^3 / (d_{avg}^{0.5} K_1^{1.5})$$

Where:

- D_{50} = median riprap particle size (*ft* or *m*);
- V_a = average velocity in the main channel (*ft/s* or *m/s*);
- C = correction factor (described below); and
- d_{avg} = average flow depth in the main flow channel (*ft* or *m*)

K_1 is defined with the equation below:

$$(19) \quad K_1 = [1 - (\sin^2\theta/\sin^2\phi)]^{0.5}$$

Where:

- θ = the bank angle with the horizontal ($^\circ$); and
- ϕ = the riprap material's angle of repose ($^\circ$)

It is important to note that average flow depth and velocity values used in Equation 18 are main channel values, as in the area between the channel banks. Equation 18 assumes a rock riprap specific gravity of 2.65 and a stability factor of 1.2. If these assumptions are not applicable to a site specific location, then a correction factor must be used. The

specific gravity correction is for rock riprap with a specific gravity greater or less than 2.65 as presented in Equation 20.

$$(20) \quad C_{sg} = 2.12 / (S_g - 1)^{1.5}$$

Where:

SG = the specific gravity of the rock riprap

The stability factor correction is for rock riprap with a stability factor greater or less than 1.2 and is provided in Equation 21.

$$(21) \quad C_{sf} = (SF/1.2)^{1.5}$$

Where:

SF = the stability factor to be applied

The correction factors calculated in Equations 20 and 21 are multiplied forming a single correction factor, C . Correction factor C is integrated into Equation 18 for determining the median rock riprap size. Stability factors range from 1.0 to 2.0 depending on the flow conditions encountered along the reach. Table 2.2 presents the guidelines for the selection of the stability factors.

TABLE 2.2. Guide for selecting stability factors

Conditions	Stability Factor Range
Uniform flow	1.0 - 1.2
Gradually varying flow	1.3 - 1.6
Approaching rapidly varying flow	1.6 - 2.0

HEC-15 HEC-15 (2005) presents a riprap design procedure based on the concept of maximum permissible depth of flow and hydraulic resistance of the lining material. The procedure was initially developed from reports published by Anderson *et al.* (1970) and Simon and Lewis (1971). Hydraulic modeling and field observations were used to verify the methods presented in HEC-15 (2005). It is important to note that the HEC-15 procedure is only applicable to: fully-lined channels carrying discharges up to 1,000 ft^3/s , triangular channels with a maximum discharge of 100 ft^3/s , and channels with maximum slopes of 0.10 ft/ft .

As a key parameter in flow hydraulics, Mannings roughness is essential in determining the relationships between flow depth, velocity, slope, grain size, and friction slope. Blodgett (1986) proposed the following relationship for Mannings roughness coefficient, n , as a function of flow depth and relative flow depth:

$$(22) \quad n = \frac{\alpha d_a^{1/6}}{2.25 + 5.23 \log\left(\frac{d_a}{D_{50}}\right)}$$

Where:

- n = Manning's roughness coefficient (dimensionless);
- d_a = average flow depth in the main channel (ft , m);
- D_{50} = median riprap/gravel size (ft , m); and
- α = unit conversion constant, 0.319 (SI) and 0.262 (CU)

It is important to note that Equation 22 is applicable for flow conditions where $1.5 < d_a/D_{50} < 185$ in small channel applications. If d_a/D_{50} is less than 1.5, the channel has flow conditions in which the projection of the riprap into the flow field has a significant effect on the roughness relationship as commonly observed in steep and moderate channels. Bathurst (1991) developed a relationship for steep and moderate slopes as presented in Equation 23.

$$(23) \quad n = \frac{\alpha d_a^{1/6}}{\sqrt{g} f(Fr) f(REG) f(CG)}$$

Where:

g = acceleration due to gravity, 9.81 m/s^2 (32.2 ft/s^2);

Fr = Froude number;

REG = roughness element geometry;

CG = channel geometry; and

α = unit conversion constant, 1.0 (SI) and 1.49 (CU)

Equation 23 is semi-empirically based, therefore, it is applicable for $0.3 < d_a/D_{50} < 8.0$.

The three functions in the denominator of Equation 23 are defined by Equations 24, 25, and 26.

$$(24) \quad f(Fr) = \left(\frac{0.28 Fr}{b} \right)^{\log\left(\frac{0.755}{b}\right)}$$

$$(25) \quad f(REG) = 13.43 \left(\frac{T}{D_{50}} \right)^{0.492} b^{1.025} \left(\frac{T}{D_{50}} \right)^{0.118}$$

$$(26) \quad f(CG) = \left(\frac{T}{d_a} \right)^{-b}$$

Where:

T = channel top width (ft , m); and

b = parameter describing the effective roughness concentration (Equation 27)

The parameter b defines a relationship between the effective roughness concentration and relative submergence of the roughness bed. The relationship is:

$$(27) \quad b = 1.14 \left(\frac{D_{50}}{T} \right)^{0.453} \left(\frac{d_a}{D_{50}} \right)^{0.814}$$

HEC-15 (2005) also presents a "hydraulic resistance of the lining" method that addresses the permissible shear stress approach for both riprap and gravel linings. The method is primarily based on field and laboratory experimental research. The permissible shear stress is defined as:

$$(28) \quad \tau_p = F^*(\gamma_s - \gamma)D_{50}$$

Where:

- τ_p = permissible shear stress (N/m^2 , lb/ft^2);
- F^* = Shield's parameter (dimensionless);
- γ_s = specific weight of stone (N/m^2 , lb/ft^2);
- γ = specific weight of water, $9810 N/m^2$ or $62.4 lb/ft^2$; and
- D_{50} = mean riprap size (ft , m)

Equation 28 can then be transformed into a rock sizing equation as:

$$(29) \quad D_{50} \geq \frac{SF * d * S_0}{F^* * (SG - 1)}$$

Where:

- d = maximum channel depth (m , ft); and
- SG = specific gravity of rock (dimensionless)

Equation 29 integrates the importance of skin friction, form drag, and channel bed slope in developing a minimum design riprap size for the channel bottom. An important component of using this method is selecting the Shields parameter and safety factor. The selection of these parameters is normally based on the Reynolds number of the flow. Table 2.3 provides a guide for the selection process:

TABLE 2.3. Guidelines for selection of Shields parameter and safety factor

Reynolds number	F^*	SF
$\leq 4 * 10^4$	0.047	1
$4 * 10^4 < R_e < 2 * 10^5$	Linear interpolation	Linear interpolation
$\geq 2 * 10^5$	0.15	1.5

Simons and Senturk (1977) derived a relationship that is applicable for channels with steeper slopes and is expressed as:

$$(30) \quad D_{50} \geq \frac{SF * d * S * \Delta}{F^* * (SG - 1)}$$

Where:

Δ = function of channel geometry and riprap size (Equation 31)

The parameter Δ is a function of the side slope angle, channel bottom slope, and riprap properties and is:

$$(31) \quad \Delta = \frac{K_1(1 + \sin(\alpha + \beta))\tan \phi}{2(\cos \theta \tan \phi - SF \sin \theta \cos \beta)}$$

Where:

α = angle of the channel bottom slope ($^\circ$);

β = angle between weight and the weight resultant vectors along the side slope ($^\circ$);

ϕ = angle of repose of the riprap ($^{\circ}$); and
 θ = angle of the channel side slope ($^{\circ}$)

In addition, the angle between the weight vector and the weight/drag resultant vector in the plane of the side slope β can be defined as:

$$(32) \quad \beta = \tan^{-1} \left(\frac{\cos \alpha}{\frac{2 \sin \theta}{\eta \tan \phi} + \sin \alpha} \right)$$

Where:

η = stability number (equation below)

Finally,

$$(33) \quad \eta = \frac{\tau_s}{F^* * (\gamma_s - \gamma) D_{50}}$$

The size of rock riprap increases dramatically as the discharge and channel gradient increase, and it is recommended that Equation 30 be used for channels with bed slopes greater than 10%. The equation is also helpful as its sizes riprap for both the channel bottom and side slopes. Equation 29 is recommended for slopes less than 5%. If channel slopes are between 5 to 10%, it is recommended that both methods be applied and the more conservative riprap size be selected.

It is important to recognize the difference between HEC-11 (1989) and HEC-15 (2005). HEC-15 (2005) is intended for use in the design of small roadside drainage channels where the entire channel section is lined. The HEC-15 methods are applicable for channels carrying less than 50 *cfs* and flow conditions are generally uniform in a manner that average hydraulic

conditions are sufficient for design. HEC-11 (1989) design guidelines are appropriate for more uniform and dynamic streams and rivers with sizes much greater than small roadside canals.

2.2.2.2. *California Department of Transportation method (Cal-B&SP)*. In 2000, the California Department of Transportation re-evaluated and revised a rock slope protection procedure that was introduced in the 1960 Bank and Shore Protection (BSP) manual. Subsequently, a California Bank and Shore Rock Slope Protection Design (2000) report was released that focuses on rock slope protection and redefines a bank and shore layered rock slope protection design method. An investigation was performed where sixty-five field sites in five states were analyzed and properties of the site were recorded. The rock slope protection design relationship presented in 2000 is the same expression found in the California Bank and Shore Protection Design (1960) and is presented in Equation 34. Equation 34 provides the minimum standard rock weight for the surface layer of the layered rock slope protection.

$$(34) \quad W = \frac{0.00002}{(G_s - 1)^3} * \frac{VM * V^6 * G_s}{\sin^3(r - a)}$$

Where:

W = minimum rock weight (*lb*);

V = velocity (*ft/s*);

VM = velocity coefficient for types of flow;

= 0.67 if flow is parallel

= 1.33 if flow is impinging

G_s = specific gravity of rock (typically 2.65);

r = angle of repose (70° for randomly placed rock); and

a = outside slope face angle to the horizontal (typically a maximum of 33°)

2.2.2.3. *USACE EM-1601 Method.* In 1991, the United States Army Corps of Engineers (USACE) published riprap design guidelines for "open channels not immediately downstream of stilling basins or other highly turbulent areas" [10]. EM-1601 presents a low-energy technique for channel bank protection or revetments using riprap. USACE developed the EM-1601 method for application in the design of riprap in constructed and natural channels with a slope of 2% or less and Froude number less than or equal to 1.2. The method uses a depth-averaged local velocity based upon the assumption that a designer can obtain a better estimation of local velocity rather than local boundary shear stress. Equation 35 can be applied to both uniform and gradually varying flow.

$$(35) \quad D_{30} = d * FS * C_s * C_v * C_T * \left[\left(\frac{\gamma_w}{\gamma_s - \gamma_w} \right)^{0.5} * \frac{V_{des}}{\sqrt{K_1 * g * d}} \right]^{2.5}$$

Where:

D_{30} = stone size (*ft, m*) of which 30% is finer by weight;

d = local depth of flow (*ft, m*);

FS = factor of safety (usually 1.1 to 1.5), suggested 1.2;

C_s = stability coefficient;

= 0.30 for angular rock

= 0.375 for rounded rock

C_v = velocity distribution coefficient;

= 1.0 for straight channels or the inside of bends

= Equation 36 below for outside of bends (1.0 for $R_c/W > 26$)

= 1.25 downstream from concrete channels

= 1.25 at the end of dikes

C_T = blanket thickness coefficient given as a function of the uniformity ratio d_{85}/d_{15} ;

= 1.0, recommended because it is based on very limited data

γ_w = specific weight of water (*weight/volume*);

γ_s = specific weight of stone (*weight/volume*);

V_{des} = characteristic velocity for design as in Equations 37 and 38 (*ft/s, m/s*);

V_{avg} = channel cross-sectional average velocity (*ft/s, m/s*);

R_c = centerline radius of curvature of channel bend (*ft, m*);
 W = width of water surface at upstream end of channel bend (*ft, m*);
 S_g = specific gravity of riprap (usually taken as 2.65);
 g = acceleration due to gravity ($32.2 \text{ ft/s}^2, 9.81 \text{ m/s}^2$); and
 K_1 = side slope correction as computed in Equation 39

For outside bends, the velocity coefficient can be calculated as:

$$(36) \quad C_v = 1.283 - 0.2 \log \frac{R_c}{W}$$

The characteristic velocity (V_{des}) is defined as the depth-averaged velocity at a point 20% upslope from the toe of the revetment and is calculated differently for natural and trapezoidal channels. For natural channels:

$$(37) \quad \begin{aligned} V_{des} &= V_{avg}(1.74 - 0.52 \log(R_c/W)) \\ V_{des} &= V_{avg} \text{ for } R_c/W > 26 \end{aligned}$$

For trapezoidal channels:

$$(38) \quad \begin{aligned} V_{des} &= V_{avg}(1.71 - 0.78 \log(R_c/W)) \\ V_{des} &= V_{avg} \text{ for } R_c/W > 8 \end{aligned}$$

The side slope correction factor K_1 is calculated as:

$$(39) \quad K_1 = [1 - (\sin^2 \theta / \sin^2 \phi)]^{0.5}$$

Where:

θ = angle of rock from the horizontal ($^\circ$); and
 ϕ = angle of repose (typically 40°)

The flow depth y utilized in EM-1601 is defined as a local flow depth and can have two different meanings depending on the application of the equation. The flow depth at the toe of the channel side slope is used for bank revetment applications, while the average water depth is used for most other applications.

It is important to note that EM-1601 utilizes a D_{30} instead of D_{50} that is used in other techniques. As a result, the resulting riprap size from EM-1601 is approximately 15% smaller than the riprap size calculated through other published riprap sizing techniques. If the median stone diameter is desired, the National Cooperative Highway Research Program (NCHRP) Report 568 (2006) provides a method for converting D_{30} to D_{50} :

$$(40) \quad D_{50} = 1.2D_{30}$$

Equation 35 was developed primarily for stream bank revetments, therefore application of Equation 35 to in-stream transverse structure design is an approximation. When designing for spur dikes, a C_v value of 1.25 is recommended, and a higher safety of factor and/or higher average channel velocity should be considered. Riprap should be designed to extend below the bed elevation to a depth that is protected from long term scour and degradation. Special attention should focus on the tip of the spur where a riprap foundation should be considered for scour protection.

FHWA's circular HEC-23 (2001) also discusses the EM-1601 method and its applicability in the field. HEC-23 (2001) identifies and provides design guidelines for countermeasures against bridge scour and stream instability. Nineteen detailed design guidelines are provided for stream instability, streambank and roadway embankment protection. Four of nineteen

design guidelines provide guidance on revetment riprap design including in-stream structure design.

2.2.2.4. *American Society of Civil Engineers method (Man-110)*. In 1975, Vanoni and the American Society of Civil Engineering (ASCE) published Sedimentation Engineering (ASCE Manual No. 54). The manual was updated and renamed to Sedimentation Engineering (ASCE Manual No. 110) by Garcia in 2006. A section of ASCE Manual No. 110 (2006) discusses channel control structures for reducing/preventing erosion. One approach to prevent erosion is the use of a rock riprap layer. ASCE Manual No. 110 (2006) determines the median rock size D_{50} based on flow velocity and restricts the gradation of the riprap such that the maximum stone size is 1.5 times the median stone size calculated. The median stone size is determined in units of weight similar to Cal-B&SP (2000). Equation 41, as proposed by Isbash, was modified in ASCE Manual No. 110 (2006) for sloping banks, and expressed as:

$$(41) \quad W = \frac{0.000041G_s V^6}{(G_s - 1)^3 \cos^3 \phi}$$

Where:

- W = weight of stone (lb);
- G_s = specific gravity of stone;
- V = velocity (ft/s); and
- ϕ = angle of side slope to horizontal ($^\circ$)

Unlike other methods, ASCE Manual No. 110 (2006) uses the flow velocity to estimate the hydraulic stresses on the bed and banks instead of parameters such as flow depth or hydraulic radius. The use of flow velocity simplifies Equation 41 since other parameters

used to determine boundary shear stress can be difficult to determine at field sites. Further, ASCE Manual No. 110 (2006) states that the thickness of the riprap layer should be 1.5 times the median rock size, and the use of rock riprap should be restricted to channels with flow depths less than 40 *ft*, and preferably less than 30 *ft*.

2.2.2.5. *U.S. Bureau of Reclamation method (USBR EM-25)*. In 1958, Peterka and the United States Bureau of Reclamation (USBR) published Engineering Monograph No.25 titled "Hydraulic Design of Stilling Basins and Energy Dissipators" (1984) i.e. USBR EM-25. Two reasons for riprap failure are presented including (1) underestimation of stone size, and (2) availability of correctly sized riprap at site. USBR EM-25 presented a set of design procedures to determine the individual stone size required to resist a range of flow velocities impacting stilling basins at downstream locations. The stone size relationship is based on laboratory flume test data. An empirical relationship was developed from the flume dataset in which the stone diameter could be determined from the flow velocity on the channel bottom. Figure 2.2 presents the maximum stone size relationship.

The effectiveness of the design curve was evaluated using field tests on constructed stilling basins. The USBR concluded that a well-graded riprap containing 40% of rocks smaller than required was more stable than a blanket of rock composed entirely of required size. This phenomena can be related to the interlocking of different sized rock and the flow turbulence caused by a rough boundary layer [11].

Figure 2.2 was logarithmically transformed and an analytical approach was produced for median rock riprap size. The analytical approach is expressed as:

$$(42) \quad D_{50} = 0.0122V_a^{2.06}$$

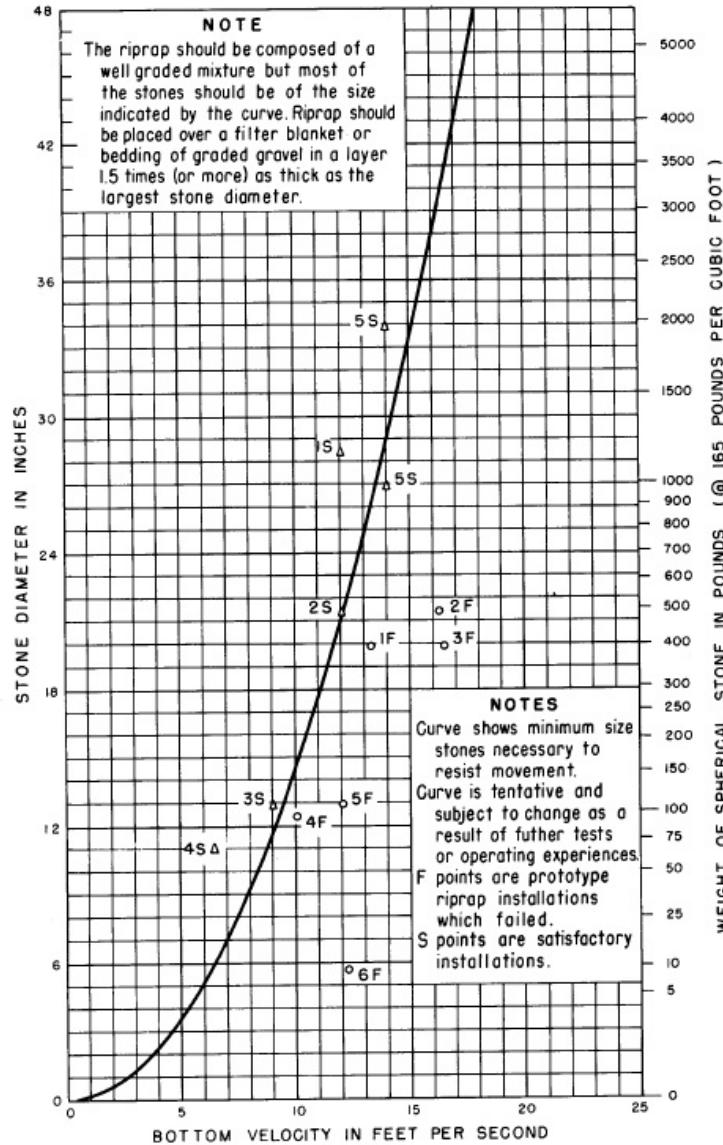


FIGURE 2.2. Curve to determine maximum stone size in riprap mixture

Where:

$$V_a = \text{average channel velocity (ft/s)}$$

2.2.2.6. *U.S. Geological Survey method (USGS Vol. 2)*. In 1986, The United States Geological Survey (USGS) published the report "Rock Riprap Design for the Protection of Stream Channels Near Highway Structures" (USGS Vol. 2, 1986) that presents hydraulic characteristics of open channels and guidelines for rock riprap design. USGS Vol. 2 (1986) by Blodgett and McConaughy evaluates seven procedures being used for the design of rock

riprap. Four types of riprap failure are recognized in the report, and a new relationship between median riprap size and flow velocity is presented. Thirty-nine (39) flow events at twenty-six (26) sites were used for the development of the relationship. Seventeen (17) events initiated riprap movement causing damage. Particle erosion is identified as the primary cause of damage in these seventeen events. The velocity and median riprap relationship established by HEC-11 were correlated resulting in Equation 43.

$$(43) \quad D_{50} = 0.01V_a^{2.44}$$

Where:

V_a = average channel velocity (*ft/s*)

2.2.2.7. *Summary of Agency Methodologies for Bank Stabilization.* The agency bank stabilization methods presented in Section 2.2.2 are used for bank and toe revetments. Revetment protects the banks of a channel similar to in-stream structures, in that, a riprap layer is installed to dissipate high velocity flows and reduce or prevent the erosion of bank material. In-stream structures are subjected to stresses higher than bank revetment. In-stream structures extend into the channel and encounter impacting flows creating zones of high shear stress, while bank revetments are contained along the channel bank resulting in high velocity flows impacting in a near parallel manner.

The HEC-11, Cal-B&SP, Man-110, USBR EM-25, and USGS methodologies utilize an average channel velocity in the computation of median riprap size. The principles behind using an in-stream structure for bank protection (further described in Section 2.3) suggests that flow velocities along in-stream structures are significantly higher than average channel

velocities. The riprap size for in-stream structures must be designed to account for higher flow velocities and shear stresses that occur along the structure and particularly at the structure tip. The implementation of an average flow velocity in agency bank revetment methodologies could underestimate the necessary riprap size for in-stream structure design. Thus, evidence strongly suggests that the design flow velocity utilized in the agency relationships may require reevaluation to account for increased flow velocities impacting the structures.

2.3. TYPES OF IN-STREAM STRUCTURES

2.3.1. BENDWAY WEIRS. Bendway weirs are defined as submerged rock structures that protrude/extend into a channel reach at angles upstream, downstream, or perpendicular to the channel bank. These structures are placed in a series along the outer bank of a bend to provide protection from channel bank erosion. They serve as a channel bank protection measure by redirecting high flow velocities away from the outside bank and reducing the magnitude of secondary flows in channel bends [4]. Redirected flow accelerates around the weir, such that significant differences have been observed between the average flow velocity and the velocities measured along bendway weirs, particularly at their tips [3]. The redirection of flow shifts high shear stresses away from the bank towards the riverward ends of the bendway weirs.

Bank stabilization schemes that are primarily constructed parallel to the channel bank (i.e. revetments, longitudinal dikes, and bulkheads) must be designed to protect against the undermining along the entire length of the bank, while localized protection at the weir tips is required for a bendway weir stabilization scheme. A catastrophic failure of a bendway weir stabilization scheme is less probable than other bank stabilization schemes because the tips

of the weirs are the most impacted at any given time. Failure of the weir tip leaves additional spur length to provide partial protection for the bank until repairs can be performed [12].

Bendway weirs are advantageous as they reduce construction right-of-way and bank alteration compared to other countermeasures such as riprap revetment [12]. Aquatic species and riparian vegetation are supported by the installation of bendway weirs as eddies and pools are favorable for fish habitat and protect vegetative growth created behind the weirs. River navigation is significantly improved by the deepening of the channel and stabilization of the channel banks caused by bendway weirs [13]. An example of a series of bendway weirs in the field is provided in Figure 2.3.



FIGURE 2.3. Series of bendway weirs in the field during low flow conditions [4]

There are five significant design parameters that have been defined for the development of bendway weir design criteria. These parameters include weir angle, height, profile, length, and spacing [4]. A plan and cross-section view of the significant bendway weir parameters is provided in Figure 2.4 and Figure 2.5. The weir angle, θ , is defined as the angle between the weir orientation and the axis tangent to the channel bank. In this manner, a weir angle of 0° to 90° indicates a weir that is oriented upstream, while an weir angle of 90° to 180° describes a weir oriented downstream. The angle at which a bendway weir is installed is dependent upon the intended purpose of the structure. Brown (1985) presented a theory that upstream-oriented weirs repel flow, while downstream-oriented weirs attract flow. Downstream-facing weirs are less susceptible to scour at the toe of the structure and collect less debris than upstream-oriented weirs. An issue that has been observed with downstream-oriented weirs is the redirection of overtopping flow towards eroding channel banks [13]. Upstream-oriented weirs are more effective at redirecting high velocity flows away from eroding channel banks. A movable bed study by Derrick *et al.* (1994) indicated that a weir angle of 60° was appropriate for efficient weir performance. Derrick *et al.* (1994) also concluded that an adjustment of weir angle as little as 5° can have a significant effect on the efficiency of a bendway weir. As a result, the weir angle is a significant part of the design of a bendway weir system.

The weir height, $H_{w-crest}$, is defined as the distance the crest of a weir rises above the channel bed. Brown (1985) recommends weir heights be designed as a function of the height of channel bank to be protected. Five design guidelines have been presented for the design of weir height by Brown (1985) that include:

- (1) Weir heights should be tall enough to adequately protects the areas of the channel bank affected by the erosion process

- (2) Weir heights should be designed no more than three feet below the design flow stage if the design flow stage is lower than the channel bank height
- (3) Weir heights should be designed to meet channel bank height when the design flow stage is higher than the channel bank height
- (4) Permeable weirs should be designed at a height where heavy debris can pass over the weir crest without causing structural damage
- (5) Impermeable weirs should be submerged by at least 3-*ft* below the worst design flow condition to protect against local scour and flow concentration at the weir tip

The profile of a weir is related to the weir height and is typically sloped or level. Sloping crests are advantageous because they allow for the adjustment of the meander trace and amount of flow constriction with flow stage. Brown (1985) recommends the use of a sloping crest for impermeable weirs. Sloping crests are typically used when the affected channel has high banks. Brown (1985) recommends a level crest design for permeable weirs unless bank heights are sufficiently tall to warrant a sloping crest [12].

The bendway weir length, L_{w-proj} , is defined as the projected length of the weir from the channel bank to the tip of the weir crest perpendicular to the main direction of flow [4]. Brown (1985) investigated weir length for permeable and impermeable weirs and identified four trends. The four trends provided are:

- (1) Scour depth at the tip of the weir increases with weir length
- (2) Magnitude of flow concentration at the structure tip increases with weir length
- (3) Flow deflection increases with weir length
- (4) The amount of channel bank protection increases with weir length [4]

Brown (1985) recommends an impermeable weir less than 15% of the bankfull channel width. Permeable weirs are recommended to be less than 25% of the channel width at dominant discharge.

Bendway weir spacing, L_{arc} , is defined as the arc distance between the weirs measured from where the bendway weir meets the channel bank. Weir spacing is a significant design parameter because a compromise between economic efficiency and structure effectiveness. Excessively large weir spacings may result in further bank erosion from high velocity flows; however, tightly-spaced weirs may result in economic inefficiency and incomplete effectiveness of individual structures. Weir length, angle, permeability, and channel bend geometry must also be considered in the design of weir spacing. Copeland (1983) and Brown (1985) investigated spacing ratios in bendway weir fields. Spacing ratios are defined by Brown (1985) as the ratio of the weir's spacing length to the its projected length, L_{w-proj} . Copeland (1983) recommends spacing ratios up to 3, but expressed a need for additional bank protection in some cases. Copeland suggested that spacing ratios should be significantly influenced by observations in channels of similar nature or site-specific models. Spacing ratios of 4 to 6 and 3 to 4 were recommended for large and small radius bends, respectively [4]. Heintz (2002) asserts that a method of determining optimal bendway weir spacing ratios is not clearly defined, and most literature recommends basing spacing ratios on site-specific conditions.

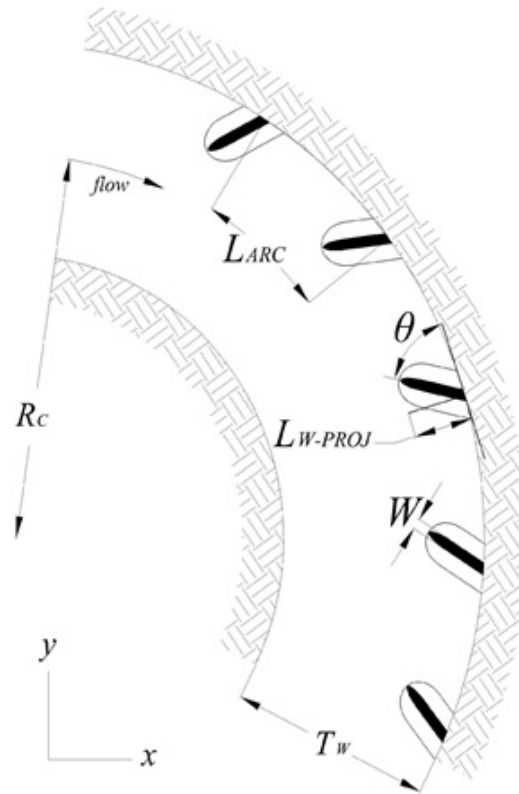


FIGURE 2.4. Planview of Bendway Weir Parameters [5]



FIGURE 2.5. Cross-Section View of Bendway Weir Parameters [5]

2.3.2. SPUR DIKES. Spur dikes are types of bendway weirs designed with a crest elevation matching the cross-section averaged design flow depth. Spur dikes are placed on the outer bank of a channel bend to provide bank protection and to redirect high velocity flows towards the middle of the channel preventing unwanted migration. Spur dikes have been extensively used to manage and train rivers. Spur dikes can be permeable or impermeable depending upon their composition, i.e. concrete, earth, stone, etc. The guidelines presented

in Section 2.3.1 are applicable to spur dikes. Figure 2.6 provides a cross-section schematic of a spur dike.

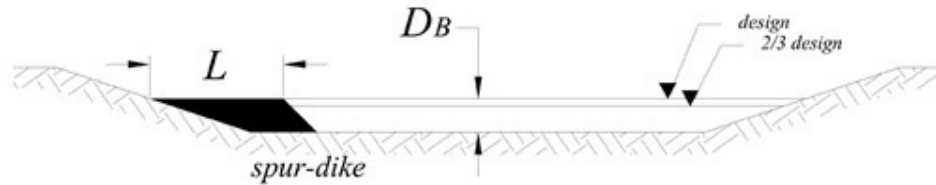


FIGURE 2.6. Schematic of a Spur Dike [5]

2.3.3. VANES. Vanes are types of bendway weirs designed with a crest that slopes downward from the bank to the thalweg of the channel. Therefore, the height of the weir at the toe of the structure is lower than where the vane ties into the outer bank. Flow is conveyed over the vane and away from the bank as it moves downstream. Similar to bendway weirs and spur dikes, vanes guide flow away from the bank, reduce bank erosion, and encourage vegetation growth. The guidelines presented in Section 2.3.1 are applicable to vanes. Figure 2.7 provides a cross-section schematic of a vane.

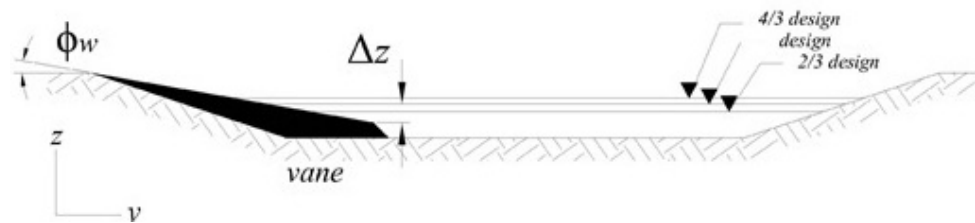


FIGURE 2.7. Schematic of a Vane [5]

2.3.4. SUMMARY. In-stream structures are designed to protect banks by redirecting high velocity flows away from eroding channel banks. Multiple techniques have been used to protect channel banks, but in-stream structures are used extensively because of the secondary effects resulting from their installation. These structures support the enhancement of riparian vegetation and fish habitats by creating pools and eddies in channel bends. Navigation is

improved by the channel deepening and bank stability that in-stream structures provide as well. The installation of bendway weirs uses less right-of-way and less bank alteration, so bendway weirs are also an efficient way to manage and train channels.

Heintz (2002) identified five key parameters for the design of bendway weirs including weir angle, height, profile, length, and spacing. Brown (1985) provided recommendations for these five weir parameters, but weir design continues to be based on field observations and physical modelling data. Three types of in-stream structures were identified including bendway weirs, spur dikes, and vanes. Spur dikes are bendway weirs that are designed with a crest elevation that meets a design flow stage for the channel. Vanes are bendway weirs designed with a crest that slopes towards the thalweg of the channel which forces the flow over the vane and away from the bank.

In-stream structures are predominantly comprised of rock riprap material. The common application of rock riprap for prevention of bank erosion and degradation has led to the development of numerous riprap sizing relationships and methodologies. Established design procedures for sizing rock riprap have been applied to channel bank, embankment, and spillway revetment with minor applicability to in-stream structure design. An analysis of the relationship between in-stream structures and channel flow conditions contributes to redefining current riprap sizing methodologies for specific application in in-stream structure design.

CHAPTER 3

PHYSICAL MODEL DESCRIPTION

3.1. INTRODUCTION

The United States Bureau of Reclamation (USBR) elected to evaluate the ability of in-stream structures to mitigate the migration of river channels. Colorado State University (CSU) was commissioned to design and construct a physical model for use in the evaluation of in-stream structures. In response, an undistorted, hard boundary physical model was constructed at the Colorado State University Hydraulics Laboratory to test and evaluate a series of twenty-two structure configurations that included bendway weirs, spur-dikes, vanes, and submerged spur-dikes.

3.2. MODEL GEOMETRY AND FLOW CONDITIONS

A concrete, trapezoidal physical model of two representative channel bends of the Middle Rio Grande was constructed at CSU in 2001 [3]. Heintz (2002) designed and oversaw the construction of the physical model. The physical model represents a twenty-nine (29) mile reach of the Middle Rio Grande and contains two separate geometric channel bends that are connected by a transition section. The Middle Rio Grande reach was scaled using a 1:12 Froude scale. Table 3.1 provides the scaling factors used for the physical parameters of the model.

A representative geometry of the twenty-nine mile reach of the Middle Rio Grande was modeled to examine trends in the hydraulic conditions. Three types of channel bends were established, and two of the three types were represented in the physical model. The geometric characteristics of the modeled bends are provided in Table 3.2. The similitude relationships

TABLE 3.1. Similitude Scaling Used for the Physical Model (1:12 Froude Scale)

Parameter	Scaling Factor
Length	$L_r = 12$
Depth	$h_r = L_r = 12$
Width	$W_r = L_r = 12$
Velocity	$V_r = L_r^{1/2} = 3.46$
Discharge	$Q_r = L_r^{5/2} = 500$
Slope	$S_r = 1$
Roughness	$n_r = L_r^{1/6} = 1.51$

that were presented in Table 3.1 were applied to the geometric characteristics in Table 3.2 to determine the model dimensions. The results of the scaling procedure for the model are provided in Table 3.3.

TABLE 3.2. Geometric characteristics of Type 1 and 3 bends in the field

Bend	Channel Width <i>ft (m)</i>	Radius of Curvature <i>ft (m)</i>	Bend Angle (°)	Relative Curvature <i>r/b</i>	Channel Length <i>ft (m)</i>
Type 1	230.4 (70.2)	465 (141.7)	125	2.02	1,014 (309)
Type 3	180 (54.9)	790 (240.8)	73	4.39	1,002 (305)

TABLE 3.3. Geometric characteristics of Type 1 and 3 bends in the model

Bend	Channel Width <i>ft (m)</i>	Radius of Curvature <i>ft (m)</i>	Bend Angle (°)	Relative Curvature <i>r/b</i>	Channel Length <i>ft (m)</i>
Type 1	19.2 (5.9)	38.8 (11.8)	125	2.02	84.5 (25.8)
Type 3	15 (4.6)	65.8 (20.1)	73	4.39	83.5 (25.4)

The cross-sectional geometry of both upstream and downstream bends is trapezoidal with 3H:1V side slopes and a total channel depth of 1.5-*ft* to accommodate the model flow rates. The upstream bend has a 10.2-*ft* bottom width, while the downstream bend has a 6-*ft* bottom width. The cross-sectional geometry of each bend remains constant and prismatic for consistency. The model was constructed to match the prototype bed slope of

approximately 0.000863 ft/ft . A straight transition was included to separate the upstream and downstream bends. The channel width is contracted from 19.2-ft to 15.0-ft by the straight transition at a ratio of 10:1. A 10:1 ratio was chosen to fit model constraints of the available laboratory floor space, and equates to a 42-ft straight transition. Figure 3.1 provides a planview of the model and the Type 1 and 3 bends [4].

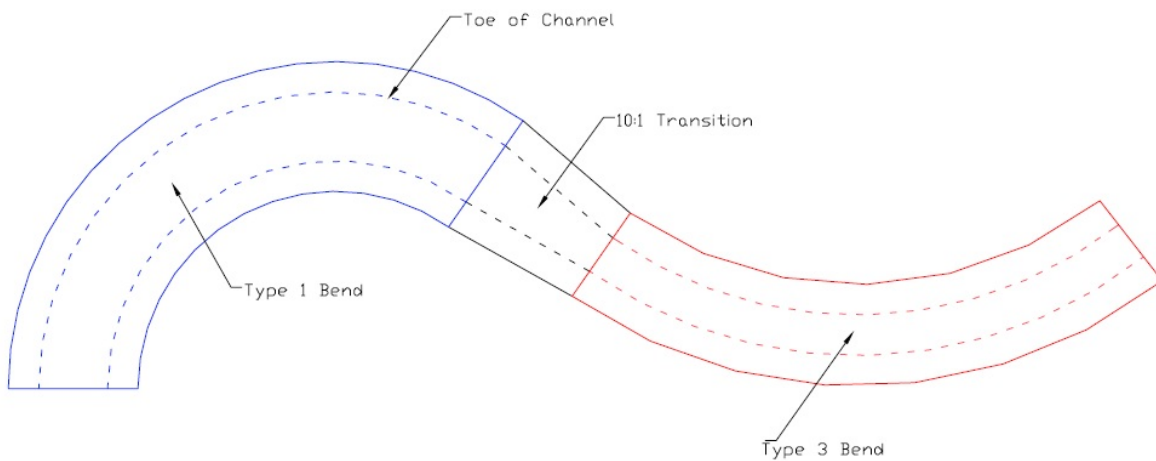


FIGURE 3.1. Planview of Model Layout of Type 1 and 3 Bends [4]

The twenty-nine mile reach of Middle Rio Grande has Manning's n values ranging from 0.026 to 0.035. The model was constructed with a roughened concrete surface providing a Mannings value of 0.018, which equates to a prototype roughness of approximately 0.027 [4]. Three prototype flow conditions were modeled for a comprehensive study of the flow conditions found in the Middle Rio Grande. The prototype flow conditions modeled included 4,000, 6,000, and 8,000 cfs [14]. The three prototype discharges were scaled using the similitude relationship in Table 3.1 resulting in model discharges of 8, 12, and 16 cfs .

3.3. MODEL CONSTRUCTION, COMPONENTS AND STARTUP

The construction of the physical model began in August of 2000 and required approximately 8 months to complete. The model consists of three major components including a headbox, main channel, and tailbox. The headbox was constructed at the upstream end of the model and creates uniform flow conditions as water enters the model. The headbox delivers flow to the model through a pipe manifold. A 2-*in* rock baffle flow diffuser downstream of the pipe manifold is used to dissipate energy and evenly distribute the flow at the inlet. Curves in the hard boundary of the headbox provide a transition from the headbox into the main channel cross-section and transition the flow smoothly into the model. Water is supplied to the model through a direct 12-*in* pipeline from Horsetooth Reservoir in Fort Collins, CO. The 12-*in* pipeline connects to the pipe manifold and supplies water to the headbox. Figure 3.2 shows the headbox during testing [4].



FIGURE 3.2. Physical Model Headbox for Flow Delivery [4]

The main channel was constructed with 4-*ft* tall wood walls. Plywood cross-sectional templates were installed between the 4-*ft* walls to form the channel bend geometry. Eight cross-section templates were used for each bend. The plywood templates were installed at a predetermined elevation, and sand was backfilled between each template to meet a predetermined elevation. The sand was saturated, compacted, and leveled until reaching an appropriate level that was 2-*in* below the desired finished elevation. A roughened concrete cap 2-*in* thick was placed over the sand to form the hard channel boundary. A broom was raked across the wet concrete to provide the desired roughness in the channel. The concrete roughening process for desired channel roughness is seen Figure 3.3. Sealant was used on and between the concrete slabs to prevent leaking of the model. A total of 40 yd^3 of concrete and 600 *tons* of sand was used for the construction of the main channel [4].



FIGURE 3.3. Finishing of Concrete for Desired Channel Roughness [4]

A tailbox was constructed at the downstream end of the model to collect the flow for redistribution. A 10-*in* pipe and two 12-*in* culverts are used to convey the flows to College Lake located approximately 0.25 miles south of the Hydraulics Laboratory. A recirculation system was installed in the summer of 2003 consisting of a pump sump, two pumps, and two 12-*in* recirculation pipelines. During testing, the 10-*in* pipe and 12-*in* culverts can be closed, and the pump sump filled. Flow can then be pumped back to the headbox through the two 12-*in* recirculation pipelines [7].

Rock weirs were constructed of angular sandstone (average diameter of 3"-6") and plywood inserts. Angular sandstone was chosen because of its applicability in the Middle Rio Grande Valley area and its availability in the Fort Collins area. The design weir length and height were drawn on to the plywood and cutout to aid in the consistent and accurate construction of the weirs, as well as, to prevent the weirs from complete permeability. The plywood insert was essential in maintaining the shape and size of the structure during the construction process. Rock riprap was hand-placed on either side of the plywood cutouts, until the weir top and base were 1-*ft* and 4-*ft* wide, respectively. An example of a constructed bendway weir and series of bendway weirs in the physical model are provided in Figures 3.4 and 3.5.



FIGURE 3.4. Constructed Benway Weir during Testing [4]



FIGURE 3.5. Bendway Weir Series in Model [4]

3.4. INSTRUMENTATION AND MEASUREMENTS

3.4.1. INTRODUCTION. A mobile instrumentation cart was constructed on the main channel that spanned the entire width of the model and allowed for the collection of data at all points within the model. Cross-sections were surveyed and labeled on the edge of the model. There were a total of 18 cross-sections designated. The upstream bend contains cross-sections 1 through 8, and the downstream bend entails cross-sections 10 through 18 with cross-section 9 located directly between the two bends [6]. The instrumentation cart was purposefully aligned perpendicular to the main direction of flow for consistency in the coordinate system of the data. Figure 3.6 shows the locations of the cross-sections in the physical model.

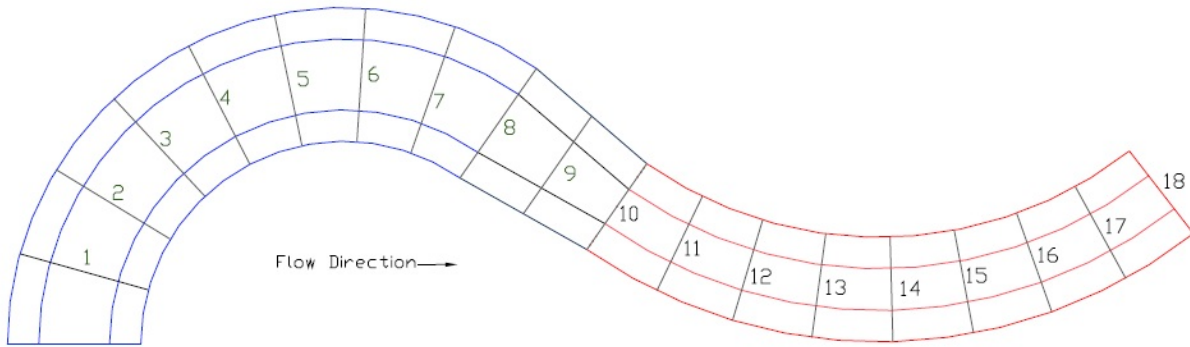


FIGURE 3.6. Planview of model with labeled cross-sections [4]

3.4.2. FLOW RATE MEASUREMENTS. Water is supplied to the model through a direct 12-*in* line from Horsetooth Reservoir in Fort Collins, CO, and released (if necessary) through an additional direct 12" line to College Lake. The 12-*in* line from Horsetooth Reservoir is controlled by a gate valve that leads to the headbox. Two SIGNET 2550 Insertion Magmeters located on the two 12-*in* recirculation pipelines are used to monitor the flow coming into

the headbox with an accuracy of plus or minus 2%. The magmeters can read DC voltages ranging from 4 to 20 *mA* converting to flow velocities from 0.3 *ft/s* to 20 *ft/s*. Figures 3.7 and 3.8 from Schmidt (2005) show the device.



FIGURE 3.7. SIGNET Meters

3.4.3. WATER DEPTH MEASUREMENTS. Water depth and water surface elevation measurements were recorded using two different methods. A standard point gauge system with ± 0.001 -*ft* accuracy was mounted on the instrumentation cart and used to measure bed and water surface elevations. A piezometer system was also constructed and implemented throughout the model for the measurement of flow depths. The piezometer taps in the model



FIGURE 3.8. Electronic Display Boxes

were constructed using a capped 1-*in* diameter, 6-*in* long copper pipe. The copper pipe was connected to a 2-*in* diameter PVC stilling well using polyurethane tubing, and a Vernier scale point gauge with an accuracy of ± 0.001 -*ft* was used to measure the water level in the PVC stilling wells. One channel center and six channel bank (three along each channel bank) piezometer taps were installed for each cross-section and labeled A-G starting along the river left bank. One-hundred and twenty-two (122) piezometer taps were placed throughout the model. Figure 3.9 and Figure 3.10 show the piezometer locations for upstream and downstream bends and the PVC stilling well station, respectively.

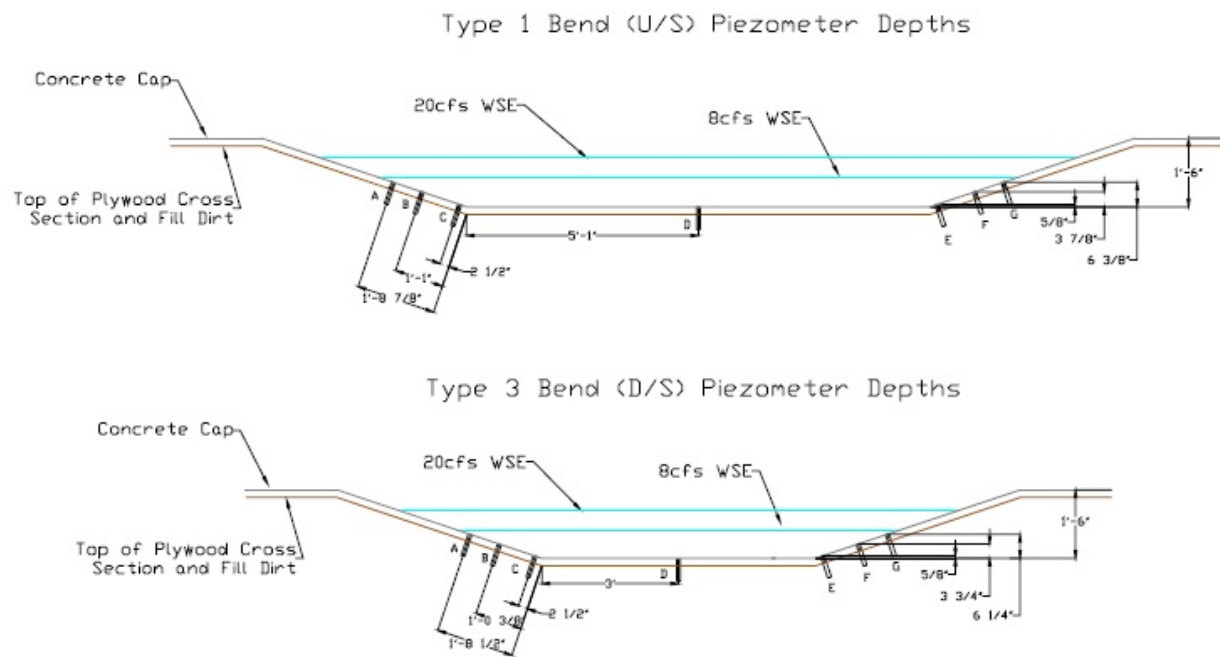


FIGURE 3.9. Piezometer locations for upstream and downstream bends [4]



FIGURE 3.10. Stilling wells to measure water surface elevations [4]

3.4.4. VELOCITY MEASUREMENTS. For each structure configuration, velocity measurements were strategically taken at each cross-section in order to comprehend flow patterns around the in-stream structures. A Sontek Acoustic Doppler Velocity (ADV) meter was used to measure flow velocity in the model. The Sontek ADV measures flow velocity three-dimensionally for the analysis of both longitudinal and secondary flow profiles and is accurate to plus or minus 1% . The ADV probe was placed perpendicular to the cart in a manner that the positive x-direction was upstream facing the main direction of flow. The y and z directions were defined as the lateral and vertical components of the flow velocity, respectively [6]. The ADV was attached to a Vernier point gauge on the instrumentation cart, the Vernier point gauge measures with an accuracy of $\pm 0.001\text{-}ft$. The personal computer on the instrumentation cart, in conjunction with the ADV's data acquisition card and software, were used for recording and averaging flow velocity values. The Sontek ADV uses a 10 Hz sampling rate measuring velocity from a sampling position 0.164- ft directly below the probe head. Figure 3.11 and Figure 3.12 show the ADV probe and test setup.



FIGURE 3.11. ADV Probe [4]



FIGURE 3.12. ADV Setup [4]

CHAPTER 4

DATA COLLECTION

4.1. BASELINE DATA COLLECTION

Preliminary baseline testing was completed to understand the principle flow characteristics and patterns through the physical model's channel bends. A comprehensive dataset was collected for the design flow rates of 8, 12, and 16 *cfs* without in-stream structure placement. Data collection locations were selected through an iterative process over several stages of testing. Depth measurements and three dimensional velocity profiles were measured at 10% increments above each of the 122 piezometer taps. Depth measurements were also taken with a point gauge for verification purposes. All baseline data were collected and logged into a database for analysis. Figure 4.1 shows the upstream bend of the model during baseline testing.

4.2. IN-STREAM STRUCTURE TEST PROGRAM

An in-stream structure test program was initiated after the baseline testing was completed. The purpose of the in-stream structure test program was to determine the effects of various bendway weir design characteristics [6]. Structure height, length, angle, and spacing were chosen for each test based on a thorough review of literature including Heintz (2002), Schmidt (2005), and Darrow (2004). Twenty-two different rock configurations were tested during the in-stream structure data collection process. Fifteen structures configurations were completed for spur dikes and bendway weirs, and seven structure configurations were completed for vanes. Each of the twenty-two structure configurations were evaluated based upon three design flow discharges (8, 12, and 16 *cfs*) resulting in a comprehensive program of sixty-six (66) tests. Previous studies by Darrow (2004) and Schmidt (2005) required that



FIGURE 4.1. Upstream bend of model during baseline testing [4]

only one variable be adjusted between each in-stream structure configuration. Variables that were changed from configuration to configuration included projected weir length (L_{w-proj}), weir height ($H_{w-crest}$), angle (θ), and spacing (L_{arc}). The three variables that were held constant through each configuration were the weir crest width ($\sim 1\text{ ft}$), bottom width ($\sim 4\text{ ft}$), and median riprap size ($\sim 3''\text{-}6''$). A 1-ft crest width is necessary in the field construction of the weirs for mobility of the construction equipment along the weir, and a bottom width of 4-ft was necessary due to the angle of repose of the rock used in the model. A planview schematic of the structure parameters is provided in Figure 2.4.

The alteration of projected weir length, weir height, angle, and spacing between each structure configuration allowed for twenty-two (22) individual weir designs. Projected weir lengths ranging from 1.6 to 5.1-ft were designated for a comprehensive analysis of the effects

of weir length on channel flow conditions. Weir heights of 0.77 and 0.78-*ft* were used for the upstream and downstream bends, respectively, in the bendway weir and spur dike tests. For vane testing, weir heights of 0.13 and 0.42-*ft* were used for the upstream and downstream bends, respectively, for five of the seven structure configurations, while weir heights of 0.44 and 0.69-*ft* were used for the upstream and downstream bends, respectively, for two of the seven structure configurations. Weir heights for spur dikes and bendway weirs were kept consistent for correlation with the design discharges of 8, 12, and 16 *cfs*. Weir spacings ranged from 8.5 to 29.6-*ft* for comparison with results obtained by Heintz (2002). Weir angles of 60°, 75°, and 90° were used as recommended from Heintz (2002) and Darrow (2004).

The test matrix was developed to facilitate an efficient and orderly program of in-stream structure testing. Table 4.1 presents the test matrix developed for the in-stream structure program. Sixty-six (66) tests are represented in Table 4.1. Each test is segmented into upstream (US) and downstream (DS) bends because each bend has a separate structure design. Test W01-W15 represent spur dike and bendway weir testing, and Tests W16-W22 represent vanes testing. Within tests W01-W15, spur dikes were tested at flow discharges of 8 and 12 *cfs*, while bendway weirs were tested at 16 *cfs* for submergence purposes. Vanes were tested at all three design flow discharges (8, 12, and 16 *cfs*).

Table 4.1: In-stream Structure Design Program

Test	Flow Rate (ft^3/s)	Bend	Weir Angle ($^{\circ}$)	Proj. Weir Length (ft)	Weir Spacing (ft)	Weir Height (ft)	% of XS Blocked
W01	8	US	90	4.1	16.9	0.77	27.0
W01	8	DS	90	3.0	20.9	0.78	27.0
W01	12	US	90	4.1	16.9	0.77	27.0
W01	12	DS	90	3.0	20.9	0.78	27.0
W01	16	US	90	4.1	16.9	0.77	27.0
W01	16	DS	90	3.0	20.9	0.78	27.0
W02	8	US	90	4.1	21.1	0.77	27.0
W02	8	DS	90	3.0	29.6	0.78	27.0
W02	12	US	90	4.1	21.1	0.77	27.0
W02	12	DS	90	3.0	29.6	0.78	27.0
W02	16	US	90	4.1	21.1	0.77	27.0
W02	16	DS	90	3.0	29.6	0.78	27.0
W03	8	US	90	4.1	14.0	0.77	27.0
W03	8	DS	90	3.0	16.7	0.78	27.0
W03	12	US	90	4.1	14.0	0.77	27.0
W03	12	DS	90	3.0	16.7	0.78	27.0
W03	16	US	90	4.1	14.0	0.77	27.0
W03	16	DS	90	3.0	16.7	0.78	27.0

Table 4.1 – Continued

Test	Flow Rate (ft^3/s)	Bend	Weir Angle ($^\circ$)	Proj. Weir Length (ft)	Weir Spacing (ft)	Weir Height (ft)	% of XS Blocked
W04	8	US	90	2.2	8.5	0.77	10.8
W04	8	DS	90	1.6	13.0	0.78	10.8
W04	12	US	90	2.2	8.5	0.77	10.8
W04	12	DS	90	1.6	13.0	0.78	10.8
W04	16	US	90	2.2	8.5	0.77	10.8
W04	16	DS	90	1.6	13.0	0.78	10.8
W05	8	US	90	2.2	10.3	0.77	10.8
W05	8	DS	90	1.6	16.8	0.78	10.8
W05	12	US	90	2.2	10.3	0.77	10.8
W05	12	DS	90	1.6	16.8	0.78	10.8
W05	16	US	90	2.2	10.3	0.77	10.8
W05	16	DS	90	1.6	16.8	0.78	10.8
W06	8	US	90	3.3	11.5	0.77	19.4
W06	8	DS	90	2.4	17.1	0.78	19.4
W06	12	US	90	3.3	11.5	0.77	19.4
W06	12	DS	90	2.4	17.1	0.78	19.4
W06	16	US	90	3.3	11.5	0.77	9.4
W06	16	DS	90	2.4	17.1	0.78	19.4
W07	8	US	90	3.3	13.9	0.77	19.4

Table 4.1 – Continued

Test	Flow Rate (ft^3/s)	Bend	Weir Angle ($^\circ$)	Proj. Weir Length (ft)	Weir Spacing (ft)	Weir Height (ft)	% of XS Blocked
W07	8	DS	90	2.4	22.1	0.78	19.4
W07	12	US	90	3.3	13.9	0.77	19.4
W07	12	DS	90	2.4	22.1	0.78	19.4
W07	16	US	90	3.3	13.9	0.77	19.4
W07	16	DS	90	2.4	22.1	0.78	19.4
W08	8	US	60	2.3	8.5	0.77	10.8
W08	8	DS	60	1.7	13.0	0.78	10.8
W08	12	US	60	2.3	8.5	0.77	10.8
W08	12	DS	60	1.7	13.0	0.78	10.8
W08	16	US	60	2.3	8.5	0.77	10.8
W08	16	DS	60	1.7	13.0	0.78	10.8
W09	8	US	60	2.3	10.3	0.77	10.8
W09	8	DS	60	1.7	16.8	0.78	10.8
W09	12	US	60	2.3	10.3	0.77	10.8
W09	12	DS	60	1.7	16.8	0.78	10.8
W09	16	US	60	2.3	10.3	0.77	10.8
W09	16	DS	60	1.7	16.8	0.78	10.8
W10	8	US	60	3.2	11.2	0.77	19.4
W10	8	DS	60	2.4	16.5	0.78	19.4

Table 4.1 – Continued

Test	Flow Rate (ft^3/s)	Bend	Weir Angle ($^\circ$)	Proj. Weir Length (ft)	Weir Spacing (ft)	Weir Height (ft)	% of XS Blocked
W10	12	US	60	3.2	11.2	0.77	19.4
W10	12	DS	60	2.4	16.5	0.78	19.4
W10	16	US	60	3.2	11.2	0.77	19.4
W10	16	DS	60	2.4	16.5	0.78	19.4
W11	8	US	60	3.2	13.5	0.77	19.4
W11	8	DS	60	2.4	21.3	0.78	19.4
W11	12	US	60	3.2	13.5	0.77	19.4
W11	12	DS	60	2.4	21.3	0.78	19.4
W11	16	US	60	3.2	13.5	0.77	19.4
W11	16	DS	60	2.4	21.3	0.78	19.4
W12	8	US	60	4.0	13.7	0.77	27.0
W12	8	DS	60	3.0	20.3	0.78	27.0
W12	12	US	60	4.0	13.7	0.77	27.0
W12	12	DS	60	3.0	20.3	0.78	27.0
W12	16	US	60	4.0	13.7	0.77	27.0
W12	16	DS	60	3.0	20.3	0.78	27.0
W13	8	US	60	4.0	16.5	0.77	27.0
W13	8	DS	60	3.0	26.2	0.78	27.0
W13	12	US	60	4.0	16.5	0.77	27.0

Table 4.1 – Continued

Test	Flow Rate (ft^3/s)	Bend	Weir Angle ($^{\circ}$)	Proj. Weir Length (ft)	Weir Spacing (ft)	Weir Height (ft)	% of XS Blocked
W13	12	DS	60	3.0	26.2	0.78	27.0
W13	16	US	60	4.0	16.5	0.77	27.0
W13	16	DS	60	3.0	26.2	0.78	27.0
W14	8	US	75	4.1	14.0	0.77	27.0
W14	8	DS	75	3.0	20.4	0.78	27.0
W14	12	US	75	4.1	14.0	0.77	27.0
W14	12	DS	75	3.0	20.4	0.78	27.0
W14	16	US	75	4.1	14.0	0.77	27.0
W14	16	DS	75	3.0	20.4	0.78	27.0
W15	8	US	75	4.1	16.8	0.77	27.0
W15	8	DS	75	3.0	26.4	0.78	27.0
W15	12	US	75	4.1	16.8	0.77	27.0
W15	12	DS	75	3.0	26.4	0.78	27.0
W15	16	US	75	4.1	16.8	0.77	27.0
W15	16	DS	75	3.0	26.4	0.78	27.0
W16	8	US	90	5.1	15.0	0.13	19.4
W16	8	DS	90	3.1	19.2	0.42	19.4
W16	12	US	90	5.1	15.0	0.13	19.4
W16	12	DS	90	3.1	19.2	0.42	19.4

Table 4.1 – Continued

Test	Flow Rate (ft^3/s)	Bend	Weir Angle ($^\circ$)	Proj. Weir Length (ft)	Weir Spacing (ft)	Weir Height (ft)	% of XS Blocked
W16	16	US	90	5.1	15.0	0.13	19.4
W16	16	DS	90	3.1	19.2	0.42	19.4
W17	8	US	90	5.1	11.5	0.13	19.4
W17	8	DS	90	3.1	17.1	0.42	19.4
W17	12	US	90	5.1	11.5	0.13	19.4
W17	12	DS	90	3.1	17.1	0.42	19.4
W17	16	US	90	5.1	11.5	0.13	19.4
W17	16	DS	90	3.1	17.1	0.42	19.4
W18	8	US	60	4.9	11.5	0.13	19.4
W18	8	DS	60	3.0	17.1	0.42	19.4
W18	12	US	60	4.9	11.5	0.13	19.4
W18	12	DS	60	3.0	17.1	0.42	19.4
W18	16	US	60	4.9	11.5	0.13	19.4
W18	16	DS	60	3.0	17.1	0.42	19.4
W19	8	US	90	5.1	13.9	0.13	19.4
W19	8	DS	90	3.1	22.1	0.42	19.4
W19	12	US	90	5.1	13.9	0.13	19.4
W19	12	DS	90	3.1	22.1	0.42	19.4
W19	16	US	90	5.1	13.9	0.13	19.4

Table 4.1 – Continued

Test	Flow Rate (ft^3/s)	Bend	Weir Angle ($^{\circ}$)	Proj. Weir Length (ft)	Weir Spacing (ft)	Weir Height (ft)	% of XS Blocked
W19	16	DS	90	3.1	22.1	0.42	19.4
W20	8	US	60	4.9	13.5	0.13	19.4
W20	8	DS	60	3.0	21.3	0.42	19.4
W20	12	US	60	4.9	13.5	0.13	19.4
W20	12	DS	60	3.0	21.3	0.42	19.4
W20	16	US	60	4.9	13.5	0.13	19.4
W20	16	DS	60	3.0	21.3	0.42	19.4
W21	8	US	90	2.9	8.5	0.44	10.8
W21	12	US	90	2.9	8.5	0.44	10.8
W21	12	DS	90	1.7	16.8	0.69	10.8
W21	16	US	90	2.9	8.5	0.44	10.8
W21	16	DS	90	1.7	16.8	0.69	10.8
W22	8	US	60	2.8	8.5	0.44	10.8
W22	12	US	60	2.8	8.5	0.44	10.8
W22	12	DS	60	1.7	16.8	0.69	10.8
W22	16	US	60	2.8	8.5	0.44	10.8
W22	16	DS	60	1.7	16.8	0.69	10.8

Data were collected during each test along each cross-section and around each weir. Along the cross-sections, data were collected at the river left bank toe, center, and river right bank toe. For in-stream structure locations, data were collected one-foot upstream and downstream from the structure along the channel toe; one-foot from the tip of the structure; and along the opposite bank at the channel toe. A 60% depth-averaged velocity was recorded at each location. Figure 4.2 provides an example of the data collection locations in the upstream bend.

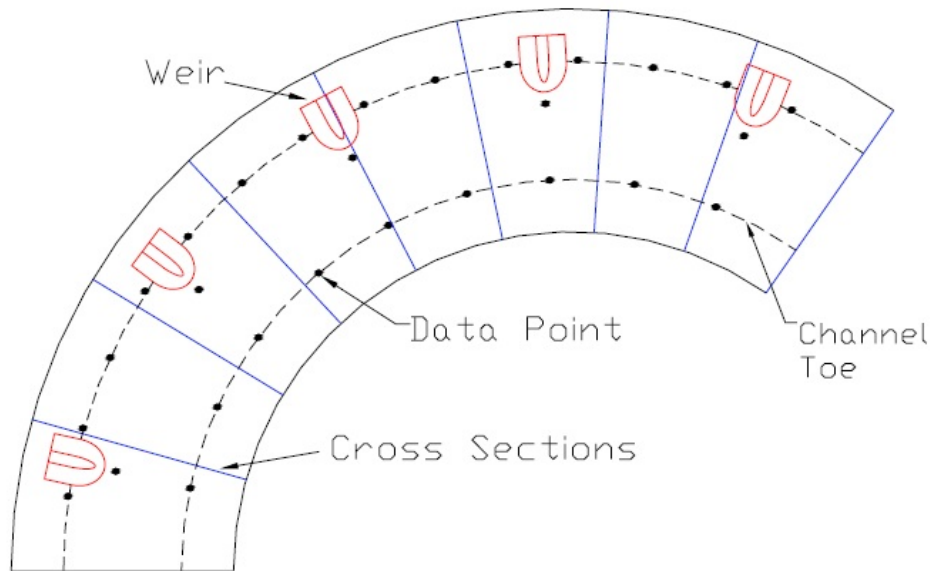


FIGURE 4.2. Data collection locations [4]

Flow velocities of particular interest were those located at the tip of the in-stream structures due to their vulnerability during high velocity flow events. The measurement one-foot from the structure tip was assumed to be an accurate and conservative representation of the velocity experienced at the structure tip in the model due to the acceleration of flows around in-stream structures. Maximum (V_{max}) and average ($V_{average}$) flow velocities at the in-stream structures' tips in both channel bends were analyzed for each configuration. Additionally, a cross-section averaged velocity in the channel bend (V_{bend}) was required for

analysis. Cross-section averaged velocities were obtained using the hydraulic principle of continuity ($Q = V \times A$). A representative cross-section averaged flow velocity is obtained by dividing the flow discharge by the representative cross-section area. Two cross-section averaged representative flow velocities were calculated for each structure configuration, one each for the upstream and downstream bends. Table 4.2 provides the velocity dataset obtained during the in-stream structure testing.

Table 4.2: Velocity Results from Data Collection

Test	Discharge (ft^3/s)	Bend	Test Number	V_{bend} (ft/s)	V_{max} (ft/s)	$V_{average}$ (ft/s)
W01	8	US	1	1.12	1.36	1.23
W01	8	DS	1	1.71	2.49	2.35
W01	12	US	2	1.25	1.54	1.38
W01	12	DS	2	1.84	2.82	2.65
W01	16	US	3	1.36	1.57	1.47
W01	16	DS	3	2.04	3.28	3.01
W02	8	US	4	1.12	1.41	1.32
W02	8	DS	4	1.71	2.36	2.28
W02	12	US	5	1.25	1.51	1.38
W02	12	DS	5	1.84	2.63	2.53
W02	16	US	6	1.36	1.75	1.63
W02	16	DS	6	2.04	3.27	3.06
W03	8	US	7	1.12	1.56	1.28

Table 4.2 – Continued

Test	Discharge (ft^3/s)	Bend	Test Number	V_{bend} (ft/s)	V_{max} (ft/s)	$V_{average}$ (ft/s)
W03	8	DS	7	1.71	2.59	2.36
W03	12	US	8	1.25	1.89	1.40
W03	12	DS	8	1.84	2.80	2.57
W03	16	US	9	1.36	1.57	1.45
W03	16	DS	9	2.04	2.97	2.84
W04	8	US	10	1.12	1.27	1.18
W04	8	DS	10	1.71	2.14	1.96
W04	12	US	11	1.25	1.49	1.35
W04	12	DS	11	1.84	2.24	2.09
W04	16	US	12	1.36	1.59	1.45
W04	16	DS	12	2.04	2.56	2.45
W05	8	US	13	1.12	1.24	1.16
W05	8	DS	13	1.71	2.13	1.97
W05	12	US	14	1.25	1.44	1.33
W05	12	DS	14	1.84	2.13	2.05
W05	16	US	15	1.36	1.64	1.50
W05	16	DS	15	2.04	2.76	2.59
W06	8	US	16	1.12	1.38	1.26
W06	8	DS	16	1.71	2.19	2.07
W06	12	US	17	1.25	1.53	1.42

Table 4.2 – Continued

Test	Discharge (ft^3/s)	Bend	Test Number	V_{bend} (ft/s)	V_{max} (ft/s)	$V_{average}$ (ft/s)
W06	12	DS	17	1.84	2.49	2.33
W06	16	US	18	1.36	1.72	1.59
W06	16	DS	18	2.04	2.73	2.63
W07	8	US	19	1.12	1.36	1.28
W07	8	DS	19	1.71	2.38	2.16
W07	12	US	20	1.25	1.43	1.35
W07	12	DS	20	1.84	2.34	2.25
W07	16	US	21	1.36	1.60	1.52
W07	16	DS	21	2.04	2.78	2.69
W08	8	US	22	1.12	1.16	1.08
W08	8	DS	22	1.71	2.02	1.84
W08	12	US	23	1.25	1.32	1.26
W08	12	DS	23	1.84	1.85	1.69
W08	16	US	24	1.36	1.40	1.29
W08	16	DS	24	2.04	2.58	2.26
W09	8	US	25	1.12	1.13	1.07
W09	8	DS	25	1.71	1.90	1.77
W09	12	US	26	1.25	1.30	1.20
W09	12	DS	26	1.84	2.15	1.94
W09	16	US	27	1.36	1.40	1.29

Table 4.2 – Continued

Test	Discharge (ft^3/s)	Bend	Test Number	V_{bend} (ft/s)	V_{max} (ft/s)	$V_{average}$ (ft/s)
W09	16	DS	27	2.04	2.31	2.23
W10	8	US	28	1.12	1.29	1.19
W10	8	DS	28	1.71	2.39	2.11
W10	12	US	29	1.25	1.31	1.24
W10	12	DS	29	1.84	2.33	2.19
W10	16	US	30	1.36	1.52	1.46
W10	16	DS	30	2.04	2.92	2.68
W11	8	US	31	1.12	1.24	1.14
W11	8	DS	31	1.71	2.26	2.11
W11	12	US	32	1.25	1.35	1.21
W11	12	DS	32	1.84	2.52	2.34
W11	16	US	33	1.36	1.43	1.34
W11	16	DS	33	2.04	2.95	2.66
W12	8	US	34	1.12	1.32	1.18
W12	8	DS	34	1.71	2.68	2.41
W12	12	US	35	1.25	1.39	1.31
W12	12	DS	35	1.84	2.74	2.49
W12	16	US	36	1.36	1.62	1.48
W12	16	DS	36	2.04	2.96	2.86
W13	8	US	37	1.12	1.29	1.18

Table 4.2 – Continued

Test	Discharge (ft^3/s)	Bend	Test Number	V_{bend} (ft/s)	V_{max} (ft/s)	$V_{average}$ (ft/s)
W13	8	DS	37	1.71	2.31	2.15
W13	12	US	38	1.25	1.39	1.25
W13	12	DS	38	1.84	2.40	2.32
W13	16	US	39	1.36	1.61	1.48
W13	16	DS	39	2.04	3.00	2.82
W14	8	US	40	1.12	1.37	1.28
W14	8	DS	40	1.71	2.61	2.41
W14	12	US	41	1.25	1.47	1.38
W14	12	DS	41	1.84	2.68	2.59
W14	16	US	42	1.36	1.62	1.49
W14	16	DS	42	2.04	3.26	2.97
W15	8	US	43	1.12	1.44	1.35
W15	8	DS	43	1.71	2.60	2.34
W15	12	US	44	1.25	1.47	1.39
W15	12	DS	44	1.84	2.53	2.50
W15	16	US	45	1.36	1.62	1.57
W15	16	DS	45	2.04	2.99	2.89
W16	8	US	46	1.12	1.47	1.33
W16	8	DS	46	1.71	2.52	2.31
W16	12	US	47	1.25	1.62	1.45

Table 4.2 – Continued

Test	Discharge (ft^3/s)	Bend	Test Number	V_{bend} (ft/s)	V_{max} (ft/s)	$V_{average}$ (ft/s)
W16	12	DS	47	1.84	2.43	2.35
W16	16	US	48	1.36	1.69	1.60
W16	16	DS	48	2.04	2.92	2.83
W17	8	US	49	1.12	1.38	1.31
W17	8	DS	49	1.71	2.38	2.05
W17	12	US	50	1.25	1.58	1.47
W17	12	DS	50	1.84	2.61	2.47
W17	16	US	51	1.36	1.78	1.64
W17	16	DS	51	2.04	3.08	2.86
W18	8	US	52	1.12	1.44	1.33
W18	8	DS	52	1.71	2.20	2.06
W18	12	US	53	1.25	1.54	1.43
W18	12	DS	53	1.84	2.53	2.42
W18	16	US	54	1.36	1.68	1.61
W18	16	DS	54	2.04	2.96	2.87
W19	8	US	55	1.12	1.37	1.29
W19	8	DS	55	1.71	2.01	1.93
W19	12	US	56	1.25	1.50	1.38
W19	12	DS	56	1.84	2.47	2.34
W19	16	US	57	1.36	1.63	1.52

Table 4.2 – Continued

Test	Discharge (ft^3/s)	Bend	Test Number	V_{bend} (ft/s)	V_{max} (ft/s)	$V_{average}$ (ft/s)
W19	16	DS	57	2.04	2.71	2.59
W20	8	US	58	1.12	1.41	1.34
W20	8	DS	58	1.71	2.54	2.26
W20	12	US	59	1.25	1.56	1.48
W20	12	DS	59	1.84	2.52	2.43
W20	16	US	60	1.36	1.78	1.68
W20	16	DS	60	2.04	2.85	2.75
W21	8	US	61	1.12	1.29	1.21
W21	12	US	62	1.25	1.33	1.26
W21	12	DS	62	1.84	2.07	2.00
W21	16	US	63	1.36	1.46	1.41
W21	16	DS	63	2.04	2.54	2.42
W22	8	US	64	1.12	1.29	1.06
W22	12	US	65	1.25	1.35	1.26
W22	12	DS	65	1.84	2.04	1.96
W22	16	US	66	1.36	1.50	1.39
W22	16	DS	66	2.04	2.42	2.32

CHAPTER 5

DATA ANALYSIS

A dimensional analysis was performed to determine an appropriate method for arranging structure variables for the development of the predictive model. Additionally, multivariable regression analysis was identified as the most efficient method for deriving the predictive model from the in-stream structure dimensionless parameters.

5.1. TERMS FOR ANALYSIS

Intricate hydraulic systems may be fully explained by fundamental equations, and systematic relationships must be developed from experimental data. Dimensional analysis is a tool that reduces physical properties of a system to a fundamental dimensional form so interrelationships within the system can be analyzed. Dimensional analysis is used to create similitude between similar physical systems. Similitude allows the development of equations that are applicable to real systems using experimental model studies.

A set of significant model variables must be selected to begin developing predictive equations based on the concept of similitude. A comprehensive understanding of hydraulics and the specified hydraulic system is essential in selecting the parameters that will be the basis of the developed relationship [7]. The compilation of variables must completely and accurately describe the entire physical system. Heintz (2002), Darrow (2004), and Schmidt (2005) identified a set of the most influential properties for bed materials, channels, water flow, and weirs. For this particular study, additional properties focusing on the tip of in-stream structures were identified. All the properties that were identified are provided in Tables 5.1, 5.2, 5.3, and 5.4.

TABLE 5.1. Material Properties

Variable	Description	Dimensions
ρ_w	Density of water	M/L^3
ν_w	Kinematic viscosity of water	L^2/T
ν_w	Dynamic viscosity of water	M/LT

TABLE 5.2. Channel Properties

Variable	Description	Dimensions
S_0	Channel bed slope	L/L
T_w	Channel top width	L
b	Base width	L
S_s	Channel bank side slope	L/L
n	Manning's roughness	$T/L^{1/3}$
y	Flow depth	L
R_c	Radius of curvature of channel bend	L
k	Conveyance	L^3/T
A_c	Area of the channel at test flow	L^2

TABLE 5.3. Flow Properties

Variable	Description	Dimensions
Q	Flow discharge	L^3/T
g	Gravitational acceleration	L/T^2
V_{bend}	Cross-section bend-averaged velocity	L/T
$V_{max,tip}$	Maximum velocity at the tip of in-stream structures	L/T
$V_{average,tip}$	Average velocity at the tip of in-stream structures	L/T

TABLE 5.4. Weir Properties

Variable	Description	Dimensions
L_{w-proj}	Projected length of weir	L
L_w	Weir length	L
$L_{cw-proj}$	Projected length of weir crest	L
L_{cw}	Weir crest length	L
$H_{w-crest}$	Height of weir crest	L
L_{arc}	Arc distance between weirs	L
θ	Angle of weir relative to tangent from shore	L/L
A_w	Projected area of weir	L^2
A^*	Percentage of flow blocked by weir	L^2/L^2
D_B	Averaged cross-sectional flow depth in bend	L
Δz	Distance from weir crest to water surface	L

5.2. MAXIMUM AND AVERAGE VELOCITY RATIOS (MVR & AVR)

Heintz (2002) developed a hydraulic variable termed the maximum velocity ratio (*MVR*) during the process of formulating a method for predicting velocities along the outer channel bank. *MVR*, defined by Heintz (2002), is "the ratio of the maximum velocity found in a weir field along a specific axis of the bend to the maximum velocity found along the centerline of the bend during baseline conditions" [6]. Scurlock *et al.* (2012) altered and defined *MVR* as the ratio of the maximum velocity found in a weir field along a specific axis of the bend to the baseline average velocity found along the thalweg of the bend.

Scurlock *et al.* (2012) additionally defined an average velocity ratio (*AVR*) term, which is the ratio of the average velocity found in a weir field along a specific axis of the bend to the baseline average velocity found along the thalweg of the bend. The *AVR* provides a consistent prediction of the flow hydraulics through the full channel bend by not focusing on maximum values. The concept of *MVR* is significant for bank protection and offers an inherent factor of safety for design, but *AVR* provides a more typical quantification of flow conditions in channel bends. Julien (2002) indicated that the "non-localized maximum velocity data can be difficult to capture spatiotemporally, and may behave erratically; therefore, the concept of *AVR* may represent a more reliable predictive method."

For this study, maximum and average velocity ratios were defined that focus on the vulnerability of the in-stream structure's tips during high velocity flow events. In-stream structures redirect and constrict flow in the channel to protect the outer channel banks. A consequence of the flow-constricting is a concentration of flow lines along the tip of each structure. The flow accelerates around the structures and results in an increase in shear stress and subsequent channelbed erosion within the vicinity of the structure tip [12]. The structural

integrity of an in-stream transverse structure is founded at the structure tip. Channelbed erosion at the structure tip could lead to significant maintenance issues or structure failure. The maximum tip velocity ratio (MVR_{tip}) and average tip velocity ratio (AVR_{tip}) were developed to describe the high velocity fields located at the tip of in-stream structures. The maximum and average velocity ratios are mathematically defined in Equations 44 and 45.

$$(44) \quad MVR_{tip} = \frac{MaxV_{tip}}{V_{AveBaseline}}$$

Where:

MVR_{tip} = maximum velocity ratio (dimensionless);

$MaxV_{tip}$ = maximum velocity at the tips of the in-stream structures (L/T); and

$V_{AveBaseline}$ = cross-section averaged velocity during baseline conditions (L/T)

and

$$(45) \quad AVR_{tip} = \frac{AveV_{tip}}{V_{AveBaseline}}$$

Where:

AVR_{tip} = average velocity ratio (dimensionless); and

$AveV_{tip}$ = average velocity at the tips of the in-stream structures (L/T)

MVR_{tip} and AVR_{tip} can be expressed as a function of flow and weir variables for a practical understanding of how weirs affect flow conditions [6]. Nine parameters were selected from Tables 5.1, 5.2, 5.3, and 5.4 for analysis with MVR_{tip} and AVR_{tip} . The variables selected for analysis are presented in Table 5.5. Figures 2.4 and 2.5 presented in Chapter 2 provide planview and cross-section schematics of the analysis parameters.

TABLE 5.5. Parameters used for analysis

Variable	Description	Dimensions
A^*	Percentage of flow blocked by weir	L^2/L^2
L_{arc}	Arc distance between weirs	L
T_w	Channel top width	L
R_c	Radius of curvature of channel bend	L
L_{w-proj}	Projected length of weir	L
D_B	Averaged cross-sectional flow depth in bend	L
$H_{w-crest}$	Height of weir crest	L
θ	Angle of weir relative to tangent from shore	L/L
Δz	Distance from weir crest to water surface	L

Scurlock *et al.* (2012) proposed a functional relationship between MVR_{tip} , AVR_{tip} , and the parameters in Table 5.5 to evaluate the effects of the parameters on the maximum and average velocities experienced at the tips of the in-stream structures. The proposed MVR_{tip} and AVR_{tip} relationships are provided in Equation 46.

$$(46) \quad MVR_{tip}, AVR_{tip} = f(L_{w-proj}, L_{arc}, R_c, T_w, D_B, \Delta z, \theta)$$

Scurlock *et al.* (2012) arranged the parameters in Equation 46 into dimensionless groups sharing similar physical properties. Equation 47 provides the relationship proposed by Scurlock *et al.* (2012) in power function format. The dimensionless terms (in parenthesis) are defined from left to right as the percentage of cross-section blocked by the weirs, structure spacing ratio, curvature ratio, lateral contraction ratio, vertical contraction ratio, and normalized structure plan form angle. Equation 48 presents Equation 47 in a logarithmic form. The logarithmic form is provided to evaluate trends in the data when plotted.

$$(47) \quad MVR_{tip}, AVR_{tip} = a_1(A^*)^{a_2} \left(\frac{L_{arc}}{T_w}\right)^{a_3} \left(\frac{R_c}{T_w}\right)^{a_4} \left(\frac{L_{w-proj}}{T_w}\right)^{a_5} \left(\frac{D_B}{D_B - \Delta z}\right)^{a_6} \left(\frac{2\theta}{\pi}\right)^{a_7}$$

and

$$(48) \quad \ln(MVR_{tip}, AVR_{tip}) = a_1 + a_2 \ln(A^*) + a_3 \ln\left(\frac{L_{arc}}{T_w}\right) + a_4 \ln\left(\frac{R_c}{T_w}\right) + a_5 \ln\left(\frac{L_{w-proj}}{T_w}\right) + a_6 \ln\left(\frac{D_B}{D_B - \Delta z}\right) + a_7 \ln\left(\frac{2\theta}{\pi}\right)$$

5.3. REGRESSION ANALYSIS

A multivariate regression analysis was performed with the in-stream structure dataset to develop Equation 48 for spur dikes, bendway weirs, and vanes. Multivariate regression analysis is a technique that allows for the statistical analysis of datasets with more than one variable; therefore, effects of multiple weir and model variables are represented. A multivariate regression considers the interrelationships between designated independent variables and the dependent variable and weights the independent variables accordingly. The prediction of the dependent variable is expressed in the general form of Equation 49.

$$(49) \quad Y = b_0 + b_1X_1 + b_2X_2 + \dots b_kX_k$$

Where:

- Y = dependent variable;
- b = regression weights; and

X = independent variables

Predictive equations were thereby created with the dimensionless groups proposed by Scurlock *et al.* (2012) in Equations 47 and 48 using a multivariate regression analysis. It is important to note that "tailoring a mathematical model to data through regression procedures is a process dependent upon how data are scattered relative to the predictive parameters" [3]. Therefore, the assumption that a dataset is linearly related must be tested and confirmed through other statistical methods before the accuracy of the predictive equations can be assured.

Microsoft Excel® and its statistical analysis toolset were used to perform a backwards linear regression on the natural logarithms of the collected dataset at a statistical significance level of $p = 0.05$. The multivariate regression analysis procedure requires sets of data for the dependent variable and its correlated independent variables. The dependent variables are defined as MVR_{tip} & AVR_{tip} , while the independent variables are defined as the in-stream structure dimensionless groups. The datasets for the MVR_{tip} & AVR_{tip} regression analyses are provided in Appendix A.1 and Appendix A.2.

The results of a regression analysis in Microsoft Excel® include a regression statistics table and a regression coefficients table. The regression statistics table provides a goodness-of-fit measure for the regression analysis. The statistics that are calculated for goodness-of-fit measure include a coefficient of determination (R^2), adjusted coefficient of determination ($Adj. R^2$), and standard error (SE). The regression coefficients table provides the estimated regression line information including: estimated coefficients (a_1 through a_7), calculated t-statistics, corresponding p-values, and bounds of the 95% and 90% confidence intervals. A more detailed description of multivariate regression analysis results is presented in Kleinbaum *et al.* (2007).

With the estimated regression line p-values and coefficients, "the full numerical model is analyzed and the parameter with the least significance or highest p-value above a specified level is removed by determination on the basis of a null F-distribution" [3]. P-values are determined by the amount of change each parameter creates in the sum of square error or the coefficient of determination when it is either added or removed. A large p-value for an independent variable implies that the parameter does not have a significant influence on the dependent variable, in that there is a minimal change in the sum of square error when the parameter is added or removed. A p-value of 0.05 corresponds to a confidence level of 95% and was used as a maximum p-value for independent variables in the regression analyses. As a result, parameters with p-values greater than 0.05 were removed from further statistical analysis, and the regression process was repeated. The regression analysis became iterative until all parameters remaining within the model had associated p-values less than the specified level of 0.05. Independent variables can partially interact with other independent variables, so backwards linear regression procedures account for the interaction within the dataset by eliminating one of the two highly correlated terms.

5.4. MVR_{tip} & AVR_{tip} RESULTS

A comprehensive multivariate regression analysis was performed yielding four sets of MVR_{tip} & AVR_{tip} predictive equations. The four analyses included complete regression procedures for spur dikes, bendway weirs, vanes, and a composite of in-stream structures tested. The composite in-stream structures' analysis utilized the complete in-stream structure dataset of sixty-six (66) individual tests, which includes twenty-two (22) structure configurations at design discharges of 8, 12, and 16 *cfs*. The spur dike analysis utilized a dataset of thirty (30) tests, which includes fifteen (15) structure configurations at discharges of 8

and 12 *cfs*. The bendway weir dataset utilized fifteen (15) tests, which included fifteen (15) structure configurations at a discharge of 16 *cfs*, and the vane dataset utilized twenty-one (21) tests, which included seven (7) structure configurations at discharges of 8, 12, and 16 *cfs*.

Tables 5.6 and 5.7 provide the MVR_{tip} and AVR_{tip} parameter coefficients (a_1 through a_7) and coefficients of determination (R^2) for the composite in-stream structure, spur dike, bendway weir, and vane regression analyses, respectively. The complete regression analyses results are provided in Appendix B.

TABLE 5.6. MVR_{tip} Regression Results

Coefficients	Dimensionless Groups	Composite	Spur Dikes	Bendway Weirs	Vanes
-	R^2	0.74	0.80	0.83	0.74
a_1	MVR_{tip}	-0.76	0.48	-0.47	-1.43
a_2	A^*	0.23	-	0.14	0.52
a_3	L_{arc}/TW	-0.11	-0.12	-	-
a_4	RC/TW	0.26	0.24	0.23	-
a_5	L_{w-proj}/TW	-	0.36	-	-0.19
a_6	D_{ratio}	0.04	-	-	-0.05
a_7	$2\theta/\pi$	0.11	0.19	0.14	-

TABLE 5.7. AVR_{tip} Regression Results

Coefficients	Dimensionless Groups	Composite	Spur Dikes	Bendway Weirs	Vanes
-	R^2	0.81	0.84	0.90	0.82
a_1	MVR_{tip}	-1.05	-0.57	-0.58	-2.26
a_2	A^*	0.25	0.17	0.16	0.69
a_3	L_{arc}/TW	-	-	-	-
a_4	RC/TW	0.19	0.17	0.24	-
a_5	L_{w-proj}/TW	-0.14	-	-	-0.40
a_6	D_{ratio}	0.08	-	-	-0.03
a_7	$2\theta/\pi$	0.11	0.18	0.17	-

The parameter coefficients in Tables 5.6 and 5.7 quantify the relative importance of each term in the predictive equation. The larger the coefficient, the more significant the parameter is for the predictive relationship. It is important to note that larger parameter coefficients represent significance with respect to the amount of influence on the shape of the multi-dimensional curve being created [3]. If a parameter coefficient is not defined, the parameter was eliminated during the regression analysis procedure. Many parameters are interrelated (i.e. projected length of weir and percentage of cross-section blocked by weir); therefore, a parameter that is eliminated can be represented through another separate parameter. For example, the percentage of flow blocked by weir (A^*) parameter is directly influenced by the distance the weir protrudes parallel to shore (L_{w-proj}) parameter. Therefore, if one of these two terms is removed during the regression, its influence on the MVR_{tip} & AVR_{tip} can be indirectly accounted for by the other parameter.

During the composite in-stream structures' regression, the (L_{w-proj}/T_w) term for MVR_{tip} and (L_{arc}/T_w) term for AVR_{tip} were removed. The R^2 values for the MVR_{tip} and AVR_{tip} were 0.74 and 0.81, respectively. During the spur dike regression, the (A^*) and (D_{ratio}) terms were eliminated from MVR_{tip} , and the (L_{arc}/T_w), (L_{w-proj}/T_w), and (D_{ratio}) terms were eliminated from AVR_{tip} . The R^2 values for the MVR_{tip} and AVR_{tip} relationships were 0.80 and 0.84, respectively. During the bendway weir regression, the (L_{arc}/T_w), (L_{w-proj}/T_w), and (D_{ratio}) terms were eliminated for both MVR_{tip} and AVR_{tip} . The R^2 values for the MVR_{tip} and AVR_{tip} relationships were 0.83 and 0.90, respectively. During the vane regression, the (L_{arc}/T_w), (R_c/T_w), and ($2\theta/\pi$) terms were removed from both MVR_{tip} and AVR_{tip} . The R^2 values for the MVR_{tip} and AVR_{tip} relationships were 0.74 and 0.82, respectively. The four AVR_{tip} regressions and two of the MVR_{tip} regressions eliminated the

weir spacing ratio (L_{arc}/T_w). The removal of the weir spacing term contributed to the irrelevance of weir spacing to the maximum and average velocity encountered at the tips of the weirs or the relative insignificance of the design spacing configurations for the model. Similar observations were noted for the (L_{w-proj}/T_w) term. Observed vs. predicted MVR_{tip} and AVR_{tip} plots are provided in Figures 5.1 through 5.4.

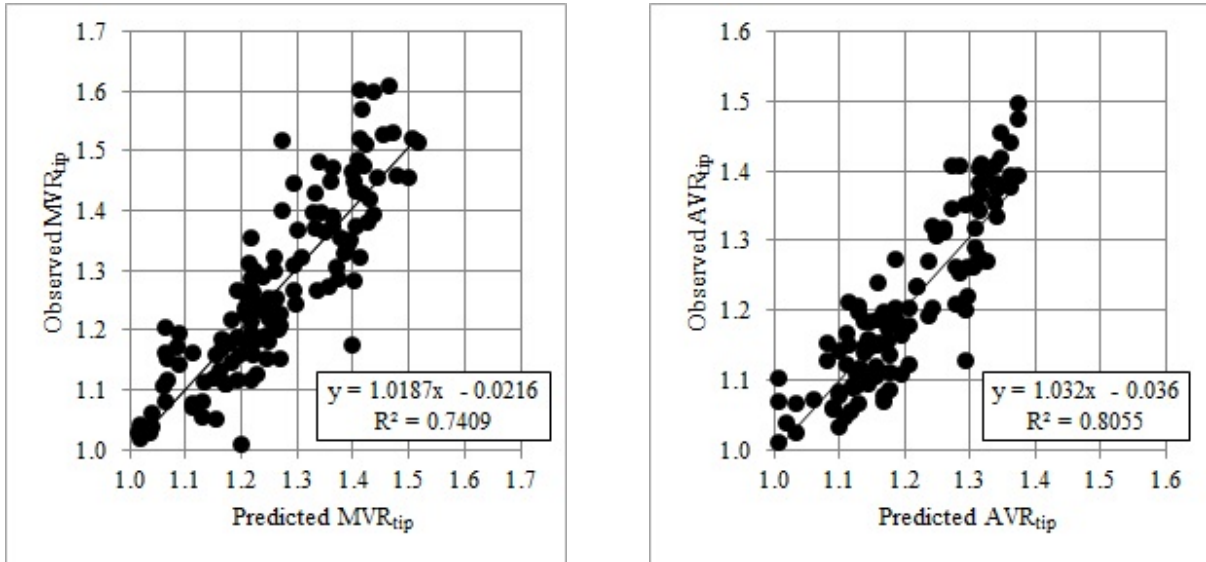


FIGURE 5.1. Observed vs. predicted MVR_{tip} and AVR_{tip} for all in-stream structure types

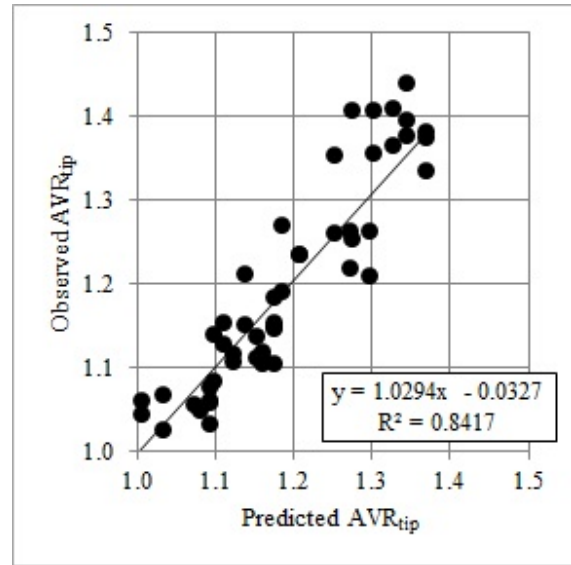
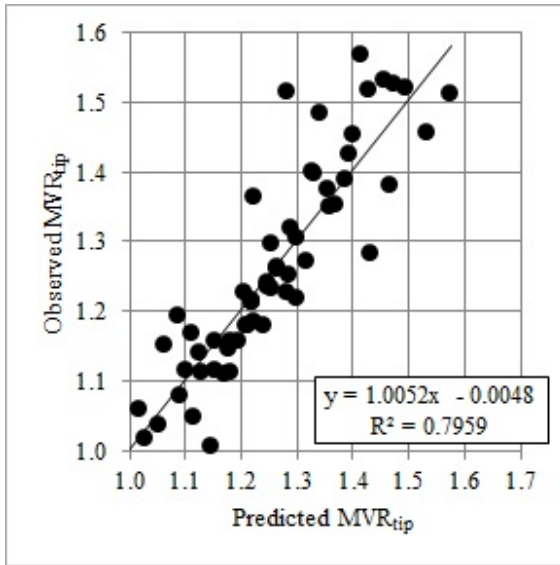


FIGURE 5.2. Observed vs. predicted MVR_{tip} and AVR_{tip} for spur dikes

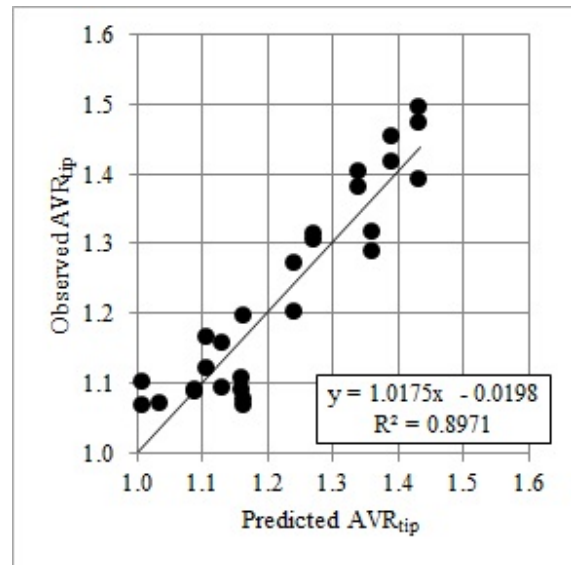
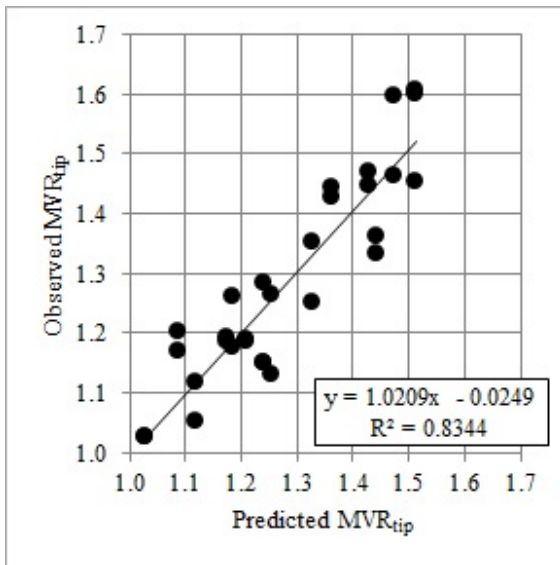


FIGURE 5.3. Observed vs. predicted MVR_{tip} and AVR_{tip} for bendway weirs

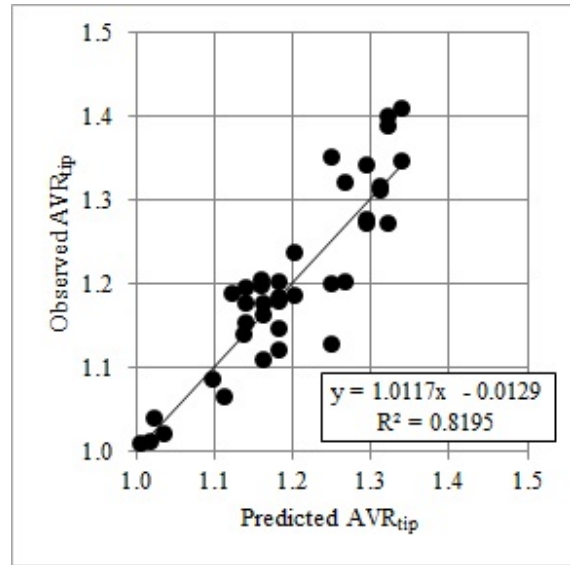
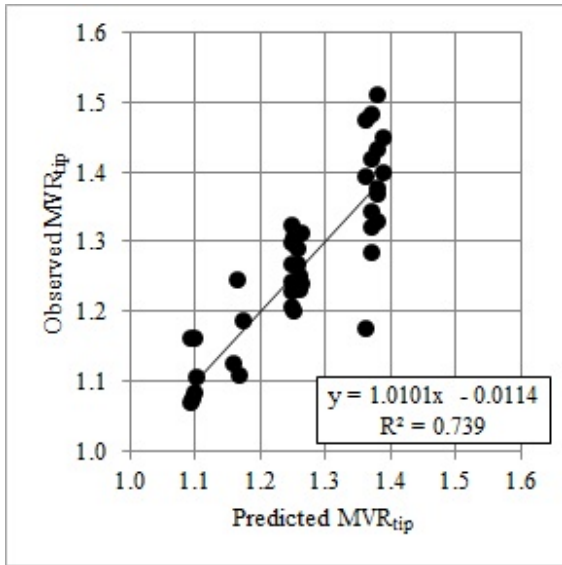


FIGURE 5.4. Observed vs. predicted MVR_{tip} and AVR_{tip} for vanes

Percent errors were calculated for each plot to quantify the accuracy of the predictive equations. It is important to note that error between predicted and observed data can be attributed to errors in the observed data (i.e. measurement accuracy). Average and maximum percent errors for the composite, spur dike, bendway weir, and vane analyses are provided in Tables 5.8 and 5.9.

TABLE 5.8. Observed vs. Predicted MVR_{tip} Percent Errors

	Average % Error	Max % Error
Composite	4.5	19.7
Spur Dikes	3.9	15.1
Bendway Weirs	4.3	11.1
Vanes	3.9	16.3

TABLE 5.9. Observed vs. Predicted AVR_{tip} Percent Errors

	Average % Error	Max % Error
Composite	4.2	22.0
Spur Dikes	3.9	17.2
Bendway Weirs	3.7	9.5
Vanes	3.3	11.3

The plots in Figures 5.1 through 5.4 present relatively accurate predictions for MVR_{tip} and AVR_{tip} in comparison to the MVR_{tip} and AVR_{tip} values measured in the model. The ideal linear trendline between observed and predicted MVR_{tip} 's and AVR_{tip} 's has a slope of 1:1. The slopes of all linear trendlines in Figures 5.1 through 5.4 were within ± 0.032 of 1. The average coefficient of determination (R^2) for the trendlines was 0.81 which relates to 81% of the total variation in predicted ratios explained by the observed ratios. The lowest and highest R^2 values were 0.74 and 0.90 as produced by observed vs. predicted MVR_{tip} 's for vanes and AVR_{tip} 's for bendway weirs, respectively. A 0.16 range and 0.81 average of R^2 values demonstrates reasonably accurate and consistent predictions for MVR_{tip} and AVR_{tip} in the model. The maximum and average percent errors recorded in Tables 5.8 and 5.9 were

22.0% and 3.96%, respectively. With an average percent error less than 5%, the predictive equations further demonstrated consistent accuracy for estimating MVR_{tip} 's and AVR_{tip} 's within the range of structure parameters tested in the physical model. Significant erroneous predictions were not estimated with a maximum percent error value less than 25% as well. The equation form of the predictive equations are presented in Equations 50 through 57.

Composite In-Stream Structures

$$\begin{aligned}
 \ln(MVR_{tip,total}) = & -0.760165041 + 0.227241121 \ln(A^*) - 0.107111017 \ln\left(\frac{L_{arc}}{T_w}\right) \\
 (50) \qquad \qquad \qquad & + 0.259392 \ln\left(\frac{R_c}{T_w}\right) + 0.039931097 \ln\left(\frac{D_B}{D_B - \Delta z}\right) \\
 & + 0.113941299 \ln\left(\frac{2\theta}{\pi}\right)
 \end{aligned}$$

$$\begin{aligned}
 \ln(AVR_{tip,total}) = & -1.045689529 + 0.253417693 \ln(A^*) + 0.193625055 \ln\left(\frac{R_c}{T_w}\right) \\
 (51) \qquad \qquad \qquad & + 0.135634965 \ln\left(\frac{L_{w-proj}}{T_w}\right) + 0.081461823 \ln\left(\frac{D_B}{D_B - \Delta z}\right) \\
 & + 0.113588457 \ln\left(\frac{2\theta}{\pi}\right)
 \end{aligned}$$

Spur Dikes

$$\begin{aligned}
 \ln(MVR_{tip,spur}) = & 0.474920663 - 0.123049032 \ln\left(\frac{L_{arc}}{T_w}\right) + 0.242738229 \ln\left(\frac{R_c}{T_w}\right) \\
 (52) \qquad \qquad \qquad & + 0.364267154 \ln\left(\frac{L_{w-proj}}{T_w}\right) + 0.193748496 \ln\left(\frac{2\theta}{\pi}\right)
 \end{aligned}$$

$$\begin{aligned}
(53) \quad \ln (AV R_{tip,spur}) &= -0.56572806 + 0.166881983 \ln(A^*) + 0.172746993 \ln \left(\frac{R_c}{T_w} \right) \\
&+ 0.176569803 \ln \left(\frac{2\theta}{\pi} \right)
\end{aligned}$$

Bendway Weirs

$$\begin{aligned}
(54) \quad \ln (MV R_{tip,BW}) &= -0.46509 + 0.142747444 \ln(A^*) + 0.233884711 \ln \left(\frac{R_c}{T_w} \right) \\
&+ 0.140842158 \ln \left(\frac{2\theta}{\pi} \right)
\end{aligned}$$

$$\begin{aligned}
(55) \quad \ln (AV R_{tip,BW}) &= -0.577237515 + 0.154603567 \ln(A^*) + 0.244272986 \ln \left(\frac{R_c}{T_w} \right) \\
&+ 0.166388438 \ln \left(\frac{2\theta}{\pi} \right)
\end{aligned}$$

Vanes

$$\begin{aligned}
(56) \quad \ln (MV R_{tip,vanes}) &= -1.42861 + 0.519502623 \ln(A^*) - 0.193256713 \ln \left(\frac{L_{w-proj}}{T_w} \right) \\
&- 0.051044608 \ln \left(\frac{D_B}{D_B - \Delta z} \right)
\end{aligned}$$

$$\begin{aligned}
(57) \quad \ln (AV R_{tip,vanes}) &= -2.261364661 + 0.69368224 \ln(A^*) - 0.391394672 \ln \left(\frac{L_{w-proj}}{T_w} \right) \\
&- 0.031455954 \ln \left(\frac{D_B}{D_B - \Delta z} \right)
\end{aligned}$$

The relative accuracy of the MVR_{tip} and AVR_{tip} predictive equations indicate that they can serve as an initial approximation in the design of in-stream transverse structures. Equations 50 through 57 represent one of the first toolsets applicable for in-stream structure design that is tip-oriented, structure-specific, and bend-averaged.

CHAPTER 6

BERNALILLO PRIORITY SITE CASE STUDY

6.1. INTRODUCTION

The installation of a series of bendway weirs at the Bernalillo Priority Site in Bernalillo, NM presented an opportunity to analyze the design, installation, and effectiveness of in-stream structures in the field. The United States Bureau of Reclamation (USBR) collected velocity measurements to evaluate the flow conditions along the Bernalillo Priority Site reach. The USBR velocity measurements were used to determine MVR_{tip} 's at the Bernalillo Priority Site. The Bernalillo Priority Site MVR_{tip} 's were compared to the MVR_{tip} 's from the CSU physical model for analysis of accuracy and applicability.

6.2. BERNALILLO PRIORITY SITE BACKGROUND

In 2007, the United States Bureau of Reclamation (USBR) constructed a series of bendway weirs at the Bernalillo Priority Site of the Middle Rio Grande to prevent lateral channel migration. The Bernalillo Priority Site is located 3,300-*ft* south of the US Highway 550 bridge in Bernalillo, NM. A set of twelve weirs were constructed with four weirs intentionally buried as part of the design [1]. A plan view of the Bernalillo Priority Site is provided in Figure 6.1. Aerial photographs of the bendway weir site pre- and post-construction from Cox *et al.* (2012) are provided in Figures 6.2 and 6.3.



FIGURE 6.1. Map of Bernalillo Site [1]



FIGURE 6.2. Pre-construction aerial photograph date March 31, 2006 (left) and post-construction aerial photograph dated February 25, 2007 (right)



FIGURE 6.3. Planview of Bernalillo Site Weir Configuration [1]

The weirs were installed to protect the levee on the east side of the Rio Grande River where lateral migration has re-located the channel to within 100-*ft* of the levee structure toe. The objective was for the bendway weirs to redirect high velocity flows to the center of the channel to prevent continued erosion of the east bank. The design parameters of the bendway weir design are provided in Table 6.1, and sketches of the bendway weir design are provided in Figures 6.4 through 6.6.

TABLE 6.1. Design parameters of bendway weir design [1]

Variable	Symbol	Value	Units
Total length of weir	L_w	25.0	<i>ft</i>
Projected length of weir into channel	L_{w-proj}	23.5	<i>ft</i>
Bendway weir crest slope	S_c	0.04	<i>ft/ft</i>
Planform bendway weir angle	θ	70.0	<i>degrees</i>
Arc length (bankline distance) between centerline of weirs	L_{arc}	75.0	<i>ft</i>
Bendway weir cross-sectional area	A_w	87.5	<i>ft</i> ²

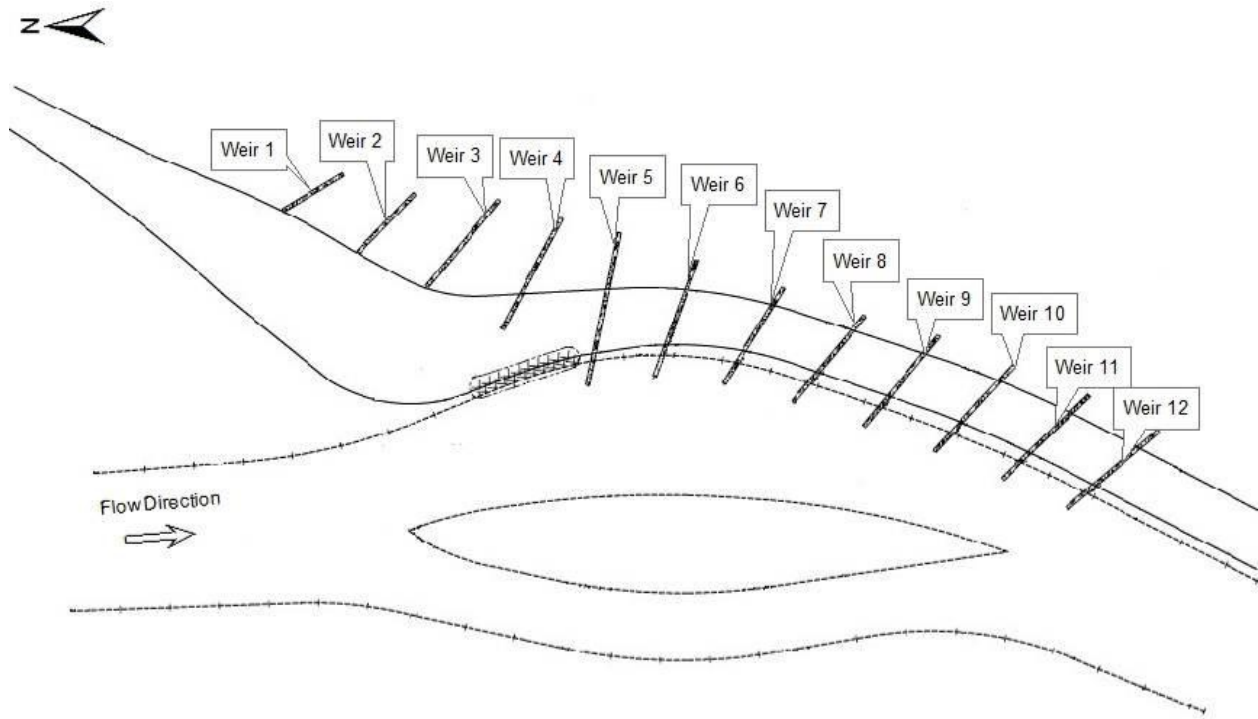


FIGURE 6.4. Planview sketch of bendway weir field design [?]

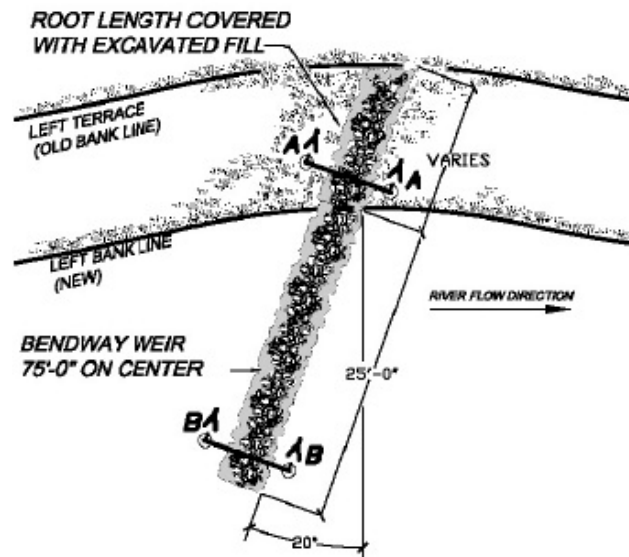


FIGURE 6.5. Bendway weir design planview [?]

6.3. HEC-RAS® MODEL

A HEC-RAS® model was developed by the USBR's Albuquerque Area Office for the simulation of flow conditions through the Middle Rio Grande River and was provided to

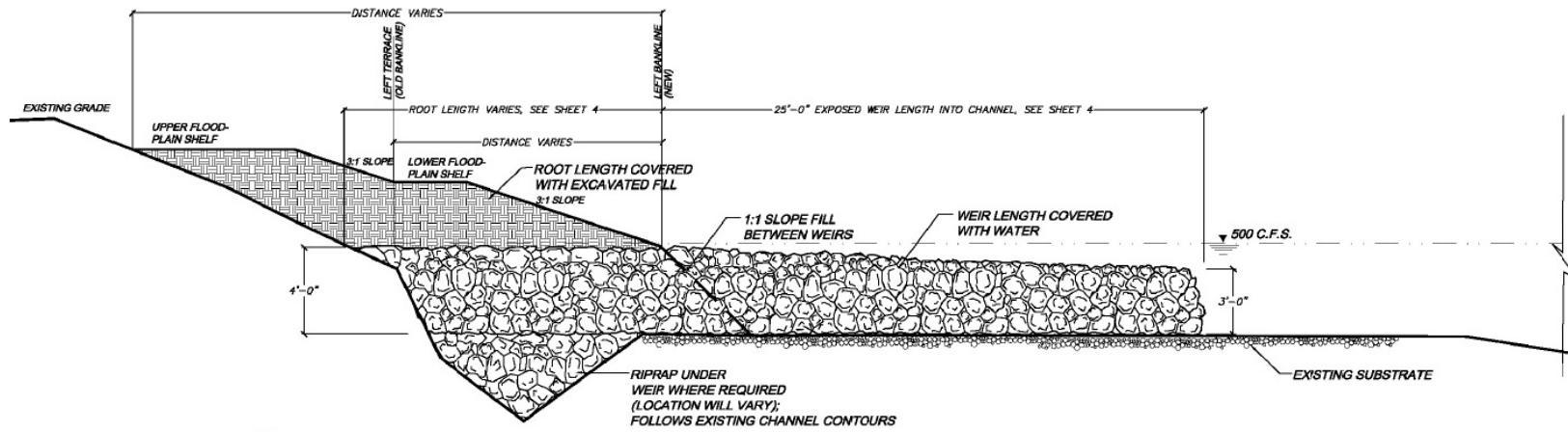


FIGURE 6.6. Bendway weir design cross-section view [?]

Colorado State University [1]. The USBR surveyed eight cross-sections of the Middle Rio Grande in May 2007 and May 2008 labeled BB 303.7 through BB 306.6. Figure 6.7 provides a planview of the surveyed cross-sections. Three of the eight cross-sections (BB 304.8, BB 305.2, and BB 305.4) were located within the bendway weir field, while the other five cross-sections were surveyed to examine the flow conditions upstream and downstream of the weir field. The cross-section survey data were imported into HEC-RAS® where additional cross-sections were interpolated. Water depths and flow discharges at the BB 303.7 and BB 304.8 cross-sections were observed on May 22nd and 23rd of 2008 and used to calibrate and validate the one-dimensional model [1].

A cross-section that was representative of baseline conditions was chosen by Cox *et al.* (2012) after the model was validated. High roughness values in the downstream section of the reach resulted in the predicted flow velocities from the model to be lower than those measured within the downstream section of the weir field. Cox *et al.* (2012) chose Cross-section BB 304.8 as the representative cross-section for baseline conditions because of its location upstream of the weir field and its accurate correlation between predicted and measured values [1].

6.4. USBR VELOCITY DATA AND OBSERVED MVR_{tip} 'S

The USBR collected flow velocity field data at the Bernalillio Priority Site on May 14, 2007 and May 19 through May 23, 2008. Velocity measurements were collected around multiple weir tips and between several weirs. Flow velocities were recorded at 0.5-*ft* depth increments starting from 0.5-*ft* above the channel bed for tip velocity measurements and 0.5-*ft* below the water surface for velocity measurements between the weirs. Flow velocities were recorded at a 60% depth of the flow, as measured from the water surface, and used as



Legend

- Cross Sections Surveyed in 2007
 - Rangelines
- 0 200 400 800 Feet
- Aerial Photograph dated 2-25-2007 ©2012 Google Earth

FIGURE 6.7. Middle Rio Grande cross-section surveyed for HEC-RAS model [1] an approximation of the average flow velocity within a water column [1]. There were eight structure tip locations where velocity data were collected. It is important to note that four of these eight locations were also considered channel centerline locations by Cox *et al.* (2012) for evaluation of the Scurlock *et al.* (2012) *MVR* and *AVR* equations.

Velocity measurements were obtained 12-*ft* from the structure tips (towards the channel centerline) at the Bernalillo Priority Site and termed "structure tip velocities" by the USBR. The design length of the weirs at the Bernalillo Priority Site was 25-*ft*; therefore, the USBR structure tip velocities represent velocity measurements approximately 48% of the weir length away from the structure tip. For analysis, a structure tip velocity will be considered any velocity measurement that is taken within a distance $\leq 50\%$ of the weir length from the upstream rounded edge of the structure to 135° around the structure tip. A schematic of this designated area is provided in Figure 6.8. The green area that is not hatched represents the area in which a velocity measurement is considered a structure tip velocity measurement and has been designated as the primary zone for tip velocities. The primary zone is the area most likely to experience the maximum flow velocities around the weir tip. The hatched section along the downstream rounded edge of the weir represents a secondary zone for tip velocities. Flow velocities in the secondary zone are affected by secondary currents behind the weirs but the velocity impacts are unknown.

Cox *et al.* (2012) defined the USBR structure tip velocities as centerline channel velocities due to the measurement's proximity with the thalweg of the channel; however, the USBR initially collected the data as weir tip velocity measurements. The velocity measurements meet the criteria established in Figure 6.8, so the field $MVR_{centerline}$'s presented by Cox *et al.* (2012) will be considered MVR_{tip} 's for analysis. Observed MVR_{tip} 's by Cox *et al.* (2012) were compared to the MVR_{tip} 's computed from CSU's physical model dataset. The observed MVR_{tip} 's for Cox *et al.* (2012) were computed from USBR field velocity measurements and HEC-RAS® baseline velocity data. The CSU physical model MVR_{tip} 's were calculated from

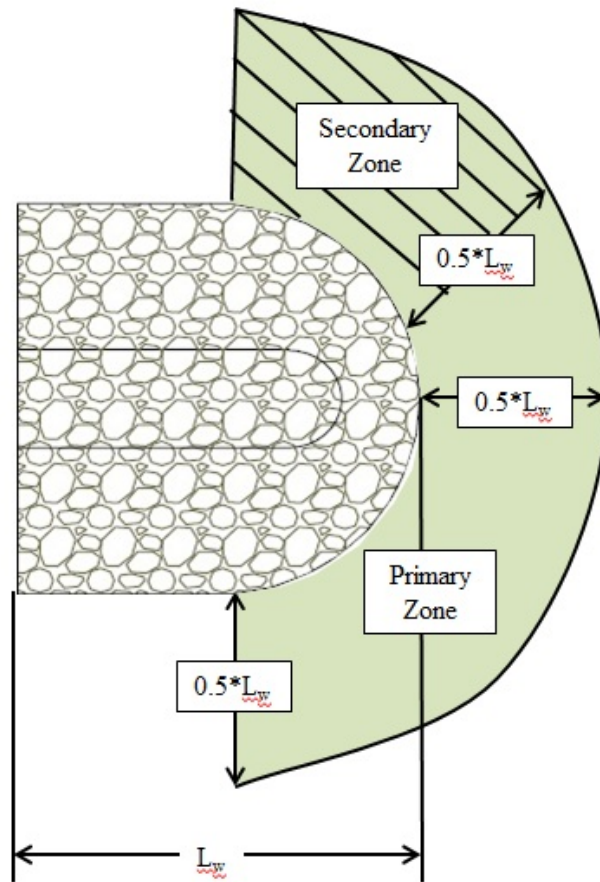


FIGURE 6.8. Structure Tip Velocity Measurement Area

the velocity data collected in the laboratory model at the locations presented in Chapter 4.

The two sets of maximum velocity ratios are presented in Tables 6.2 and 6.3.

TABLE 6.2. Cox (2012) Observed Field MVR_{tip} 's (Natural Channel)

Prototype Discharge (<i>cfs</i>)	Model Discharge (<i>cfs</i>)	Field MVR_{tip}
2,237	4.48	1.46
2,944	5.90	1.16

TABLE 6.3. CSU Physical Model Data MVR_{tip} 's (Trapezoidal Channel)

Model Discharge (<i>cfs</i>)	Prototype Discharge (<i>cfs</i>)	Average (\pm Range) Model MVR_{tip}
8	3,990.6	1.28 (\pm 0.29)
12	5,985.9	1.24 (\pm 0.28)
16	7,981.3	1.29 (\pm 0.32)

Table 6.2 presents the highest (1.46) and lowest (1.16) MVR_{tip} values for natural channels. The 0.3 difference indicates that flow conditions around weir tips in natural channels vary significantly depending on the flow discharge. The average trapezoidal channel MVR_{tip} 's in Table 6.3 were consistent for various flow discharges with a 0.05 difference between the lowest (1.24) and highest (1.29) average values. Flow conditions in trapezoidal channels are not as significantly affected by weir installation as natural channels as indicated by the 0.17 difference between the maximum natural channel MVR_{tip} of 1.46 and maximum average trapezoidal channel MVR_{tip} of 1.29. The uniformity of a trapezoidal channel and non-uniformity of a natural channel account for the large difference in maximum values. Natural channels have greater irregularity and topographic deviation that affect the acceleration and deceleration of flow around the weir tips.

6.5. DESIGN VELOCITY CALCULATION FROM MVR_{tip} 'S

MVR_{tip} , as described by Equation 44, is the ratio of a maximum velocity experienced at the tips of an in-stream structure series to a cross-section averaged velocity during baseline conditions. As a result, maximum structure tip velocities in a weir field can be estimated with a MVR_{tip} if a cross-section averaged baseline velocity can be obtained. The USBR HEC-RAS® model [1] described in Section 6.3 provides a method for obtaining cross-section averaged baseline velocities for the Bernalillo Priority Site.

Maximum structure tip velocities at the Bernalillo Priority Site will be utilized as design velocities for the evaluation of riprap sizing relationships. The observed MVR_{tip} 's presented by Cox *et al.* (2012) were used to calculate design velocities for natural channels, while the CSU physical model MVR_{tip} 's were used to estimate design velocities for trapezoidal channels. The 1.46 MVR_{tip} value in Table 6.2 was applied to natural channels, and the MVR_{tip} value of 1.29 in Table 6.3 was applied to trapezoidal-shaped channels. The 1.46 and 1.29 MVR_{tip} 's will be termed as structure tip velocity coefficients (C_{TV}) for clarity for design velocity calculations. The design velocity (V_{des}) calculation is defined with Equation 58. The premise of determining design velocities using MVR_{tip} 's is to identify and quantify an accelerated flow velocity field at the tips of in-stream structures.

$$(58) \quad V_{des} = C_{TV} * V_{avg}$$

Where:

- V_{des} = design velocity for in-stream structure riprap design (*ft/s*);
- C_{TV} = structure tip velocity coefficient;
- = 1.46 for natural channels
- = 1.29 for uniform or trapezoidal channels
- V_{avg} = cross-section averaged channel velocity (*ft/s*)

6.6. SUMMARY

A series of twelve bendway weirs were installed at the Bernalillo Priority Site in Bernalillo, NM for the protection of the levee along the east bank of the Middle Rio Grande River. Velocity measurements between weirs and around the weir tips were collected by the USBR in May of 2007 and 2008. Cox *et al.* (2012) determined a set of observed MVR_{tip} 's for

the Bernalillo Priority site from collected velocity measurements and HEC-RAS® baseline velocity data. The observed Cox *et al.* (2012) field MVR_{tip} 's were significantly larger and more variable than the MVR_{tip} 's derived from the CSU physical model velocity data.

Estimates of MVR_{tip} from the Bernalillo Priority Site and the CSU physical model are used to obtain a design velocity for the analysis of the bank revetment riprap sizing. An observed MVR_{tip} of 1.46 presented by Cox *et al.* (2012) is used to calculate design velocities for natural channels, while a CSU physical model MVR_{tip} of 1.29 is used to estimate design velocities for trapezoidal channels. The 1.46 and 1.29 MVR_{tip} 's were termed as structure tip velocity coefficients (C_{TV}) for natural and trapezoidal-shaped channels, respectively. Design velocities are calculated by multiplying C_{TV} by a bend-averaged channel velocity (Equation 58).

CHAPTER 7

ANALYSIS OF RIPRAP SIZING RELATIONSHIPS

7.1. INTRODUCTION

In-stream structures are routinely comprised of placed rock riprap. The sizing of the incremental stone within an in-stream structure is critical to assuring structural stability. The agency bank revetment design techniques presented in Chapter 2 appear to be the most applicable methods for designing in-stream structure riprap size. The principal design parameter for stone-sizing in each of the agency techniques is an average channel flow velocity. As prescribed in Chapter 5, the most critical velocity associated with in-stream structure stability is the maximum weir tip velocity. Maximum weir tip velocities may be calculated using the $MV R_{tip}$ relationship with a cross-section averaged channel velocity as presented in Chapter 6. Maximum weir tip velocities were input into the agency methodologies as design flow velocities for rock riprap design, and median riprap sizes were calculated. The median riprap sizes calculated from the agency methodologies were evaluated and compared to the riprap stone size utilized at the Bernalillo Priority Site described in Chapter 6.

7.2. MEDIAN RIPRAP SIZE RESULTS

Six agency bank revetment methodologies and one overtopping flow method presented in Chapter 2 were applied to the Bernalillo Priority Site. The resulting rock riprap sizes were compared to the USBR design stone size for the Bernalillo Priority Site. The six agency bank revetment methodologies are the USACE EM-1601 (1991) method, the FHWA HEC-11 (1989) method, the CALTRANS Cal-B&SP (2000) method, the ASCE Man-110 (2006) method, the USBR EM-25 (1984) method, and the USGS Vol. 2 (1986) method.

Design velocities for implementation into the rock riprap sizing techniques were obtained with Equation 58. Cross-section averaged baseline velocities were extracted from the USBR HEC-RAS® model [1] in 500 *cfs* increments from 200 to 60,000 *cfs*. A large range of extrapolated cross-section averaged velocities (provided in Appendix C.1) was utilized to present a detailed representation of the agency methodologies' relationship between flow velocity and rock riprap size. In addition to design velocity, other variables required for riprap sizing include the unit weight of water (γ_w) and stone (γ_s) which were assumed to be 62.4 *lb/ft³* and 165 *lb/ft³*, respectively. The acceleration of gravity (g) was assumed to be 32.2 *ft/s²*. The bank angle (θ) and angle of repose of rock riprap (ϕ) utilized were 24.75° and 32.2°, respectively, as provided in Holste (2012) for the Middle Rio Grande reach.

7.2.1. USACE EM-1601 (1991) METHOD ANALYSIS. The riprap sizing equation for the USACE EM-1601 (1991) method [10] is presented in Equation 35 in Chapter 2. The calculation of riprap size using this method requires the estimation of a safety factor (FS), stability coefficient (C_s), vertical velocity coefficient (C_v), blanket thickness coefficient (C_T), local flow depth above particle (d), and side slope correction factor (K_1). The variable values that were used for analysis based on recommendation from the USACE EM-1601 (1991) manual are:

FS = suggested as 1.2;

C_s = stability coefficient = 0.30 for angular rock;

C_v = velocity distribution coefficient = 1.25 at the end of dikes; and

C_T = blanket thickness coefficient = recommended as 1.0

The side slope correction factor (K_1) was estimated as 0.74 using Equation 39 with an angle of rock from the horizontal (θ) of 24.75° and angle of repose (ϕ) of 32.2°. Equations 37

and 38 are used to calculate an adjusted design velocity for use in the EM-1601 method. The radius of curvature (R_c) was provided in Cox *et al* (2012) as 675-*ft* for the Bernalillo Priority Site post-construction of the bendway weir series. Channel top width (TW) and local flow depth (d) values were extracted from the USBR HEC-RAS® model [1]. The explicit result for the USACE EM-1601 (1991) method is D_{30} . Equation 40 provides a means to convert D_{30} to D_{50} . The median riprap size results for incremental design maximum weir tip velocities from 5.12 *ft/s* to 12.77 *ft/s* are provided in Table 7.1. A comprehensive set of median riprap results for the USACE EM-1601 (1991) method is provided in Table D.1 of Appendix D.

TABLE 7.1. USACE EM-1601 (1991) Median Riprap Size Results

Flow Depth (d) (<i>ft</i>)	Design Velocity (V_{des}) (<i>ft/s</i>)	Adj. Design Velocity (V_{des}) (<i>ft/s</i>)	Riprap Size (D_{30}) (<i>ft</i>)	Riprap Size (D_{50}) (<i>ft</i>)	Riprap Size (D_{50}) (<i>in</i>)
1.9	4.10	5.12	0.23	0.28	3.36
5.8	3.94	6.47	0.32	0.38	4.56
6.9	4.32	7.21	0.40	0.48	5.74
8.4	5.10	8.63	0.60	0.72	8.58
9.4	5.55	9.57	0.75	0.90	10.77
10.1	6.10	10.67	0.97	1.16	13.90
10.8	6.57	11.49	1.14	1.37	16.45
11.9	7.30	12.77	1.45	1.74	20.90

7.2.2. FHWA HEC-11 (1989) METHOD ANALYSIS. The median riprap sizing equation for the FHWA HEC-11 (1989) method [15] is presented in Equation 18 in Chapter 2. The calculation of median riprap size using this method requires the estimation of a correction factor (C), an average flow depth in main flow channel (d_{avg}), and a side slope correction factor (K_1). The rock riprap specific gravity and stability factor are assumed to be 2.65 and 1.2, respectively; therefore, the correction factor was assumed to be 1. Local cross-section averaged flow depths in the channel (d) were extracted from the USBR HEC-RAS® model

[1]. The side slope correction factor (K_1) was estimated as 0.74 using Equation 19 with an bank angle with the horizontal (θ) of 24.75° and angle of repose (ϕ) of 32.2° . The median riprap size results for incremental design maximum weir tip velocities from 4.10 ft/s to 12.82 ft/s are provided in Table 7.2. A comprehensive set of median riprap results for the FHWA HEC-11 (1989) method is provided in Table D.2 of Appendix D.

TABLE 7.2. FHWA HEC-11 (1989) Median Riprap Size Results

Flow Depth (d) (ft)	Design Velocity (V_{des}) (ft/s)	Riprap Size (D_{50}) (ft)	Riprap Size (D_{50}) (in)
1.9	4.1	0.08	0.95
8.8	5.36	0.08	0.98
10.8	6.57	0.14	1.63
12.7	7.85	0.21	2.56
14.5	9.07	0.31	3.68
16.5	10.35	0.43	5.14
18.6	11.59	0.57	6.81
20.7	12.82	0.73	8.73

7.2.3. CALTRANS CAL-B&SP (2000) METHOD. The median riprap sizing equation for the CALTRANS Cal-B&SP (2000) method [16] is presented in Equation 34 in Chapter 2. The calculation of median riprap size using this method requires the estimation of a velocity coefficient (VM) and specific gravity of rock (G_s). The velocity coefficient is designated based on identification of the flow type as parallel or impinging. The nature of the flow requiring in-stream structures is impinging; therefore, a recommended VM value of 1.33 was used for analysis. The specific gravity of rock riprap was assumed to be 2.65. The explicit result from Equation 34 is a weight of rock riprap required for adequate protection of a channel bank. The rock riprap weight must be transformed into a median riprap size as prescribed with Equation 59. The median riprap size results for incremental design maximum weir tip velocities from 4.10 ft/s to 12.82 ft/s are provided in Table 7.3. A comprehensive set of

median riprap results for the CALTRANS Cal-B&SP (2000) method is provided in Table D.3 of Appendix D.

$$(59) \quad D_s = \left(\frac{6W}{\pi\gamma_s} \right)^{1/3}$$

Where:

W = minimum rock weight (lb); and
 γ_s = unit weight of rock riprap (lb/ft^3)

TABLE 7.3. CALTRANS Cal-B&SP (2000) Median Riprap Size Results

Design Velocity (V_{des}) (ft/s)	Total Rock Riprap Weight (lb)	Riprap Size (D_{50}) (ft)	Riprap Size (D_{50}) (in)
4.1	34.3	0.74	8.82
5.36	170.4	1.25	15.05
6.57	578.9	1.89	22.62
7.85	1690.7	2.69	32.34
9.07	3998.7	3.59	43.08
10.35	8856.1	4.68	56.16
11.59	17469.8	5.87	70.43
12.82	31939.8	7.18	86.13

7.2.4. ASCE MAN-110 (2006) METHOD. The median riprap sizing equation for the ASCE Man-110 (2006) method [17] is presented in Equation 41 in Chapter 2. The calculation of median riprap size using this method requires the estimation of a specific gravity of rock (G_s). The specific gravity of rock riprap was assumed to be 2.65. The explicit result from Equation 41 is a weight of rock riprap required for adequate protection of a channel bank, same as the CALTRANS Cal-B&SP (2000) method. The rock riprap weight was transformed into a median riprap size using Equation 59. The median riprap size results for incremental design maximum weir tip velocities from 4.10 ft/s to 12.82 ft/s are provided in Table 7.4. A

comprehensive set of median riprap results for the ASCE Man-110 (2006) method is provided in Table D.4 of Appendix D.

TABLE 7.4. ASCE Man-110 (2006) Median Riprap Size Results

Design Velocity (V_{des}) (<i>ft/s</i>)	Total Rock Riprap Weight (<i>lb</i>)	Riprap Size (D_{50}) (<i>ft</i>)	Riprap Size (D_{50}) (<i>in</i>)
4.1	0.17	0.12	1.50
5.36	0.83	0.21	2.55
6.57	2.83	0.32	3.84
7.85	8.28	0.46	5.49
9.07	19.57	0.61	7.32
10.35	43.35	0.79	9.54
11.59	85.51	1.00	11.96
12.82	156.34	1.22	14.62

7.2.5. USBR EM-25 (1984) METHOD. The median riprap sizing equation for the USBR EM-25 (1984) method [18] is presented in Equation 42 in Chapter 2. The calculation of median riprap size using this method requires only a design flow velocity. The median riprap size results for incremental design maximum weir tip velocities from 4.10 *ft/s* to 12.82 *ft/s* are provided in Table 7.5. A comprehensive set of median riprap results for the USBR EM-25 (1984) method is provided in Table D.5 of Appendix D.

TABLE 7.5. USBR EM-25 (1984) Median Riprap Size Results

Design Velocity (V_{des}) (<i>ft/s</i>)	Riprap Size (D_{50}) (<i>ft</i>)	Riprap Size (D_{50}) (<i>in</i>)
4.10	0.22	2.68
5.36	0.39	4.65
6.57	0.59	7.07
7.85	0.85	10.22
9.07	1.14	13.74
10.35	1.50	18.05
11.59	1.90	22.79
12.82	2.34	28.04

7.2.6. USGS VOL. 2 (1986) METHOD. The median riprap sizing equation for the USGS Vol. 2 (1986) method [11] is presented in Equation 43 in Chapter 2. The calculation of median riprap size using this method requires an average channel velocity. The median riprap size results for incremental design maximum weir tip velocities from 4.10 *ft/s* to 12.82 *ft/s* are provided in Table 7.6. A comprehensive set of median riprap results for the USGS Vol. 2 (1986) method is provided in Table D.6 of Appendix D.

TABLE 7.6. USGS Vol. 2 (1986) Median Riprap Size Results

Design Velocity (V_{des}) (<i>ft/s</i>)	Riprap Size (D_{50}) (<i>ft</i>)	Riprap Size (D_{50}) (<i>in</i>)
4.10	0.31	3.76
5.36	0.60	7.21
6.57	0.99	11.86
7.85	1.53	18.34
9.07	2.17	26.02
10.35	3.00	35.96
11.59	3.95	47.40
12.82	5.05	60.58

7.2.7. ISBASH (1936) METHOD. The median riprap sizing equation for the Isbash (1936) method is presented in Equation 1 in Chapter 2. The calculation of median riprap size using this method requires a design flow velocity, unit weight of water and unit weight of rock. The unit weight of water (γ_w) and riprap (γ_s) was assumed to be 62.4 *lb/ft³* and 165 *lb/ft³*. The median riprap size results for incremental design maximum weir tip velocities from 4.10 *ft/s* to 12.82 *ft/s* are provided in Table 7.7. A comprehensive set of median riprap results for the Isbash (1936) is provided in Table D.7 of Appendix D.

TABLE 7.7. Isbash Median Riprap Size Results

Design Velocity (V_{des}) (<i>ft/s</i>)	Riprap Size (D_{50}) (<i>ft</i>)	Riprap Size (D_{50}) (<i>in</i>)
4.10	0.11	1.32
5.36	0.19	2.26
6.57	0.28	3.40
7.85	0.40	4.86
9.07	0.54	6.47
10.35	0.70	8.43
11.59	0.88	10.58
12.82	1.08	12.93

7.3. COMPARISON OF METHODS

A graphical representation of the agency methodology results was produced in which the cross-section averaged velocity values extrapolated from the USBR HEC-RAS® model [1] were plotted against the resulting median riprap sizes. For comparison purposes, the median riprap size for each agency methodology at a design velocity of 10 *ft/s* was obtained. The graphical representation of the agency methodology results is provided in Figure 7.1, and the median riprap sizes at a design velocity of 10 *ft/s* for each method are presented in Table 7.8.

TABLE 7.8. Extrapolated Median Riprap Size Results for a Design Velocity of 10 *ft/s*

Agency Method	D_{50} (<i>in</i>)
USACE EM-1601 (1991)	12.0
FHWA HEC-11 (1989)	4.7
CALTRANS Cal-B&SP (2000)	52.4
ASCE Man-110 (2006)	8.9
USBR EM-25 (1984)	16.8
USGS Vol. 2 (1986)	33.1
Isbash (1936)	7.9

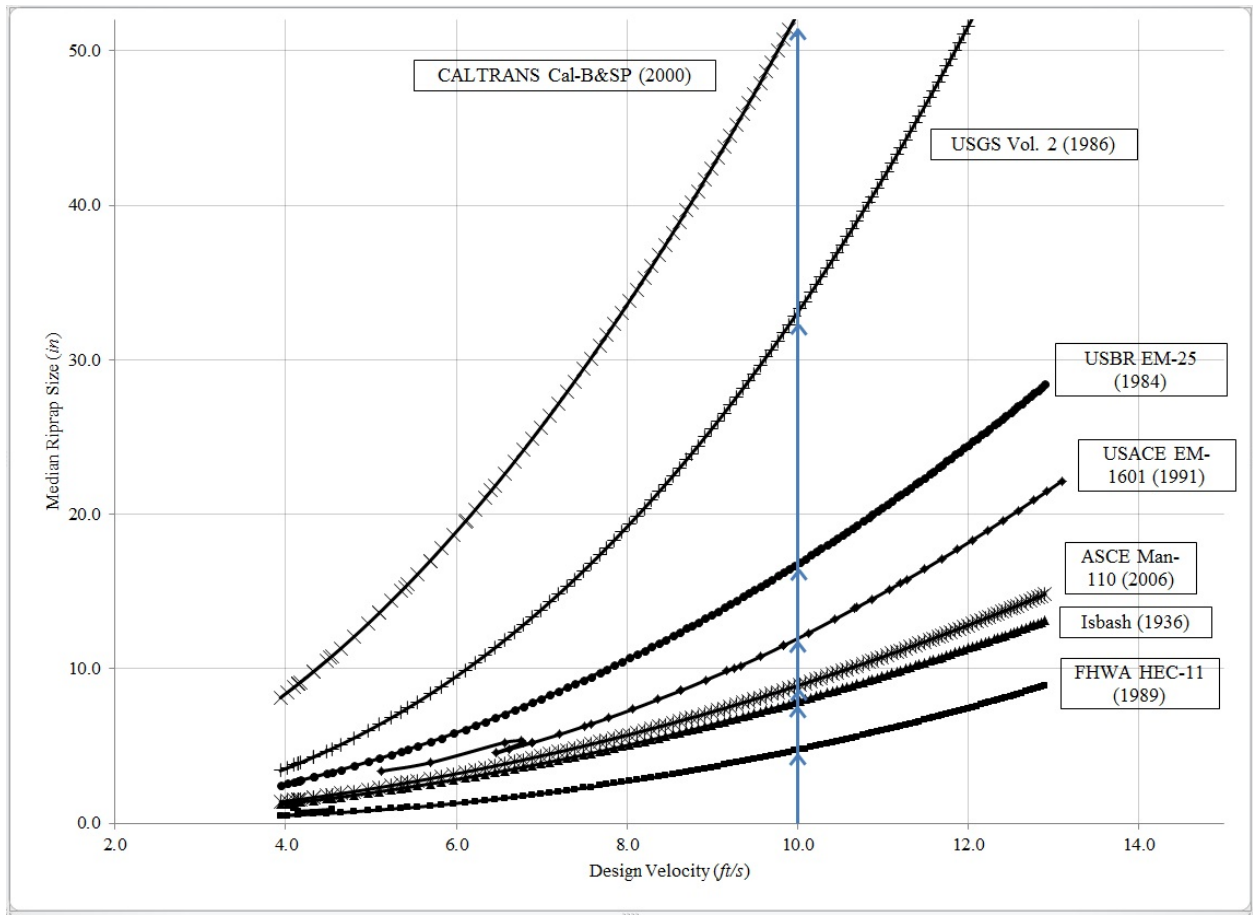


FIGURE 7.1. Extrapolated Results for Design Velocity vs. Median Riprap Size

7.4. DISCUSSION OF RESULTS

The USBR EM-25 (1984), USGS Vol. 2 (1986), and Isbash (1936) techniques exclusively use the average channel velocity to calculate riprap size, but each technique produced largely-varying riprap sizes (1.3 to 61.6-*in*). Therefore, calculation of a design riprap size exclusively with an average channel velocity is difficult, and the results vary significantly. The USACE EM-1601 (1991), FHWA HEC-11 (1989), CALTRANS Cal-B&SP (2000), and ASCE Man-110 (2006) techniques are detailed design approaches that account for significant geomorphic, hydraulic, and river characteristics such as water depth, flow top width, and radius of curvature of a channel bend. Design methods that do not incorporate significant geomorphic and hydraulic characteristics of river reaches cannot assure comprehensive applicability and accuracy.

The agency methodologies were segmented into three groups based on similarity of rock riprap size results. The first group consisted of the FHWA HEC-11 (1989), Isbash (1936), and ASCE Man-110 (2006) methods which produced the least conservative rock riprap sizes. The third group consisted of the CALTRANS Cal-B&SP (2000) and USGS Vol. 2 (1986) methods which produced the most conservative rock riprap size results. The second group consisted of the USBR EM-25 (1984) and USACE EM-1601 (1991) methods, which produced rock riprap sizes between the first and third groups. Table 7.9 presents the three groups and their respective calculated rock riprap sizes at a design velocity of 10 *ft/s*.

TABLE 7.9. Methodology Groups for Analysis

Group	Agency Method	Rock Riprap Sizes (<i>in</i>)
Group 1	FHWA HEC-11 (1989)	4.7
	Isbash (1936)	7.9
	ASCE Man-110 (2006)	8.9
Group 2	EM-1601	12.0
	USBR EM-25 (1984)	16.8
Group 3	USGS	33.1
	CALTRANS Cal-B&SP (2000)	52.4

For a design velocity of 10 *ft/s*, the calculated rock riprap sizes ranged from 4.7 to 52.4-*in*, which presents a 47.7-*in* differential. This is a large difference between the lowest and highest riprap sizes indicating substantial variation in design approaches. Group 1 produced results of 4.7-*in* (FHWA HEC-11 (1989)), 7.9-*in* (Isbash (1936)), and 8.9-*in* (ASCE Man-110 (2006)) which are generally undersized for a river as large as the Middle Rio Grande experiencing flow velocities of 10 *ft/s*. Using undersized rock riprap for the design of a set of in-stream structures could lead to significant maintenance issues or failure of the structure set. Group 3 calculated riprap sizes of 33.1-*in* (USGS Vol. 2 (1986)) and 52.4-*in* (CALTRANS Cal-B&SP (2000)), which are inefficient and costly although stable for an in-stream structure design. Group 2 calculated riprap sizes of 12.0-*in* (USACE EM-1601 (1991)) and 16.8-*in* (USBR EM-25 (1984)) which appear to be more reasonable rock riprap sizes for a flow velocity of 10 *ft/s* in the Middle Rio Grande.

There are typically four classes of machined rock riprap that are available from suppliers that include rock sizes from 2 to 36-*in* diameter [19]. The Group 2 methodologies produced riprap results within this generally available riprap size range and provide reasonable riprap sizes for stable in-stream structures. The USACE EM-1601 (1991) and USBR EM-25 (1984)

methodologies utilized with structure tip velocity coefficients (C_{TV}) will be initially recommended and further analyzed for use in the design of in-stream structures. Average velocity adjustment procedures to the current USACE EM-1601 (1991) and USBR EM-25 (1984) methodologies will be presented.

7.5. AVERAGE VELOCITY ADJUSTMENT PROCEDURES FOR THE USACE EM-1601 (1991) AND USBR EM-25 (1984) METHODS

The USACE EM-1601 (1991) technique is unique in that it is the only agency methodology that does not use an average channel velocity for computation of rock riprap size. An average flow velocity is adjusted with Equations 37 and 38. The USACE EM-1601 (1991) method has been used for previous bendway weir designs and has been recommended for the stone-sizing of in-stream structures by the National Cooperative Highway Research Program (NCHRP) (2006). NCHRP (2006) recommended the USACE EM-1601 (1991) method because it presents bank and bend correction factors, qualifications for safety/stability factors, and a detailed explanation of the difference between stable or failed riprap [20]. The USBR EM-25 (1984) method is simplistic in nature requiring a design velocity for the calculation of a median riprap size. The USBR EM-25 (1984) relationship was developed using laboratory flume tests and verified by applying it to stilling basins in the field [11].

Average velocity adjustment procedures were developed for the USACE EM-1601 (1991) and USBR EM-25 (1984) methodologies which include a conversion procedure for average channel velocities to maximum structure tip velocities. For the USACE EM-1601 (1991) methodology, Equations 37 and 38 are currently used as velocity correction equations to determine the characteristic velocity defined as the depth-averaged velocity at a point 20% upslope from the toe of the revetment for natural and trapezoidal channels, respectively

[10]. The velocity adjustment procedure is initiated by transforming the average channel velocity to a characteristic velocity with Equation 37 or 38. The characteristic velocity is adjusted by multiplying by a C_{TV} as presented in Equation 58. The resulting velocity is deemed the design velocity for in-stream structures as described in Chapter 6 and Section 7.2. The updated average channel velocity adjustment procedure for the USACE EM-1601 (1991) methodology is described mathematically as follows:

Design Velocity Calculations for USACE EM – 1601 (1991) Method

(1) Calculate a characteristic velocity (V_{char}):

For natural channels:

$$(37) \quad \begin{aligned} V_{char} &= V_{avg}(1.74 - 0.52\log(R_c/W)) \\ V_{char} &= V_{avg} \text{ for } R_c/W > 26 \end{aligned}$$

For trapezoidal channels:

$$(38) \quad \begin{aligned} V_{char} &= V_{avg}(1.71 - 0.78\log(R_c/W)) \\ V_{char} &= V_{avg} \text{ for } R_c/W > 8 \end{aligned}$$

(2) Calculate a design velocity with the structure tip velocity coefficients (C_{TV}):

$$(58) \quad V_{des} = C_{TV} * V_{char}$$

Where:

V_{des} = design velocity for in-stream structure riprap design (ft/s);
 C_{TV} = structure tip velocity coefficient;
= 1.46 for natural channels
= 1.29 for uniform or trapezoidal channels
 V_{char} = depth-averaged velocity at toe of bank revetment (ft/s)

The USACE EM-1601 (1991) manual provides a recommended factor of safety range (SF) of 1.1 to 1.5 for application in Equation 35. The general factor of safety suggested in longitudinal revetment design is 1.2. Adjustments to the USACE EM-1601 (1991) methodology include an increase in the suggested 1.2 factor of safety to safety factors on the higher end of the typical 1.1 to 1.5 range. A 1.4 to 1.5 range of safety factors is recommended to ensure adequate rock riprap sizes for transverse protection design. Safety factors from 1.4 to 1.5 remain within the typical factor of safety range provided in the USACE EM-1601 (1991) manual and produces a more conservative median rock riprap size.

The velocity adjustment procedure for the USBR EM-25 (1984) methodology is the same as the velocity adjustment procedure for the USACE EM-1601 (1991) method. Characteristic velocities are estimated from Equation 37 or 38. Maximum structure tip velocities are determined by multiplying a C_{TV} by the characteristic velocity. The average channel velocity adjustment procedure for the USBR EM-25 (1984) method is described mathematically as follows:

Design Velocity Calculations for USBR EM – 25 (1984) Method

- (1) Calculate a characteristic velocity (V_{char}):

For natural channels:

$$(37) \quad \begin{aligned} V_{char} &= V_{avg}(1.74 - 0.52\log(R_c/W)) \\ V_{char} &= V_{avg} \text{ for } R_c/W > 26 \end{aligned}$$

For trapezoidal channels:

$$(38) \quad \begin{aligned} V_{char} &= V_{avg}(1.71 - 0.78\log(R_c/W)) \\ V_{char} &= V_{avg} \text{ for } R_c/W > 8 \end{aligned}$$

(2) Calculate a design velocity with the structure tip velocity coefficients (C_{TV}):

$$(58) \quad V_{des} = C_{TV} * V_{char}$$

Where:

V_{des} = design velocity for in-stream structure riprap design (ft/s);

C_{TV} = structure tip velocity coefficient;

= 1.46 for natural channels

= 1.29 for uniform or trapezoidal channels

V_{char} = depth-averaged velocity at toe of bank revetment (ft/s)

7.6. EXAMPLE PROCEDURES FOR IN-STREAM STRUCTURE RIPRAP DESIGN

The design for the bendway series at the Bernalillo Priority Site was based upon the successful bendway weir series design at the San Ildefonso Priority Site outside of Verlarde, NM. The San Ildefonso Priority Site is located ~50 miles upstream of the Bernalillo Priority Site along the Middle Rio Grande. A river maintenance project was initiated by the USBR to provide protection of the east bankline of the Middle Rio Grande and the San Ildefonso fishing pond from progressive erosion. The project consisted of installing seven buried bendway weirs and a diagonal key at the downstream portion of the channel bend at the site. Construction of the weir field was completed during the spring of 2007. Field observations indicate that the 2007 bendway weirs remain intact, but some noticeable rock displacement has been observed [2].

A design riprap size for the bendway weirs at the San Ildefonso Priority Site was determined using the USACE EM-1601 (1991) and USACE-Maynard (1988) techniques with San Ildefonso Priority Site hydraulic parameters. A discontinuity factor proposed in de Almeida and Martin-Vide (2009) for the USACE-Maynard (1988) technique was employed to adjust

the riprap size from bank revetment design to transverse in-stream structure design. It is important to note that the singular difference between the USACE-Maynard (1988) equation and the USACE EM-1601 (1991) equation is that the USACE-Maynard (1988) equation does not include the terms FS , C_v , C_T , and K_1 . The variables C_s , d , γ_w , γ_s , V_{des} , and g remain the same for both techniques. The hydraulic parameters of the San Ildefonso Priority Site used for the design riprap size calculation are presented in Table 7.10.

TABLE 7.10. Hydraulic Parameters of San Ildefonso Priority Site [2]

Parameter	Value	Definition
Q_{des}	14,200 <i>cfs</i>	Design Flow Discharge
V_{avg}	5.81 <i>ft/s</i>	Bend-averaged Channel Flow Velocity
TW	202 <i>ft</i>	Bend-averaged Channel Top Width
W	195.6 <i>ft</i>	Width of Water Surface at Upstream End of Channel Bend
d	10.01 <i>ft</i>	Local Depth of Flow at V_{des} Location
R_c	360 <i>ft</i>	Centerline Radius of Curvature of Channel Bend

The design flowrate of 14,200 *cfs* was estimated as a flow discharge for a 10-yr regulated peak flow return period [21]. The hydraulic parameters presented in Table 7.10 were based upon the 14,200 *cfs* design flow rate. The V_{avg} and TW parameters are bend-averaged by using length-weighted averages based on the number of cross-sections that describe the channel bend. The V_{avg} and TW parameters describe only the main channel hydraulics such that the floodplain area was not included in the calculation [2]. A design velocity of 12.65 *ft/s* was derived from a maximum permissible velocity methodology presented in Holste (2013). The other parameters necessary for riprap size calculation are defined below:

$$FS = \text{suggested as } 1.2;$$

$$C_s = \text{stability coefficient} = 0.30 \text{ for angular rock};$$

$$C_v = \text{velocity distribution coefficient} = 1.23;$$

C_T = blanket thickness coefficient = 1.0;

γ_w = specific weight of water = 62.4 lb/ft³;

γ_s = specific weight of stone = 165 lb/ft³;

K_1 = side slope correction = 0.901; and

g = acceleration due to gravity (32.2 ft/s²)

Rock riprap sizes were calculated using the USACE-Maynard (1988) and USACE EM-1601 (1991) techniques, resulting in design median riprap sizes of 9.7-in and 16.3-in, respectively. De Almeida and Martin-Vide (2009) proposed a range of discontinuity factors to convert riprap sizes from the USACE-Maynard (1988) equation for bank revetement to a riprap size for transverse protection. The maximum discontinuity factor proposed by de Almeida and Martin-Vide (2009) was 2.5, which results in a design transverse D_{50} of 24.2-in for the San Ildefonso Priority Site when multiplied by the initial USACE-Maynard (1988) riprap size result of 9.7-in. The design transverse D_{50} of 24.2-in is 1.5 times larger than the bank revetment riprap size calculated from the USACE EM-1601 (1991) method. A final USBR design riprap size of 24.2-in was specified for the San Ildefonso Priority Site [2].

Riprap sizes were calculated using the USACE EM-1601 (1991) and USBR EM-25 (1984) techniques and their velocity adjustment procedures (as discussed in Section 7.5) for comparison with the USBR design at San Ildefonso Priority Site. In addition to the design velocity, the remaining parameters presented in Wright (2010) and Holste (2013) for the San Ildefonso Priority Site were used in computing the riprap sizes for transverse protection. Design velocities were calculated with a bend-averaged channel flow velocity of 5.81 ft/s as presented in Table 7.10 and a C_{TV} of 1.46 for natural channels.

The calculation of the design velocity based on the USACE EM-1601 (1991) velocity adjustment procedure is provided with utilization of Equations 37 and 58. The calculation

of transverse D_{50} for the USACE EM-1601 (1991) method is provided with utilization of Equations 35 and 40. The USACE EM-1601 (1991) methodology procedure was repeated with a safety factor of 1.5 as recommended in Section 7.5 and an additional median riprap size was determined.

Design Velocity Calculations for USACE EM – 1601 (1991) Methods

Using Equation 37:

$$(60) \quad V_{char} = (5.81 ft/s)(1.74 - 0.52 \log \left(\frac{360 ft}{195.6 ft} \right)) = 9.31 ft/s$$

and applying Equation 58:

$$(61) \quad V_{des} = 1.46 * (9.31 ft/s) = 13.6 ft/s$$

D_{50} Calculation for USACE EM – 1601 (1991) Method

Computing D_{30} with Equation 35:

$$(62) \quad D_{30} = (10.01 ft) * 1.2 * 0.3 * 1.23 * 1 * \left[\left(\frac{(62.4 lb/ft^3)}{(165 lb/ft^3) - (62.4 lb/ft^3)} \right)^{0.5} \right]^{2.5} \\ * \left[\frac{13.6 ft/s}{\sqrt{0.901 * 32.2 ft/s^2 * 10.01 ft}} \right]^{2.5} = 1.35 ft = 16.2 in$$

and converting D_{30} to D_{50} with Equation 40:

$$(63) \quad D_{50} = 1.2 * (16.2 in) = 19.5 in$$

D₅₀ Calculation for USACE EM – 1601 (1991) Method with Safety Factor Adjustment

Computing D_{30} with Equation 35:

$$(64) \quad D_{30} = (10.01 \text{ ft}) * 1.5 * 0.3 * 1.23 * 1 * \left[\left(\frac{(62.4 \text{ lb/ft}^3)}{(165 \text{ lb/ft}^3) - (62.4 \text{ lb/ft}^3)} \right)^{0.5} \right]^{2.5} \\ * \left[\frac{13.6 \text{ ft/s}}{\sqrt{0.901 * 32.2 \text{ ft/s}^2 * 10.01 \text{ ft}}} \right]^{2.5} = 1.69 \text{ ft} = 20.3 \text{ in}$$

and converting D_{30} to D_{50} with Equation 40:

$$(65) \quad D_{50} = 1.2 * (20.3 \text{ in}) = 24.3 \text{ in}$$

The USACE EM-1601 (1991) methodology produced a median riprap size of 24.3-in which is within 0.1-in of the 24.2-in riprap size that was designed by the USBR for the San Ildefonso Priority Site. The median riprap size estimated before safety factor correction was 19.5-in; therefore, a higher safety factor (1.4 - 1.5) must be considered for in-stream structure design to potentially ensure an effective and stable in-stream structure series.

The calculation of the design velocity based on the USBR EM-25 (1984) velocity adjustment procedure is provided with utilization of Equations 37 and 58. The calculation of transverse D_{50} for the USBR EM-25 (1984) method is provided with utilization of Equation 42.

Design Velocity Calculations for USBR EM – 25 (1984) Methods

Using Equation 37:

$$(66) \quad V_{char} = (5.81 ft/s)(1.74 - 0.52 \log \left(\frac{360 ft}{195.6 ft} \right)) = 9.31 ft/s$$

and applying Equation 58:

$$(67) \quad V_{des} = 1.46 * (9.31 ft/s) = 13.6 ft/s$$

D₅₀ Calculation for USBR EM – 25 (1984) Method

Computing D_{50} with Equation 42:

$$(68) \quad D_{50} = 0.0122(13.6 ft/s)^{2.06} = 2.64 ft = 31.6 in$$

With the average velocity adjustment procedure, the USBR EM-25 (1984) methodology produced a 31.6-*in* median riprap size, which is more conservative than the USBR San Ildefonso Priority Site design. The USBR EM-25 (1984) method is recommended to be used as a secondary conservative option for an in-stream structure designer when the USACE EM-1601 (1991) methodology is non-applicable or hydraulic parameters needed for calculation cannot be obtained.

CHAPTER 8

CONCLUSION AND RECOMMENDATIONS

8.1. OVERVIEW

The U.S. Bureau of Reclamation in Albuquerque, NM identified transverse in-stream structures as a possible method for protecting the outside banks of channel bends from the harmful erosive effects of high velocity flows. Transverse in-stream structures function as a channel bank protection measure by redirecting high flow velocities away from the outside bank and reducing the magnitude of secondary flows in channel bends. The redirected flow accelerates around the structures, shifting high shear stresses away from the bank towards the riverward ends of the structures. The shifting of the high shear stresses can cause channelbed erosion and instability around the tips of the in-stream structures. Channelbed erosion and structural instability at the structure tips result in significant maintenance issues or structure failure. As a result, the structure tip velocities should be considered in in-stream structure design as structure tips are the foundation of the structure stability.

MVR_{tip} and AVR_{tip} predictive equations were developed to quantify the acceleration of flows around structure tips in relation to an average channel velocity. The MVR_{tip} and AVR_{tip} predictive equations were developed with in-stream structure and flow velocity datasets collected on a physical model at the Colorado State University hydraulics laboratory. Dimensional analysis and multivariate regression analysis were utilized on the datasets to evaluate the interrelationships between hydraulic conditions and structure parameters within a channel bend. The MVR_{tip} and AVR_{tip} predictive equations are one of the first toolsets applicable for in-stream structure design that is tip-oriented, structure-specific, and bend-averaged.

MVR_{tip} 's from the field and laboratory were utilized to create structure tip coefficients (C_{TV}) that transform average channel velocities to design velocities for in-stream structure design calculations. Flow overtopping and agency bank revetment procedures were reviewed and analyzed to identify applicability to in-stream structure design. Agency bank revetment techniques were identified as the most reasonable methods for in-stream structure riprap design. Velocity adjustment procedures were created for two agency bank revetment methods (USACE EM-1601 (1991) and USBR EM-25 (1984) methods) in an attempt to make the two methods viable options for in-stream structure riprap design.

8.2. CONCLUSION

MVR_{tip} and AVR_{tip} predictive equations are design tools for analyzing the effects of in-stream structure on flow conditions. The development of predictive equations for bendway weirs, spur dikes, and vanes allows for the analysis of the unique impacts each structure has on flow conditions. Multivariate regression analysis eliminates the insignificant structure parameters and quantifies the relationship between significant structure parameters and resulting flow conditions. In this manner, the design process can be focused on the design parameters that have most influence on flow conditions. The development of predictive equations that are tip-oriented presents a design tool that takes into account the exposed sections of the structures. More stable in-stream structures are produced when the design is based on the sections of the weir that are most susceptible to failure.

The observation of MVR_{tip} 's in the field and laboratory led to the development of structure tip velocity coefficients for uniform, trapezoidal and natural channels. The use of a structure tip velocity coefficient (C_{TV}) shifts the current practice of using average flow conditions to more applicable maximum flow conditions. The C_{TV} for natural channels was

defined as 1.46, while the C_{TV} for uniform, trapezoidal channels was defined as 1.29. The 0.17 difference indicates that the irregularity of natural channels can have a considerable effect on flow conditions.

The analysis of riprap design techniques has demonstrated that enhancements are warranted for estimating median riprap sizes for in-stream structure design. Bank revetment design techniques appear to be the most applicable methods for in-stream structure design; however, these techniques tend to underestimate in-stream structure riprap sizes. The USACE EM-1601 (1991) and USBR EM-25 (1984) agency methodologies provided the most cost-effective and reasonable results for in-stream structure design. The USACE EM-1601 (1991) method combined with an average velocity adjustment procedure provides an initial design method for any proposed in-stream structure field. The USBR EM-25 (1984) methodology combined with an average velocity adjustment procedure provides a conservative option for in-stream structure design when the USACE EM-1601 (1991) methodology cannot be applied.

8.3. RECOMMENDATIONS FOR FURTHER RESEARCH

The MVR_{tip} and AVR_{tip} predictive equations and structure tip velocity coefficients (C_{TV}) are the initial steps in the development of a comprehensive design method for in-stream structures. The recommendation of the USACE EM-1601 (1991) and USBR EM-25 (1984) methods for in-stream structure design requires further verification to determine the complete range of application. Several recommendations for further research are provided. The recommendations for further research include:

- (1) The USACE EM-1601 (1991) and USBR EM-25 (1984) methods were evaluated using hydraulic parameters from two Middle Rio Grande maintenance sites. It is

recommended that the two methods be compared to other channel reaches for further evidence of the method's ability to calculate stable and cost-efficient riprap sizes. The expanded analysis should include rivers in other regions of the United States where the interrelationships between in-stream structures and flow conditions differ from the Middle Rio Grande.

- (2) Additional testing is recommended to observe in-stream structure failure. Near-prototype in-stream structures should be constructed in the laboratory, and varying stone sizes should be used to armour the structures. Flow discharges should be increased until failure is observed. Failure conditions should be recorded and documented. With the structure failure dataset, validation of the adjusted USACE EM-1601 (1991) and USBR EM-25 (1984) methodologies should be completed to ensure stable design in-stream structure riprap sizes.
- (3) In-stream structure stability and failure should be observed in the field. Verification of effective in-stream structure riprap sizes in the field is minimal, and the observation of a long-term stable in-stream structure design would significantly help the analysis and adjustment of current riprap design procedures. Observation of stable in-stream structure design at locations other than the Middle Rio Grande could also expand the range of application for the design procedures.
- (4) The suitability of the predictive equations for in-stream structure design can be broadened with the expansion of the dataset statistically analyzed. A composite dataset from various channel sites with transverse in-stream protection is recommended for the estimation and development of future MVR_{tip} and AVR_{tip} values and relationships. The expanded dataset should include rivers in other regions of

the United States where the interrelationships between in-stream structures and flow conditions may differ.

Generally, the riprap sizing methods currently in practice are site-specific and only accurate for channels for which they were developed. A broader approach to the development of an in-stream structure design method leads to a comprehensive, accurate, and efficient methodology for the sizing of rock riprap for in-stream structures.

BIBLIOGRAPHY

- [1] A. L. Cox, S. M. Scurlock, C. I. Thornton, and S. R. Abt, *Assessment of equations for predicting flow velocities associated with transverse features using field data from the Bernalillo river maintenance site on the Middle Rio Grande*. Colorado State University, Engineering Research Center, Cooperation by U.S. Bureau of Reclamation, 2012.
- [2] N. Holste, “San ildefonso priority site bendway weir design report,” tech. rep., United States Department of Interior, United States Bureau of Reclamation, 2013.
- [3] S. M. Scurlock, A. L. Cox, D. C. Baird, and C. I. Thornton, *Transverse instream structure analysis: Maximum and average velocity ratios within the prismatic channel*. Colorado State University, Cooperation from U.S. Bureau of Reclamation, 2012.
- [4] M. L. Heintz, “Investigation of bendway weir spacing,” Master’s thesis, Colorado State University, Summer 2002.
- [5] S. M. Scurlock, A. L. Cox, D. C. Baird, and C. I. Thornton, *Instream structure analysis: Maximum outer-bank velocity reduction within the prismatic channel*. Colorado State University, Cooperation from U.S. Bureau of Reclamation, 2012.
- [6] J. D. Darrow, “Effects of bendway weir characteristics on resulting flow conditions,” Master’s thesis, Colorado State University, Spring 2004.
- [7] P. G. Schmidt, “Effects of bendway weir field geometric characteristics on channel flow conditions,” Master’s thesis, Colorado State University, Fall 2005.
- [8] S. R. Abt, C. I. Thornton, B. A. Scholl, and T. R. Bender, “Evaluation of overtopping riprap design relationships,” *Journal of the American Water Resources Association*, vol. 49, pp. 923–937, 2013.

- [9] USDA, “Technical supplement 14c: Stone sizing criteria,” tech. rep., United States Department of Agriculture, 2007.
- [10] USACE, “Hydraulic design of flood control channels,” Tech. Rep. EM 1110-2-1601, United States Army Corps of Engineers, 1991.
- [11] J. C. Blodgett and C. E. McConaughy, *Rock Riprap Design for Protection of Stream Channels Near Highway Structures: Volume 2 - Evaluation of Riprap Design Procedures*. Water Resources Investigations Report 86-4128, United States Geological Survey, 1986.
- [12] S. A. Brown, *Design of Spur-Type Streambank Stabilization Structures*. Report No. FHWA/RD-84/101, United States Department of Transportation, Federal Highway Administration, 1985.
- [13] R. R. Copeland, *Bank Protection Techniques Using Spur Dikes*. Report No. Paper HL-83-1, United States Army Corps of Engineers, U.S. Army Engineer Waterways Experiment Station, Vicksburg, MS, 1983.
- [14] P. Sclafani, “Methodology for predicting maximum velocity and shear stress in a sinuous channel with bendway weirs using 1-d hec-ras modeling results,” Master’s thesis, Colorado State University, Summer 2010.
- [15] S. A. Brown and E. S. Clyde, *Design of Riprap Revetment*. Hydraulic Engineering Circular No. 11, United States Department of Transportation, Federal Highway Administration, 1989.
- [16] CALTRANS, *California Bank and Shore Rock Slope Protection Design: Practitioner’s Guide and Field Evaluations of Riprap Methods*. Final Report No. FHWA-CA-TL-95-10, California Department of Transportation, United States Department of Transportation, 2000.

- [17] V. A. Vanoni and M. H. Garcia, *Sedimentation Engineering: Processes, Measurements, Modelling, and Practice, No. 110*. American Society of Engineers, 2006.
- [18] A. J. Peterka, *Hydraulic Design of Stilling Basins and Energy Dissipators*. Engineering Monograph No. 25, United States Bureau of Interior, U.S. Bureau of Reclamation, 1984.
- [19] TDEC, *Erosion and Sediment Control Handbook: A Stormwater Planning and Design Manual for Construction Activities*. 4th Edition, Tennessee Department of Environment and Conservation, 2012.
- [20] P. F. Lagasse, P. E. Clopper, L. W. Zevenbergen, and J. F. Ruff, *Riprap Design Criteria, Recommended Specifications, and Quality Control*. Final Report No. EPA 816-R-10-022, National Cooperative Highway Research Program, 2006.
- [21] J. M. Wright, “Middle rio grande peak discharge frequency study,” tech. rep., United States Bureau of Reclamation, Upper Colorado Region, 2010.
- [22] D. G. Kleinbaum, L. L. Kupper, A. Nizam, and K. E. Muller, *Applied Regression Analysis and Other Multivariable Methods*. Fourth Edition, Thomson Learning, Inc., 928 pages, 2008.
- [23] BIO-WEST, *Bernalillo Priority Site: Final Design, Final Design Drawings*. Bureau of Reclamation, Albuquerque Area Office, Albuquerque, NM, 2006.
- [24] P. F. Lagasse, P. E. Clopper, J. E. Pagan-Ortiz, L. W. Zevenbergen, L. A. Arneson, J. D. Schall, and L. G. Girard, *Bridge Scour and Stream Instability Countermeasures Experience, Selection, and Design Guidance: Volume 1*. Hydraulic Engineering Circular No. 23: Volume 1, United States Department of Transportation, Federal Highway Administration, 2009.

- [25] P. F. Lagasse, P. E. Clopper, J. E. Pagan-Ortiz, L. W. Zevenbergen, L. A. Arneson, J. D. Schall, and L. G. Girard, *Bridge Scour and Stream Instability Countermeasures Experience, Selection, and Design Guidance: Volume 2*. Hydraulic Engineering Circular No. 23: Volume 2, United States Department of Transportation, Federal Highway Administration, 2009.
- [26] J. Knauss, “Computation of maximum discharge at overflow rockfill dams (a comparison of different model test results),” *International Congress on Large Dams*, vol. 3, pp. 143–160, 1979.
- [27] S. V. Isbash, “Construction of dams by depositing rock in running water,” *Second Congress of Large Dams*, vol. 5, pp. 123–126, 1936.
- [28] D. L. Derrick, T. J. Pokrefke, M. B. Boyd, J. P. Crutchfield, and R. R. Henderson, “Design and development of bendway weirs for the dogtooth bend reach, mississippi river,” Tech. Rep. Paper HL-94-10, United States Army Corps of Engineers, 1994.
- [29] R. T. Kilgore and G. K. Cotton, *Design of Roadside Channels with Flexible Linings*. Hydraulic Engineering Circular No. 15, United States Department of Transportation, Federal Highway Administration, 2005.
- [30] K. M. Robinson, C. E. Rice, and K. C. Kadavy, “Design of rock chutes,” *Transactions of the ASCE*, vol. 41, pp. 621–626, 1998.
- [31] C. I. Thornton, S. R. Abt, B. A. Scholl, and T. R. Bender, “Enhanced stone sizing for overtopping flow,” *Unpublished United States Bureau of Reclamation Report*, pp. 1–16, 2013.
- [32] R. Siebel, “Experimental investigations on the stability of riprap layers on overtoppable earthdams,” *Environmental Fluid Mechanics*, vol. 7, pp. 455–467, 2007.

- [33] P. Y. Julien and J. R. Duncan, “Optimal design criteria of bendway weirs from numerical simulations and physical model studies,” tech. rep., Colorado State University, 2003.
- [34] W. L. Peirson, J. Figlus, S. E. Pells, and R. J. Cox, “Placed rock as protection against erosion by flow down steep slopes,” *Journal of Hydraulic Engineering*, vol. 134, pp. 1370–1375, 2008.
- [35] R. J. Wittler and S. R. Abt, “Riprap design for full spectrum overtopping flows,” *Unpublished United States Bureau of Reclamation Report*, pp. 1–12, 1997.
- [36] S. K. Mishra, “Riprap design for overtopped embankments,” Master’s thesis, Colorado State University, Fall 1998.
- [37] H. H. Chang, “Riprap stability on steep slopes,” *International Journal of Sediment Research*, vol. 13, pp. 40–49, 1998.
- [38] G. A. de Almeida and J. P. Martin-Vide, “Riprap stability: Transverse and longitudinal versus continuous protections,” *Journal of Hydraulic Engineering*, vol. 135(6), pp. 447–456, 2009.
- [39] P. Y. Julien, *River Mechanics*. First Edition, Cambridge University Press, 2002.
- [40] K. H. Frizell, J. F. Ruff, and S. K. Mishra, “Simplified design guidelines for riprap subjected to overtopping flow,” in *Proceeding of the Annual Association of State Dam Safety Officials (ASDSO), Conference*, 1998.
- [41] D. Khan and Z. Ahmad, “Stabilization of angular-shaped riprap under overtopping flows,” *World Academy of Science, Engineering and Technology*, vol. 59, pp. 1153–1157, 2011.
- [42] E. Richardson, M. A. Stevens, and D. B. Simons, “Stabilization of angular-shaped riprap under overtopping flows,” *Proc. XVith IAHR Congress*, vol. 59, pp. 1153–1157, 2011.

- [43] S. T. Maynard, “Stable riprap size for open channel flows,” Tech. Rep. Technical Report HL-88-4, United States Army Corps of Engineers, 1998.
- [44] C. Forbes, M. Evans, N. Hastings, and B. Peacock, *Statistical Distributions*. 4th Edition, John Wiley & Sons, Inc., 230 pages, 2011.
- [45] E. Richardson, M. A. Stevens, and D. B. Simons, “The design of spurs for river training,” Tech. Rep. XVIth, Proc. XVIth IAHR Congress, 1974.

APPENDIX A

VELOCITY AND WEIR DATA FOR REGRESSION ANALYSES

Table A.1: Weir Data for Regression Analysis

Test	Q (ft^3/s)	Bend	Test Number	θ (degrees)	L_{w-proj} (ft)	L_{arc} (ft)	TW (ft)	Radius of Curvature (ft)	$H_{w-crest}$ (ft)	DB (ft)	A^* (%)
W01	8	US	1	90	4.13	16.88	13.76	38.75	0.77	0.60	27.0
W01	8	DS	2	90	3.04	20.90	9.59	65.83	0.78	0.60	27.0
W01	12	US	3	90	4.13	16.88	14.79	38.75	0.77	0.77	27.0
W01	12	DS	4	90	3.04	20.90	10.68	65.83	0.78	0.78	27.0
W01	16	US	5	90	4.13	16.88	15.63	38.75	0.77	0.91	27.0
W01	16	DS	6	90	3.04	20.90	11.40	65.83	0.78	0.90	27.0
W02	8	US	7	90	4.13	21.08	13.76	38.75	0.77	0.60	27.0
W02	8	DS	8	90	3.04	29.60	9.59	65.83	0.78	0.60	27.0
W02	12	US	9	90	4.13	21.08	14.79	38.75	0.77	0.77	27.0
W02	12	DS	10	90	3.04	29.60	10.68	65.83	0.78	0.78	27.0
W02	16	US	11	90	4.13	21.08	15.63	38.75	0.77	0.91	27.0
W02	16	DS	12	90	3.04	29.60	11.40	65.83	0.78	0.90	27.0
W03	8	US	13	90	4.13	14.03	13.76	38.75	0.77	0.60	27.0

Test	Q (ft^3/s)	Bend	Test Number	θ (degrees)	L_{w-proj} (ft)	L_{arc} (ft)	TW (ft)	Radius of Curvature (ft)	$H_{w-crest}$ (ft)	DB (ft)	A^* (%)
W03	8	DS	14	90	3.04	16.74	9.59	65.83	0.78	0.60	27.0
W03	12	US	15	90	4.13	14.03	14.79	38.75	0.77	0.77	27.0
W03	12	DS	16	90	3.04	16.74	10.68	65.83	0.78	0.78	27.0
W03	16	US	17	90	4.13	14.03	15.63	38.75	0.77	0.91	27.0
W03	16	DS	18	90	3.04	16.74	11.40	65.83	0.78	0.90	27.0
W04	8	US	19	90	2.22	8.54	13.76	38.75	0.77	0.60	10.8
W04	8	DS	20	90	1.60	12.99	9.59	65.83	0.78	0.60	10.8
W04	12	US	21	90	2.22	8.54	14.79	38.75	0.77	0.77	10.8
W04	12	DS	22	90	1.60	12.99	10.68	65.83	0.78	0.78	10.8
W04	16	US	23	90	2.22	8.54	15.63	38.75	0.77	0.91	10.8
W04	16	DS	24	90	1.60	12.99	11.40	65.83	0.78	0.90	10.8
W05	8	US	25	90	2.22	10.30	13.76	38.75	0.77	0.60	10.8
W05	8	DS	26	90	1.60	16.78	9.59	65.83	0.78	0.60	10.8
W05	12	US	27	90	2.22	10.30	14.79	38.75	0.77	0.77	10.8
W05	12	DS	28	90	1.60	16.78	10.68	65.83	0.78	0.78	10.8
W05	16	US	29	90	2.22	10.30	15.63	38.75	0.77	0.91	10.8
W05	16	DS	30	90	1.60	16.78	11.40	65.83	0.78	0.90	10.8

Test	Q (ft^3/s)	Bend	Test Number	θ (degrees)	L_{w-proj} (ft)	L_{arc} (ft)	TW (ft)	Radius of Curvature (ft)	$H_{w-crest}$ (ft)	DB (ft)	A^* (%)
W06	8	US	31	90	3.25	11.49	13.76	38.75	0.77	0.60	19.4
W06	8	DS	32	90	2.35	17.07	9.59	65.83	0.78	0.60	19.4
W06	12	US	33	90	3.25	11.49	14.79	38.75	0.77	0.77	19.4
W06	12	DS	34	90	2.35	17.07	10.68	65.83	0.78	0.78	19.4
W06	16	US	35	90	3.25	11.49	15.63	38.75	0.77	0.91	19.4
W06	16	DS	36	90	2.35	17.07	11.40	65.83	0.78	0.90	19.4
W07	8	US	37	90	3.25	13.85	13.76	38.75	0.77	0.60	19.4
W07	8	DS	38	90	2.35	22.06	9.59	65.83	0.78	0.60	19.4
W07	12	US	39	90	3.25	13.85	14.79	38.75	0.77	0.77	19.4
W07	12	DS	40	90	2.35	22.06	10.68	65.83	0.78	0.78	19.4
W07	16	US	41	90	3.25	13.85	15.63	38.75	0.77	0.91	19.4
W07	16	DS	42	90	2.35	22.06	11.40	65.83	0.78	0.90	19.4
W08	8	US	43	60	2.30	8.54	13.76	38.75	0.77	0.60	10.8
W08	8	DS	44	60	1.67	12.99	9.59	65.83	0.78	0.60	10.8
W08	12	US	45	60	2.30	8.54	14.79	38.75	0.77	0.77	10.8
W08	12	DS	46	60	1.67	12.99	10.68	65.83	0.78	0.78	10.8
W08	16	US	47	60	2.30	8.54	15.63	38.75	0.77	0.91	10.8

Test	Q (ft^3/s)	Bend	Test Number	θ (degrees)	L_{w-proj} (ft)	L_{arc} (ft)	TW (ft)	Radius of Curvature (ft)	$H_{w-crest}$ (ft)	DB (ft)	A^* (%)
W08	16	DS	48	60	1.67	12.99	11.40	65.83	0.78	0.90	10.8
W09	8	US	49	60	2.30	10.30	13.76	38.75	0.77	0.60	10.8
W09	8	DS	50	60	1.67	16.78	9.59	65.83	0.78	0.60	10.8
W09	12	US	51	60	2.30	10.30	14.79	38.75	0.77	0.77	10.8
W09	12	DS	52	60	1.67	16.78	10.68	65.83	0.78	0.78	10.8
W09	16	US	53	60	2.30	10.30	15.63	38.75	0.77	0.91	10.8
W09	16	DS	54	60	1.67	16.78	11.40	65.83	0.78	0.90	10.8
W10	8	US	55	60	3.23	11.18	13.76	38.75	0.77	0.60	19.4
W10	8	DS	56	60	2.37	16.49	9.59	65.83	0.78	0.60	19.4
W10	12	US	57	60	3.23	11.18	14.79	38.75	0.77	0.77	19.4
W10	12	DS	58	60	2.37	16.49	10.68	65.83	0.78	0.78	19.4
W10	16	US	59	60	3.23	11.18	15.63	38.75	0.77	0.91	19.4
W10	16	DS	60	60	2.37	16.49	11.40	65.83	0.78	0.90	19.4
W11	8	US	61	60	3.23	13.48	13.76	38.75	0.77	0.60	19.4
W11	8	DS	62	60	2.37	21.30	9.59	65.83	0.78	0.60	19.4
W11	12	US	63	60	3.23	13.48	14.79	38.75	0.77	0.77	19.4
W11	12	DS	64	60	2.37	21.30	10.68	65.83	0.78	0.78	19.4
W11	16	US	65	60	3.23	13.48	15.63	38.75	0.77	0.91	19.4

Test	Q (ft^3/s)	Bend	Test Number	θ (degrees)	L_{w-proj} (ft)	L_{arc} (ft)	TW (ft)	Radius of Curvature (ft)	$H_{w-crest}$ (ft)	DB (ft)	A^* (%)
W11	16	DS	66	60	2.37	21.30	11.40	65.83	0.78	0.90	19.4
W12	8	US	67	60	4.04	13.70	13.76	38.75	0.77	0.60	27.0
W12	8	DS	68	60	2.99	20.28	9.59	65.83	0.78	0.60	27.0
W12	12	US	69	60	4.04	13.70	14.79	38.75	0.77	0.77	27.0
W12	12	DS	70	60	2.99	20.28	10.68	65.83	0.78	0.78	27.0
W12	16	US	71	60	4.04	13.70	15.63	38.75	0.77	0.91	27.0
W12	16	DS	72	60	2.99	20.28	11.40	65.83	0.78	0.90	27.0
W13	8	US	73	60	4.04	16.52	13.76	38.75	0.77	0.60	27.0
W13	8	DS	74	60	2.99	26.19	9.59	65.83	0.78	0.60	27.0
W13	12	US	75	60	4.04	16.52	14.79	38.75	0.77	0.77	27.0
W13	12	DS	76	60	2.99	26.19	10.68	65.83	0.78	0.78	27.0
W13	16	US	77	60	4.04	16.52	15.63	38.75	0.77	0.91	27.0
W13	16	DS	78	60	2.99	26.19	11.40	65.83	0.78	0.90	27.0
W14	8	US	79	75	4.13	13.95	13.76	38.75	0.77	0.60	27.0
W14	8	DS	80	75	2.99	20.43	9.59	65.83	0.78	0.60	27.0
W14	12	US	81	75	4.13	13.95	14.79	38.75	0.77	0.77	27.0
W14	12	DS	82	75	2.99	20.43	10.68	65.83	0.78	0.78	27.0
W14	16	US	83	75	4.13	13.95	15.63	38.75	0.77	0.91	27.0

Test	Q (ft^3/s)	Bend	Test Number	θ (degrees)	L_{w-proj} (ft)	L_{arc} (ft)	TW (ft)	Radius of Curvature (ft)	$H_{w-crest}$ (ft)	DB (ft)	A^* (%)
W14	16	DS	84	75	2.99	20.43	11.40	65.83	0.78	0.90	27.0
W15	8	US	85	75	4.13	16.82	13.76	38.75	0.77	0.60	27.0
W15	8	DS	86	75	2.99	26.39	9.59	65.83	0.78	0.60	27.0
W15	12	US	87	75	4.13	16.82	14.79	38.75	0.77	0.77	27.0
W15	12	DS	88	75	2.99	26.39	10.68	65.83	0.78	0.78	27.0
W15	16	US	89	75	4.13	16.82	15.63	38.75	0.77	0.91	27.0
W15	16	DS	90	75	2.99	26.39	11.40	65.83	0.78	0.90	27.0
W16	8	US	91	90	5.14	15.03	13.76	38.75	0.13	0.60	19.4
W16	8	DS	92	90	3.11	19.23	9.59	65.83	0.42	0.60	19.4
W16	12	US	93	90	5.14	15.03	14.79	38.75	0.13	0.77	19.4
W16	12	DS	94	90	3.11	19.23	10.68	65.83	0.42	0.78	19.4
W16	16	US	95	90	5.14	15.03	15.63	38.75	0.13	0.91	19.4
W16	16	DS	96	90	3.11	19.23	11.40	65.83	0.42	0.90	19.4
W17	8	US	97	90	5.14	11.49	13.76	38.75	0.13	0.60	19.4
W17	8	DS	98	90	3.11	17.07	9.59	65.83	0.42	0.60	19.4
W17	12	US	99	90	5.14	11.49	14.79	38.75	0.13	0.77	19.4
W17	12	DS	100	90	3.11	17.07	10.68	65.83	0.42	0.78	19.4
W17	16	US	101	90	5.14	11.49	15.63	38.75	0.13	0.91	19.4

Test	Q (ft^3/s)	Bend	Test Number	θ (degrees)	L_{w-proj} (ft)	L_{arc} (ft)	TW (ft)	Radius of Curvature (ft)	$H_{w-crest}$ (ft)	DB (ft)	A^* (%)
W17	16	DS	102	90	3.11	17.07	11.40	65.83	0.42	0.90	19.4
W18	8	US	103	60	4.91	11.49	13.76	38.75	0.13	0.60	19.4
W18	8	DS	104	60	3.00	17.07	9.59	65.83	0.42	0.60	19.4
W18	12	US	105	60	4.91	11.49	14.79	38.75	0.13	0.77	19.4
W18	12	DS	106	60	3.00	17.07	10.68	65.83	0.42	0.78	19.4
W18	16	US	107	60	4.91	11.49	15.63	38.75	0.13	0.91	19.4
W18	16	DS	108	60	3.00	17.07	11.40	65.83	0.42	0.90	19.4
W19	8	US	109	90	5.14	13.85	13.76	38.75	0.13	0.60	19.4
W19	8	DS	110	90	3.11	22.06	9.59	65.83	0.42	0.60	19.4
W19	12	US	111	90	5.14	13.85	14.79	38.75	0.13	0.77	19.4
W19	12	DS	112	90	3.11	22.06	10.68	65.83	0.42	0.78	19.4
W19	16	US	113	90	5.14	13.85	15.63	38.75	0.13	0.91	19.4
W19	16	DS	114	90	3.11	22.06	11.40	65.83	0.42	0.90	19.4
W20	8	US	115	60	4.91	13.48	13.76	38.75	0.13	0.60	19.4
W20	8	DS	116	60	3.00	21.30	9.59	65.83	0.42	0.60	19.4
W20	12	US	117	60	4.91	13.48	14.79	38.75	0.13	0.77	19.4
W20	12	DS	118	60	3.00	21.30	10.68	65.83	0.42	0.78	19.4
W20	16	US	119	60	4.91	13.48	15.63	38.75	0.13	0.91	19.4

Test	Q (ft^3/s)	Bend	Test Number	θ (degrees)	L_{w-proj} (ft)	L_{arc} (ft)	TW (ft)	Radius of Curvature (ft)	$H_{w-crest}$ (ft)	DB (ft)	A^* (%)
W20	16	DS	120	60	3.00	21.30	11.40	65.83	0.42	0.90	19.4
W21	8	US	121	90	2.88	8.54	13.76	38.75	0.44	0.60	10.8
W21	12	US	123	90	2.88	8.54	14.79	38.75	0.44	0.77	10.8
W21	12	DS	124	90	1.72	16.78	10.68	65.83	0.69	0.78	10.8
W21	16	US	125	90	2.88	8.54	15.63	38.75	0.44	0.91	10.8
W21	16	DS	126	90	1.72	16.78	11.40	65.83	0.69	0.90	10.8
W22	8	US	127	60	2.79	8.54	13.76	38.75	0.44	0.60	10.8
W22	12	US	129	60	2.79	8.54	14.79	38.75	0.44	0.77	10.8
W22	12	DS	130	60	1.66	16.78	10.68	65.83	0.69	0.78	10.8
W22	16	US	131	60	2.79	8.54	15.63	38.75	0.44	0.91	10.8
W22	16	DS	132	60	1.66	16.78	11.40	65.83	0.69	0.90	10.8

Table A.2: Velocity Data for Regression Analysis

Test	Q (ft^3/s)	Bend	Test No.	$V_{approach}$ (ft/s)	V_{max} (ft/s)	V_{avg} (ft/s)	MVR_{tip}	AVR_{tip}
W01	8	US	1	1.12	1.36	1.23	1.22	1.10
W01	8	DS	2	1.71	2.49	2.35	1.45	1.37
W01	12	US	3	1.25	1.54	1.38	1.23	1.10
W01	12	DS	4	1.84	2.82	2.65	1.53	1.44
W01	16	US	5	1.36	1.57	1.47	1.15	1.08
W01	16	DS	6	2.04	3.28	3.01	1.61	1.47
W02	8	US	7	1.12	1.41	1.32	1.26	1.18
W02	8	DS	8	1.71	2.36	2.28	1.38	1.33
W02	12	US	9	1.25	1.51	1.38	1.21	1.11
W02	12	DS	10	1.84	2.63	2.53	1.43	1.37
W02	16	US	11	1.36	1.75	1.63	1.28	1.20
W02	16	DS	12	2.04	3.27	3.06	1.60	1.50

Test	Q (ft^3/s)	Bend	Test No.	$V_{approach}$ (ft/s)	V_{max} (ft/s)	V_{avg} (ft/s)	MVR_{tip}	AVR_{tip}
W03	8	US	13	1.12	1.56	1.28	1.40	1.14
W03	8	DS	14	1.71	2.59	2.36	1.51	1.38
W03	12	US	15	1.25	1.89	1.40	1.51	1.12
W03	12	DS	16	1.84	2.80	2.57	1.52	1.39
W03	16	US	17	1.36	1.57	1.45	1.15	1.07
W03	16	DS	18	2.04	2.97	2.84	1.45	1.39
W04	8	US	19	1.12	1.27	1.18	1.14	1.06
W04	8	DS	20	1.71	2.14	1.96	1.25	1.15
W04	12	US	21	1.25	1.49	1.35	1.19	1.08
W04	12	DS	22	1.84	2.24	2.09	1.21	1.13
W04	16	US	23	1.36	1.59	1.45	1.17	1.07
W04	16	DS	24	2.04	2.56	2.45	1.25	1.20
W05	8	US	25	1.12	1.24	1.16	1.11	1.04
W05	8	DS	26	1.71	2.13	1.97	1.24	1.15

Test	Q (ft^3/s)	Bend	Test No.	$V_{approach}$ (ft/s)	V_{max} (ft/s)	V_{avg} (ft/s)	MVR_{tip}	AVR_{tip}
W05	12	US	27	1.25	1.44	1.33	1.15	1.07
W05	12	DS	28	1.84	2.13	2.05	1.16	1.11
W05	16	US	29	1.36	1.64	1.50	1.20	1.10
W05	16	DS	30	2.04	2.76	2.59	1.35	1.27
W06	8	US	31	1.12	1.38	1.26	1.23	1.13
W06	8	DS	32	1.71	2.19	2.07	1.28	1.21
W06	12	US	33	1.25	1.53	1.42	1.23	1.14
W06	12	DS	34	1.84	2.49	2.33	1.35	1.26
W06	16	US	35	1.36	1.72	1.59	1.26	1.16
W06	16	DS	36	2.04	2.73	2.63	1.33	1.29
W07	8	US	37	1.12	1.36	1.28	1.21	1.15
W07	8	DS	38	1.71	2.38	2.16	1.39	1.26
W07	12	US	39	1.25	1.43	1.35	1.14	1.08
W07	12	DS	40	1.84	2.34	2.25	1.27	1.22

Test	Q (ft^3/s)	Bend	Test No.	$V_{approach}$ (ft/s)	V_{max} (ft/s)	V_{avg} (ft/s)	MVR_{tip}	AVR_{tip}
W07	16	US	41	1.36	1.60	1.52	1.17	1.12
W07	16	DS	42	2.04	2.78	2.69	1.36	1.32
W08	8	US	43	1.12	1.16	1.08	1.04	0.97
W08	8	DS	44	1.71	2.02	1.84	1.18	1.07
W08	12	US	45	1.25	1.32	1.26	1.06	1.01
W08	12	DS	46	1.84	1.85	1.69	1.00	0.92
W08	16	US	47	1.36	1.40	1.29	1.02	0.95
W08	16	DS	48	2.04	2.58	2.26	1.26	1.10
W09	8	US	49	1.12	1.13	1.07	1.02	0.96
W09	8	DS	50	1.71	1.90	1.77	1.11	1.03
W09	12	US	51	1.25	1.30	1.20	1.04	0.96
W09	12	DS	52	1.84	2.15	1.94	1.17	1.05
W09	16	US	53	1.36	1.40	1.29	1.02	0.94
W09	16	DS	54	2.04	2.31	2.23	1.13	1.09

Test	Q (ft^3/s)	Bend	Test No.	$V_{approach}$ (ft/s)	V_{max} (ft/s)	V_{avg} (ft/s)	MVR_{tip}	AVR_{tip}
W10	8	US	55	1.12	1.29	1.19	1.16	1.06
W10	8	DS	56	1.71	2.39	2.11	1.40	1.23
W10	12	US	57	1.25	1.31	1.24	1.05	0.99
W10	12	DS	58	1.84	2.33	2.19	1.26	1.19
W10	16	US	59	1.36	1.52	1.46	1.12	1.07
W10	16	DS	60	2.04	2.92	2.68	1.43	1.31
W11	8	US	61	1.12	1.24	1.14	1.11	1.02
W11	8	DS	62	1.71	2.26	2.11	1.32	1.23
W11	12	US	63	1.25	1.35	1.21	1.08	0.97
W11	12	DS	64	1.84	2.52	2.34	1.36	1.27
W11	16	US	65	1.36	1.43	1.34	1.05	0.98
W11	16	DS	66	2.04	2.95	2.66	1.44	1.30
W12	8	US	67	1.12	1.32	1.18	1.18	1.06
W12	8	DS	68	1.71	2.68	2.41	1.57	1.40

Test	Q (ft^3/s)	Bend	Test No.	$V_{approach}$ (ft/s)	V_{max} (ft/s)	V_{avg} (ft/s)	MVR_{tip}	AVR_{tip}
W12	12	US	69	1.25	1.39	1.31	1.11	1.05
W12	12	DS	70	1.84	2.74	2.49	1.48	1.35
W12	16	US	71	1.36	1.62	1.48	1.19	1.09
W12	16	DS	72	2.04	2.96	2.86	1.45	1.40
W13	8	US	73	1.12	1.29	1.18	1.16	1.06
W13	8	DS	74	1.71	2.31	2.15	1.35	1.25
W13	12	US	75	1.25	1.39	1.25	1.11	1.00
W13	12	DS	76	1.84	2.40	2.32	1.30	1.26
W13	16	US	77	1.36	1.61	1.48	1.18	1.09
W13	16	DS	78	2.04	3.00	2.82	1.47	1.38
W14	8	US	79	1.12	1.37	1.28	1.23	1.15
W14	8	DS	80	1.71	2.61	2.41	1.52	1.41
W14	12	US	81	1.25	1.47	1.38	1.18	1.11
W14	12	DS	82	1.84	2.68	2.59	1.45	1.40

Test	Q (ft^3/s)	Bend	Test No.	$V_{approach}$ (ft/s)	V_{max} (ft/s)	V_{avg} (ft/s)	MVR_{tip}	AVR_{tip}
W14	16	US	83	1.36	1.62	1.49	1.19	1.09
W14	16	DS	84	2.04	3.26	2.97	1.60	1.45
W15	8	US	85	1.12	1.44	1.35	1.29	1.21
W15	8	DS	86	1.71	2.60	2.34	1.52	1.36
W15	12	US	87	1.25	1.47	1.39	1.18	1.11
W15	12	DS	88	1.84	2.53	2.50	1.37	1.35
W15	16	US	89	1.36	1.62	1.57	1.19	1.15
W15	16	DS	90	2.04	2.99	2.89	1.46	1.42
W16	8	US	91	1.12	1.47	1.33	1.32	1.19
W16	8	DS	92	1.71	2.52	2.31	1.47	1.35
W16	12	US	93	1.25	1.62	1.45	1.30	1.16
W16	12	DS	94	1.84	2.43	2.35	1.32	1.27
W16	16	US	95	1.36	1.69	1.60	1.24	1.18
W16	16	DS	96	2.04	2.92	2.83	1.43	1.39

Test	Q (ft^3/s)	Bend	Test No.	$V_{approach}$ (ft/s)	V_{max} (ft/s)	V_{avg} (ft/s)	MVR_{tip}	AVR_{tip}
W17	8	US	97	1.12	1.38	1.31	1.24	1.17
W17	8	DS	98	1.71	2.38	2.05	1.39	1.20
W17	12	US	99	1.25	1.58	1.47	1.27	1.17
W17	12	DS	100	1.84	2.61	2.47	1.42	1.34
W17	16	US	101	1.36	1.78	1.64	1.30	1.20
W17	16	DS	102	2.04	3.08	2.86	1.51	1.40
W18	8	US	103	1.12	1.44	1.33	1.29	1.19
W18	8	DS	104	1.71	2.20	2.06	1.28	1.20
W18	12	US	105	1.25	1.54	1.43	1.23	1.14
W18	12	DS	106	1.84	2.53	2.42	1.37	1.31
W18	16	US	107	1.36	1.68	1.61	1.24	1.18
W18	16	DS	108	2.04	2.96	2.87	1.45	1.41
W19	8	US	109	1.12	1.37	1.29	1.23	1.15
W19	8	DS	110	1.71	2.01	1.93	1.17	1.13

Test	Q (ft^3/s)	Bend	Test No.	$V_{approach}$ (ft/s)	V_{max} (ft/s)	V_{avg} (ft/s)	MVR_{tip}	AVR_{tip}
W19	12	US	111	1.25	1.50	1.38	1.20	1.11
W19	12	DS	112	1.84	2.47	2.34	1.34	1.27
W19	16	US	113	1.36	1.63	1.52	1.20	1.12
W19	16	DS	114	2.04	2.71	2.59	1.33	1.27
W20	8	US	115	1.12	1.41	1.34	1.26	1.20
W20	8	DS	116	1.71	2.54	2.26	1.48	1.32
W20	12	US	117	1.25	1.56	1.48	1.25	1.18
W20	12	DS	118	1.84	2.52	2.43	1.37	1.31
W20	16	US	119	1.36	1.78	1.68	1.31	1.24
W20	16	DS	120	2.04	2.85	2.75	1.40	1.34
W21	8	US	121	1.12	1.29	1.21	1.16	1.08
W21	12	US	123	1.25	1.33	1.26	1.07	1.01
W21	12	DS	124	1.84	2.07	2.00	1.12	1.08
W21	16	US	125	1.36	1.46	1.41	1.07	1.04

Test	Q (ft^3/s)	Bend	Test No.	$V_{approach}$ (ft/s)	V_{max} (ft/s)	V_{avg} (ft/s)	MVR_{tip}	AVR_{tip}
W21	16	DS	126	2.04	2.54	2.42	1.24	1.19
W22	8	US	127	1.12	1.29	1.06	1.16	0.95
W22	12	US	129	1.25	1.35	1.26	1.08	1.01
W22	12	DS	130	1.84	2.04	1.96	1.11	1.06
W22	16	US	131	1.36	1.50	1.39	1.10	1.02
W22	16	DS	132	2.04	2.42	2.32	1.18	1.14

APPENDIX B

REGRESSION ANALYSES RESULTS

$$MVR_{tip,total}$$

TABLE B.1. Regression Statistics Results for $MVR_{tip,total}$

Multiple R	0.86
R Square	0.74
Adjusted R Square	0.73
Standard Error	0.06
Observations	130

TABLE B.2. Regression Line Results for $MVR_{tip,total}$

	Coefficients	Standard Error	t-Stat	P-value	Lower 95%	Upper 95%
MVR_{tip}	-0.760	0.107	-7.107	8.23E-11	-0.972	-0.548
A^*	0.227	0.025	9.189	1.15E-15	0.178	0.276
L_{arc}/TW	-0.107	0.039	-2.778	6.32E-03	-0.183	-0.031
RC/TW	0.259	0.036	7.279	3.37E-11	0.189	0.330
D_{ratio}	0.040	0.009	4.438	1.98E-05	0.022	0.058
$2\theta/\pi$	0.114	0.027	4.215	4.76E-05	0.060	0.167

$AVR_{tip,total}$ TABLE B.3. Regression Statistics Results for $AVR_{tip,total}$

Multiple R	0.89
R Square	0.80
Adjusted R Square	0.79
Standard Error	0.05
Observations	130

TABLE B.4. Regression Line Results for $AVR_{tip,total}$

	Coefficients	Standard Error	t-Stat	P-value	Lower 95%	Upper 95%
MVR_{tip}	-1.046	0.158	-6.608	1.03E-09	-1.359	-0.732
A^*	0.253	0.031	8.053	5.65E-13	0.191	0.316
RC/TW	0.194	0.011	16.899	5.73E-34	0.171	0.216
L_{w-proj}/TW	-0.136	0.044	-3.066	2.67E-03	-0.223	-0.048
D_{ratio}	0.081	0.012	6.550	1.38E-09	0.057	0.106
$2\theta/\pi$	0.114	0.024	4.671	7.66E-06	0.065	0.162

$MVR_{tip,spur}$

 TABLE B.5. Regression Statistics Results for $MVR_{tip,spur}$

Multiple R	0.90
R Square	0.80
Adjusted R Square	0.79
Standard Error	0.05
Observations	60

 TABLE B.6. Regression Line Results for $MVR_{tip,spur}$

	Coefficients	Standard Error	t-Stat	P-value	Lower 95%	Upper 95%
MVR_{tip}	0.475	0.050	9.518	3.18E-13	0.375	0.575
L_{arc}/TW	-0.123	0.049	-2.524	1.45E-02	-0.221	-0.025
RC/TW	0.243	0.043	5.665	5.57E-07	0.157	0.329
L_{w-proj}/TW	0.364	0.047	7.820	1.72E-10	0.271	0.458
$2\theta/\pi$	0.194	0.038	5.155	3.56E-06	0.118	0.269

$$AVR_{tip,spur}$$

TABLE B.7. Regression Statistics Results for $AVR_{tip,spur}$

Multiple R	0.91
R Square	0.83
Adjusted R Square	0.82
Standard Error	0.05
Observations	60

TABLE B.8. Regression Line Results for $AVR_{tip,spur}$

	Coefficients	Standard Error	t-Stat	P-value	Lower 95%	Upper 95%
MVR_{tip}	-0.566	0.055	-10.248	1.87E-14	-0.676	-0.455
A^*	0.167	0.017	9.916	6.21E-14	0.133	0.201
RC/TW	0.173	0.015	11.911	5.57E-17	0.144	0.202
$2\theta/\pi$	0.177	0.034	5.204	2.87E-06	0.109	0.245

$$MVR_{tip,BW}$$

TABLE B.9. Regression Statistics Results for $MVR_{tip,BW}$

Multiple R	0.91
R Square	0.83
Adjusted R Square	0.81
Standard Error	0.06
Observations	30

TABLE B.10. Regression Line Results for $MVR_{tip,BW}$

	Coefficients	Standard Error	t-Stat	P-value	Lower 95%	Upper 95%
MVR_{tip}	-0.465	0.089	-5.248	1.75E-05	-0.647	-0.283
A^*	0.143	0.027	5.256	1.71E-05	0.087	0.199
RC/TW	0.234	0.024	9.624	4.68E-10	0.184	0.284
$2\theta/\pi$	0.141	0.055	2.572	1.62E-02	0.028	0.253

$AVR_{tip,BW}$ TABLE B.11. Regression Statistics Results for $AVR_{tip,BW}$

Multiple R	0.94
R Square	0.89
Adjusted R Square	0.88
Standard Error	0.05
Observations	30

TABLE B.12. Regression Line Results for $AVR_{tip,BW}$

	Coefficients	Standard Error	t-Stat	P-value	Lower 95%	Upper 95%
MVR_{tip}	-0.577	0.073	-7.878	2.36E-08	-0.728	-0.427
A^*	0.155	0.022	6.884	2.62E-07	0.108	0.201
RC/TW	0.244	0.020	12.157	3.14E-12	0.203	0.286
$2\theta/\pi$	0.166	0.045	3.675	1.08E-03	0.073	0.259

$MVR_{tip,vanes}$

TABLE B.13. Regression Statistics Results for $MVR_{tip,vanes}$

Multiple R	0.87
R Square	0.75
Adjusted R Square	0.73
Standard Error	0.05
Observations	40

TABLE B.14. Regression Line Results for $MVR_{tip,vanes}$

	Coefficients	Standard Error	t-Stat	P-value	Lower 95%	Upper 95%
MVR_{tip}	-1.429	0.325	-4.391	9.49E-05	-2.088	-0.769
A^*	0.520	0.078	6.650	9.49E-08	0.361	0.678
L_{w-proj}/TW	-0.193	0.082	-2.358	2.39E-02	-0.360	-0.027
D_{ratio}	-0.051	0.017	-3.047	4.31E-03	-0.085	-0.017

$AVR_{tip,vanes}$

 TABLE B.15. Regression Statistics Results for $AVR_{tip,vanes}$

Multiple R	0.91
R Square	0.82
Adjusted R Square	0.81
Standard Error	0.04
Observations	40

 TABLE B.16. Regression Line Results for $AVR_{tip,vanes}$

	Coefficients	Standard Error	t-Stat	P-value	Lower 95%	Upper 95%
MVR_{tip}	-2.261	0.286	-7.910	2.18E-09	-2.841	-1.682
A^*	0.694	0.069	10.106	4.69E-12	0.554	0.833
L_{w-proj}/TW	-0.391	0.072	-5.434	3.97E-06	-0.537	-0.245
D_{ratio}	-0.031	0.015	-2.137	3.95E-02	-0.061	-0.002

APPENDIX C

VELOCITIES FOR RIPRAP DESIGN ANALYSIS

Table C.1: Weir Data for Regression Analysis

		Natural	Trapezoidal
Flow Rate (ft^3/s)	Average Channel Velocity (BB 304.8) (ft/s)	Max Velocity At Weir Tip (ft/s)	Max Velocity At Weir Tip (ft/s)
200	2.81	4.10	3.62
500	2.84	4.15	3.66
1,000	3.11	4.54	4.01
1,500	2.96	4.32	3.82
2,000	2.86	4.18	3.69
2,500	2.75	4.02	3.55
3,000	2.84	4.15	3.66
3,500	2.96	4.32	3.82
4,000	3.07	4.48	3.96
4,500	3.18	4.64	4.10
5,000	3.29	4.80	4.24
5,500	3.40	4.96	4.39
6,000	3.49	5.10	4.50
6,500	3.59	5.24	4.63

		Natural	Trapezoidal
Flow Rate (<i>ft</i> ³ / <i>s</i>)	Average Channel Velocity (BB 304.8) (<i>ft</i> / <i>s</i>)	Max Velocity At Weir Tip (<i>ft</i> / <i>s</i>)	Max Velocity At Weir Tip (<i>ft</i> / <i>s</i>)
7,000	3.67	5.36	4.73
7,500	3.72	5.43	4.80
8,000	3.80	5.55	4.90
8,500	3.90	5.69	5.03
9,000	3.99	5.83	5.15
9,500	4.09	5.97	5.28
10,000	4.18	6.10	5.39
10,500	4.26	6.22	5.50
11,000	4.34	6.34	5.60
11,500	4.42	6.45	5.70
12,000	4.50	6.57	5.81
12,500	4.58	6.69	5.91
13,000	4.65	6.79	6.00
13,500	4.72	6.89	6.09
14,000	4.79	6.99	6.18
14,500	4.86	7.10	6.27
15,000	4.93	7.20	6.36
15,500	5.00	7.30	6.45
16,000	5.06	7.39	6.53

		Natural	Trapezoidal
Flow	Average Channel	Max Velocity	Max Velocity
Rate	Velocity (BB 304.8)	At Weir Tip	At Weir Tip
(<i>ft</i> ³ / <i>s</i>)	(<i>ft/s</i>)	(<i>ft/s</i>)	(<i>ft/s</i>)
16,500	5.13	7.49	6.62
17,000	5.19	7.58	6.70
17,500	5.26	7.68	6.79
18,000	5.32	7.77	6.86
18,500	5.38	7.85	6.94
19,000	5.44	7.94	7.02
19,500	5.50	8.03	7.10
20,000	5.56	8.12	7.17
20,500	5.62	8.21	7.25
21,000	5.68	8.29	7.33
21,500	5.74	8.38	7.40
22,000	5.79	8.45	7.47
22,500	5.85	8.54	7.55
23,000	5.90	8.61	7.61
23,500	5.96	8.70	7.69
24,000	6.00	8.76	7.74
24,500	6.05	8.83	7.80
25,000	6.11	8.92	7.88
25,500	6.16	8.99	7.95

		Natural	Trapezoidal
Flow Rate (<i>ft</i> ³ / <i>s</i>)	Average Channel Velocity (BB 304.8) (<i>ft</i> / <i>s</i>)	Max Velocity At Weir Tip (<i>ft</i> / <i>s</i>)	Max Velocity At Weir Tip (<i>ft</i> / <i>s</i>)
26,000	6.21	9.07	8.01
26,500	6.26	9.14	8.08
27,000	6.31	9.21	8.14
27,500	6.36	9.29	8.20
28,000	6.41	9.36	8.27
28,500	6.46	9.43	8.33
29,000	6.50	9.49	8.39
29,500	6.55	9.56	8.45
30,000	6.60	9.64	8.51
30,500	6.64	9.69	8.57
31,000	6.69	9.77	8.63
31,500	6.74	9.84	8.69
32,000	6.78	9.90	8.75
32,500	6.83	9.97	8.81
33,000	6.87	10.03	8.86
33,500	6.91	10.09	8.91
34,000	6.96	10.16	8.98
34,500	7.00	10.22	9.03
35,000	7.04	10.28	9.08

		Natural	Trapezoidal
Flow Rate (<i>ft</i> ³ / <i>s</i>)	Average Channel Velocity (BB 304.8) (<i>ft</i> / <i>s</i>)	Max Velocity At Weir Tip (<i>ft</i> / <i>s</i>)	Max Velocity At Weir Tip (<i>ft</i> / <i>s</i>)
35,500	7.09	10.35	9.15
36,000	7.13	10.41	9.20
36,500	7.17	10.47	9.25
37,000	7.21	10.53	9.30
37,500	7.25	10.59	9.35
38,000	7.29	10.64	9.40
38,500	7.33	10.70	9.46
39,000	7.38	10.77	9.52
39,500	7.42	10.83	9.57
40,000	7.45	10.88	9.61
40,500	7.49	10.94	9.66
41,000	7.53	10.99	9.71
41,500	7.57	11.05	9.77
42,000	7.61	11.11	9.82
42,500	7.65	11.17	9.87
43,000	7.68	11.21	9.91
43,500	7.72	11.27	9.96
44,000	7.76	11.33	10.01
44,500	7.80	11.39	10.06

		Natural	Trapezoidal
Flow Rate (ft^3/s)	Average Channel Velocity (BB 304.8) (ft/s)	Max Velocity At Weir Tip (ft/s)	Max Velocity At Weir Tip (ft/s)
45,000	7.83	11.43	10.10
45,500	7.87	11.49	10.15
46,000	7.91	11.55	10.20
46,500	7.94	11.59	10.24
47,000	7.98	11.65	10.29
47,500	8.01	11.69	10.33
48,000	8.05	11.75	10.38
48,500	8.08	11.80	10.42
49,000	8.12	11.86	10.47
49,500	8.15	11.90	10.51
50,000	8.19	11.96	10.57
50,500	8.22	12.00	10.60
51,000	8.26	12.06	10.66
51,500	8.29	12.10	10.69
52,000	8.33	12.16	10.75
52,500	8.36	12.21	10.78
53,000	8.39	12.25	10.82
53,500	8.43	12.31	10.87
54,000	8.46	12.35	10.91

		Natural	Trapezoidal
Flow	Average Channel	Max Velocity	Max Velocity
Rate	Velocity (BB 304.8)	At Weir Tip	At Weir Tip
<i>(ft³/s)</i>	<i>(ft/s)</i>	<i>(ft/s)</i>	<i>(ft/s)</i>
54,500	8.49	12.40	10.95
55,000	8.52	12.44	10.99
55,500	8.56	12.50	11.04
56,000	8.59	12.54	11.08
56,500	8.62	12.59	11.12
57,000	8.65	12.63	11.16
57,500	8.69	12.69	11.21
58,000	8.72	12.73	11.25
58,500	8.75	12.78	11.29
59,000	8.78	12.82	11.33
59,500	8.81	12.86	11.36
60,000	8.84	12.91	11.40

APPENDIX D

MEDIAN RIPRAP RESULTS FOR AGENCY METHODOLOGIES

Table D.1: USACE EM-1601 (1991) Median Riprap Size
Results

Flow Depth (<i>ft</i>)	V_{avg} (<i>ft/s</i>)	R_c/W (<i>ft/ft</i>)	V_{des} (<i>ft/s</i>)	D_{30} (<i>ft</i>)	D_{30} (<i>in</i>)	D_{50} (<i>ft</i>)	D_{50} (<i>in</i>)
1.89	4.10	8.86	5.12	0.23	2.80	0.28	3.36
2.99	4.15	5.05	5.70	0.27	3.27	0.33	3.92
3.93	4.54	3.65	6.57	0.36	4.36	0.44	5.24
4.78	4.32	2.19	6.76	0.37	4.45	0.45	5.34
5.44	4.18	1.66	6.79	0.36	4.36	0.44	5.24
5.84	3.94	1.55	6.47	0.32	3.80	0.38	4.56
6.08	4.02	1.49	6.62	0.33	3.99	0.40	4.79
6.44	4.15	1.41	6.89	0.36	4.34	0.43	5.21
6.47	4.15	1.41	6.90	0.36	4.34	0.43	5.21
6.50	4.15	1.40	6.90	0.36	4.34	0.43	5.21
6.85	4.32	1.38	7.21	0.40	4.78	0.48	5.74
7.19	4.48	1.33	7.51	0.44	5.23	0.52	6.28
7.26	4.53	1.33	7.58	0.45	5.36	0.54	6.43
7.49	4.64	1.31	7.79	0.47	5.68	0.57	6.82
7.77	4.80	1.30	8.07	0.51	6.15	0.62	7.38
8.04	4.96	1.27	8.37	0.56	6.68	0.67	8.01

Table D.1 – Continued

Flow Depth	V_{avg}	R_c/W	V_{des}	D_{30}	D_{30}	D_{50}	D_{50}
(<i>ft</i>)	(<i>ft/s</i>)	(<i>ft/ft</i>)	(<i>ft/s</i>)	(<i>ft</i>)	(<i>in</i>)	(<i>ft</i>)	(<i>in</i>)
8.34	5.10	1.23	8.63	0.60	7.15	0.71	8.58
8.35	5.10	1.22	8.63	0.60	7.15	0.72	8.58
8.58	5.24	1.18	8.93	0.64	7.72	0.77	9.26
8.84	5.36	1.13	9.18	0.68	8.21	0.82	9.85
9.00	5.40	1.12	9.26	0.70	8.37	0.84	10.04
9.12	5.43	1.10	9.33	0.71	8.49	0.85	10.19
9.36	5.55	1.07	9.57	0.75	8.98	0.90	10.77
9.55	5.69	1.06	9.84	0.80	9.58	0.96	11.49
9.56	5.69	1.06	9.84	0.80	9.58	0.96	11.50
9.74	5.83	1.01	10.13	0.85	10.25	1.03	12.31
9.93	5.97	0.96	10.44	0.92	11.02	1.10	13.22
10.11	6.10	0.96	10.67	0.97	11.59	1.16	13.90
10.14	6.12	0.96	10.70	0.97	11.65	1.16	13.98
10.29	6.22	0.96	10.88	1.01	12.10	1.21	14.51
10.46	6.34	0.96	11.08	1.05	12.62	1.26	15.14
10.55	6.41	0.96	11.21	1.08	12.96	1.30	15.55
10.63	6.45	0.96	11.29	1.10	13.16	1.32	15.79
10.79	6.57	0.96	11.49	1.14	13.71	1.37	16.45
10.96	6.69	0.96	11.70	1.19	14.27	1.43	17.12
11.12	6.79	0.96	11.88	1.23	14.77	1.48	17.72

Table D.1 – Continued

Flow Depth (<i>ft</i>)	V_{avg} (<i>ft/s</i>)	R_c/W (<i>ft/ft</i>)	V_{des} (<i>ft/s</i>)	D_{30} (<i>ft</i>)	D_{30} (<i>in</i>)	D_{50} (<i>ft</i>)	D_{50} (<i>in</i>)
11.27	6.89	0.96	12.05	1.27	15.28	1.53	18.33
11.43	6.99	0.96	12.23	1.32	15.79	1.58	18.95
11.58	7.10	0.96	12.41	1.36	16.32	1.63	19.59
11.73	7.20	0.96	12.59	1.41	16.86	1.69	20.24
11.87	7.30	0.96	12.77	1.45	17.42	1.74	20.90
12.02	7.39	0.96	12.92	1.49	17.89	1.79	21.47
12.16	7.49	0.96	13.10	1.54	18.46	1.85	22.15
12.30	7.58	0.96	13.25	1.58	18.95	1.90	22.74
12.43	7.68	0.96	13.43	1.63	19.54	1.95	23.45
12.57	7.77	0.96	13.59	1.67	20.05	2.01	24.06
12.70	7.85	0.96	13.74	1.71	20.57	2.06	24.68
12.83	7.94	0.96	13.89	1.76	21.09	2.11	25.31
12.96	8.03	0.96	14.05	1.80	21.62	2.16	25.95
13.09	8.12	0.96	14.20	1.85	22.16	2.22	26.60
13.21	8.21	0.96	14.35	1.89	22.71	2.27	27.26
13.34	8.29	0.96	14.51	1.94	23.27	2.33	27.92
13.46	8.38	0.96	14.66	1.99	23.83	2.38	28.60
13.58	8.45	0.96	14.79	2.03	24.30	2.43	29.16
13.71	8.54	0.96	14.94	2.07	24.88	2.49	29.85
13.83	8.61	0.96	15.07	2.11	25.36	2.54	30.43

Table D.1 – Continued

Flow Depth (<i>ft</i>)	V_{avg} (<i>ft/s</i>)	R_c/W (<i>ft/ft</i>)	V_{des} (<i>ft/s</i>)	D_{30} (<i>ft</i>)	D_{30} (<i>in</i>)	D_{50} (<i>ft</i>)	D_{50} (<i>in</i>)
13.95	8.70	0.96	15.22	2.16	25.95	2.60	31.14
14.08	8.76	0.96	15.32	2.19	26.33	2.63	31.59
14.19	8.83	0.96	15.45	2.24	26.83	2.68	32.19
14.31	8.92	0.96	15.60	2.29	27.44	2.74	32.93
14.42	8.99	0.96	15.73	2.33	27.95	2.80	33.54
14.54	9.07	0.96	15.86	2.37	28.46	2.85	34.16
14.65	9.14	0.96	15.99	2.42	28.98	2.90	34.78
14.76	9.21	0.96	16.11	2.46	29.51	2.95	35.41
14.87	9.29	0.96	16.24	2.50	30.04	3.00	36.05
14.98	9.36	0.96	16.37	2.55	30.58	3.06	36.70
15.09	9.43	0.96	16.50	2.59	31.12	3.11	37.35
15.20	9.49	0.96	16.60	2.63	31.55	3.16	37.86
15.30	9.56	0.96	16.73	2.68	32.11	3.21	38.53
15.41	9.64	0.96	16.86	2.72	32.67	3.27	39.20
15.52	9.69	0.96	16.96	2.76	33.10	3.31	39.73
15.62	9.77	0.96	17.08	2.81	33.68	3.37	40.41
15.73	9.84	0.96	17.21	2.85	34.25	3.42	41.10
15.83	9.90	0.96	17.31	2.89	34.70	3.47	41.65
15.93	9.97	0.96	17.44	2.94	35.29	3.53	42.35
16.04	10.03	0.96	17.54	2.98	35.75	3.58	42.90

Table D.1 – Continued

Flow Depth (<i>ft</i>)	V_{avg} (<i>ft/s</i>)	R_c/W (<i>ft/ft</i>)	V_{des} (<i>ft/s</i>)	D_{30} (<i>ft</i>)	D_{30} (<i>in</i>)	D_{50} (<i>ft</i>)	D_{50} (<i>in</i>)
16.14	10.09	0.96	17.65	3.02	36.22	3.62	43.46
16.24	10.16	0.96	17.77	3.07	36.82	3.68	44.18
16.34	10.22	0.96	17.88	3.11	37.29	3.73	44.75
16.44	10.28	0.96	17.98	3.15	37.77	3.78	45.32
16.54	10.35	0.96	18.11	3.20	38.39	3.84	46.06
16.64	10.41	0.96	18.21	3.24	38.87	3.89	46.64
16.73	10.47	0.96	18.31	3.28	39.37	3.94	47.24
16.83	10.53	0.96	18.41	3.32	39.86	3.99	47.83
16.93	10.59	0.96	18.52	3.36	40.35	4.04	48.42
17.03	10.64	0.96	18.62	3.40	40.85	4.09	49.02
17.12	10.70	0.96	18.72	3.45	41.36	4.14	49.63
17.21	10.77	0.96	18.85	3.50	42.01	4.20	50.42
17.31	10.83	0.96	18.95	3.54	42.52	4.25	51.03
17.40	10.88	0.96	19.03	3.57	42.90	4.29	51.48
17.50	10.94	0.96	19.13	3.62	43.41	4.34	52.10
17.59	10.99	0.96	19.23	3.66	43.94	4.39	52.73
17.69	11.05	0.96	19.33	3.71	44.46	4.45	53.36
17.78	11.11	0.96	19.43	3.75	45.00	4.50	53.99
17.87	11.17	0.96	19.54	3.79	45.53	4.55	54.64
17.96	11.21	0.96	19.61	3.83	45.92	4.59	55.11

Table D.1 – Continued

Flow Depth (<i>ft</i>)	V_{avg} (<i>ft/s</i>)	R_c/W (<i>ft/ft</i>)	V_{des} (<i>ft/s</i>)	D_{30} (<i>ft</i>)	D_{30} (<i>in</i>)	D_{50} (<i>ft</i>)	D_{50} (<i>in</i>)
18.06	11.27	0.96	19.72	3.87	46.46	4.65	55.75
18.15	11.33	0.96	19.82	3.92	47.00	4.70	56.40
18.24	11.39	0.96	19.92	3.96	47.55	4.76	57.06
18.33	11.43	0.96	20.00	4.00	47.95	4.80	57.54
18.42	11.49	0.96	20.10	4.04	48.51	4.85	58.21
18.51	11.55	0.96	20.20	4.09	49.07	4.91	58.88
18.59	11.59	0.96	20.28	4.12	49.48	4.95	59.37
18.68	11.65	0.96	20.38	4.17	50.04	5.00	60.05
18.77	11.69	0.96	20.46	4.20	50.45	5.05	60.55
18.86	11.75	0.96	20.56	4.25	51.03	5.10	61.23
18.95	11.80	0.96	20.63	4.29	51.44	5.14	61.73
19.03	11.86	0.96	20.74	4.34	52.03	5.20	62.43
19.12	11.90	0.96	20.81	4.37	52.45	5.24	62.93
19.21	11.96	0.96	20.92	4.42	53.03	5.30	63.63
19.29	12.00	0.96	20.99	4.46	53.46	5.35	64.15
19.38	12.06	0.96	21.09	4.50	54.05	5.41	64.86
19.46	12.10	0.96	21.17	4.54	54.49	5.45	65.38
19.55	12.16	0.96	21.27	4.59	55.08	5.51	66.10
19.63	12.21	0.96	21.35	4.63	55.52	5.55	66.63
19.71	12.25	0.96	21.43	4.66	55.97	5.60	67.16

Table D.1 – Continued

Flow Depth (<i>ft</i>)	V_{avg} (<i>ft/s</i>)	R_c/W (<i>ft/ft</i>)	V_{des} (<i>ft/s</i>)	D_{30} (<i>ft</i>)	D_{30} (<i>in</i>)	D_{50} (<i>ft</i>)	D_{50} (<i>in</i>)
19.79	12.31	0.96	21.53	4.71	56.58	5.66	67.89
19.88	12.35	0.96	21.61	4.75	57.02	5.70	68.42
19.97	12.40	0.96	21.68	4.79	57.46	5.75	68.95
20.05	12.44	0.96	21.76	4.83	57.91	5.79	69.49
20.13	12.50	0.96	21.86	4.88	58.53	5.85	70.24
20.21	12.54	0.96	21.94	4.92	58.99	5.90	70.79
20.29	12.59	0.96	22.01	4.95	59.45	5.94	71.34
20.37	12.63	0.96	22.09	4.99	59.91	5.99	71.89
20.45	12.69	0.96	22.19	5.05	60.54	6.05	72.65
20.53	12.73	0.96	22.27	5.08	61.01	6.10	73.21
20.62	12.78	0.96	22.35	5.12	61.47	6.15	73.76
20.69	12.82	0.96	22.42	5.16	61.94	6.19	74.33
20.78	12.86	0.96	22.50	5.20	62.40	6.24	74.89
20.86	12.91	0.96	22.58	5.24	62.88	6.29	75.45

TABLE D.2. FHWA HEC-11 (1989) Median Riprap Size Results

Flow Depth (<i>ft</i>)	V_{des} (<i>ft/s</i>)	D_{50} (<i>ft</i>)	D_{50} (<i>in</i>)
1.89	4.10	0.08	0.95
2.99	4.15	0.06	0.78
3.93	4.54	0.07	0.89
4.78	4.32	0.06	0.70
5.44	4.18	0.05	0.59
5.84	3.94	0.04	0.48
6.08	4.02	0.04	0.49
6.44	4.15	0.04	0.53
6.47	4.15	0.04	0.53
6.50	4.15	0.04	0.53
6.85	4.32	0.05	0.58
7.19	4.48	0.05	0.63
7.49	4.64	0.06	0.69
7.77	4.80	0.06	0.75
8.04	4.96	0.07	0.81
8.34	5.10	0.07	0.86
8.58	5.24	0.08	0.93
8.84	5.36	0.08	0.98
9.12	5.43	0.08	1.00
9.36	5.55	0.09	1.05
9.55	5.69	0.09	1.13
9.74	5.83	0.10	1.19
9.93	5.97	0.11	1.27
10.11	6.10	0.11	1.35
10.29	6.22	0.12	1.41

Flow Depth (<i>ft</i>)	V_{des} (<i>ft/s</i>)	D_{50} (<i>ft</i>)	D_{50} (<i>in</i>)
10.46	6.34	0.12	1.48
10.63	6.45	0.13	1.55
10.79	6.57	0.14	1.63
10.96	6.69	0.14	1.70
11.12	6.79	0.15	1.77
11.27	6.89	0.15	1.84
11.43	6.99	0.16	1.91
11.58	7.10	0.16	1.98
11.73	7.20	0.17	2.05
11.87	7.30	0.18	2.13
12.02	7.39	0.18	2.19
12.16	7.49	0.19	2.27
12.30	7.58	0.19	2.34
12.43	7.68	0.20	2.42
12.57	7.77	0.21	2.49
12.70	7.85	0.21	2.56
12.83	7.94	0.22	2.64
12.96	8.03	0.23	2.71
13.09	8.12	0.23	2.79
13.21	8.21	0.24	2.87
13.34	8.29	0.25	2.94
13.46	8.38	0.25	3.02
13.58	8.45	0.26	3.09
13.71	8.54	0.26	3.17
13.83	8.61	0.27	3.24

Flow Depth (<i>ft</i>)	V_{des} (<i>ft/s</i>)	D_{50} (<i>ft</i>)	D_{50} (<i>in</i>)
13.95	8.70	0.28	3.33
14.08	8.76	0.28	3.38
14.19	8.83	0.29	3.45
14.31	8.92	0.29	3.54
14.42	8.99	0.30	3.61
14.54	9.07	0.31	3.68
14.65	9.14	0.31	3.76
14.76	9.21	0.32	3.84
14.87	9.29	0.33	3.91
14.98	9.36	0.33	3.99
15.09	9.43	0.34	4.07
15.20	9.49	0.34	4.13
15.30	9.56	0.35	4.21
15.41	9.64	0.36	4.30
15.52	9.69	0.36	4.36
15.62	9.77	0.37	4.44
15.73	9.84	0.38	4.53
15.83	9.90	0.38	4.60
15.93	9.97	0.39	4.68
16.04	10.03	0.40	4.75
16.14	10.09	0.40	4.82
16.24	10.16	0.41	4.91
16.34	10.22	0.41	4.98
16.44	10.28	0.42	5.05
16.54	10.35	0.43	5.14

Table D.2 – Continued

Flow Depth (<i>ft</i>)	V_{des} (<i>ft/s</i>)	D_{50} (<i>ft</i>)	D_{50} (<i>in</i>)
16.64	10.41	0.43	5.21
16.73	10.47	0.44	5.29
16.83	10.53	0.45	5.36
16.93	10.59	0.45	5.43
17.03	10.64	0.46	5.51
17.12	10.70	0.47	5.58
17.21	10.77	0.47	5.68
17.31	10.83	0.48	5.76
17.40	10.88	0.48	5.82
17.50	10.94	0.49	5.89
17.59	10.99	0.50	5.97
17.69	11.05	0.50	6.05
17.78	11.11	0.51	6.13
17.87	11.17	0.52	6.21
17.96	11.21	0.52	6.27
18.06	11.27	0.53	6.35
18.15	11.33	0.54	6.43
18.24	11.39	0.54	6.52
18.33	11.43	0.55	6.58
18.42	11.49	0.56	6.66
18.51	11.55	0.56	6.75
18.59	11.59	0.57	6.81
18.68	11.65	0.57	6.90
18.77	11.69	0.58	6.96
18.86	11.75	0.59	7.05

Flow Depth (<i>ft</i>)	V_{des} (<i>ft/s</i>)	D_{50} (<i>ft</i>)	D_{50} (<i>in</i>)
18.95	11.80	0.59	7.11
19.03	11.86	0.60	7.20
19.12	11.90	0.61	7.26
19.21	11.96	0.61	7.35
19.29	12.00	0.62	7.42
19.38	12.06	0.63	7.51
19.46	12.10	0.63	7.58
19.55	12.16	0.64	7.67
19.63	12.21	0.64	7.74
19.71	12.25	0.65	7.80
19.79	12.31	0.66	7.90
19.88	12.35	0.66	7.97
19.97	12.40	0.67	8.03
20.05	12.44	0.68	8.10
20.13	12.50	0.68	8.20
20.21	12.54	0.69	8.27
20.29	12.59	0.70	8.34
20.37	12.63	0.70	8.41
20.45	12.69	0.71	8.51
20.53	12.73	0.72	8.59
20.62	12.78	0.72	8.66
20.69	12.82	0.73	8.73
20.78	12.86	0.73	8.80
20.86	12.91	0.74	8.87

TABLE D.3. CALTRANS Cal-B&SP (2000) Median Riprap Size Results

V_{des} (ft/s)	W (lb)	D_{50} (ft)	D_{50} (in)
4.10	34.32	0.74	8.82
4.15	36.58	0.75	9.01
4.54	63.09	0.90	10.81
4.32	46.89	0.82	9.79
4.18	38.16	0.76	9.14
3.94	27.01	0.68	8.14
4.02	30.16	0.70	8.45
4.15	36.58	0.75	9.01
4.15	36.58	0.75	9.01
4.15	36.58	0.75	9.01
4.32	46.89	0.82	9.79
4.48	58.37	0.88	10.53
4.53	61.88	0.89	10.74
4.64	72.10	0.94	11.30
4.80	88.42	1.01	12.09
4.96	107.71	1.08	12.92
5.10	125.98	1.13	13.61
5.10	125.98	1.13	13.61
5.24	149.26	1.20	14.40
5.36	170.36	1.25	15.05
5.40	178.89	1.27	15.29
5.43	184.77	1.29	15.46
5.55	209.93	1.34	16.13
5.69	245.33	1.42	16.99
5.69	245.33	1.42	16.99

V_{des} (ft/s)	W (lb)	D_{50} (ft)	D_{50} (in)
5.83	281.32	1.48	17.79
5.97	326.37	1.56	18.69
6.10	371.90	1.63	19.52
6.12	377.27	1.63	19.61
6.22	416.70	1.69	20.28
6.34	465.91	1.75	21.04
6.41	499.06	1.79	21.53
6.45	519.87	1.82	21.83
6.57	578.95	1.89	22.62
6.69	643.51	1.95	23.44
6.79	704.83	2.01	24.16
6.89	770.93	2.07	24.89
6.99	842.13	2.14	25.63
7.10	918.72	2.20	26.39
7.20	1,001.03	2.26	27.15
7.30	1,089.39	2.33	27.93
7.39	1,170.22	2.38	28.61
7.49	1,270.78	2.45	29.40
7.58	1,362.60	2.51	30.09
7.68	1,476.66	2.58	30.91
7.77	1,580.65	2.64	31.62
7.85	1,690.67	2.69	32.34
7.94	1,807.00	2.76	33.06
8.03	1,929.93	2.82	33.80
8.12	2,059.75	2.88	34.54

V_{des} (ft/s)	W (lb)	D_{50} (ft)	D_{50} (in)
8.21	2,196.76	2.94	35.29
8.29	2,341.29	3.00	36.04
8.38	2,493.66	3.07	36.81
8.45	2,626.86	3.12	37.45
8.54	2,794.48	3.19	38.23
8.61	2,940.88	3.24	38.89
8.70	3,124.95	3.31	39.69
8.76	3,252.92	3.35	40.22
8.83	3,418.99	3.41	40.89
8.92	3,627.54	3.48	41.71
8.99	3,809.34	3.53	42.39
9.07	3,998.66	3.59	43.08
9.14	4,195.77	3.65	43.78
9.21	4,400.90	3.71	44.48
9.29	4,614.32	3.77	45.19
9.36	4,836.30	3.83	45.90
9.43	5,067.11	3.89	46.62
9.49	5,258.30	3.93	47.20
9.56	5,505.71	3.99	47.93
9.64	5,762.74	4.06	48.67
9.69	5,975.49	4.10	49.26
9.77	6,250.60	4.17	50.00
9.84	6,536.19	4.23	50.75
9.90	6,772.41	4.28	51.36
9.97	7,077.66	4.34	52.12

Table D.3 – Continued

V_{des} (ft/s)	W (lb)	D_{50} (ft)	D_{50} (in)
10.03	7,330.03	4.39	52.73
10.09	7,589.86	4.45	53.35
10.16	7,925.39	4.51	54.12
10.22	8,202.64	4.56	54.74
10.28	8,487.92	4.61	55.37
10.35	8,856.10	4.68	56.16
10.41	9,160.15	4.73	56.80
10.47	9,472.84	4.79	57.44
10.53	9,794.38	4.84	58.08
10.59	10,124.96	4.89	58.72
10.64	10,464.79	4.95	59.37
10.70	10,814.07	5.00	60.03
10.77	11,264.28	5.07	60.85
10.83	11,635.60	5.13	61.51
10.88	11,920.73	5.17	62.01
10.94	12,309.95	5.22	62.68
10.99	12,709.70	5.28	63.35
11.05	13,120.20	5.34	64.02
11.11	13,541.70	5.39	64.70
11.17	13,974.42	5.45	65.38
11.21	14,306.47	5.49	65.90
11.27	14,759.41	5.55	66.59
11.33	15,224.24	5.61	67.28
11.39	15,701.20	5.66	67.97
11.43	16,067.04	5.71	68.50
11.49	16,565.85	5.77	69.20
11.55	17,077.50	5.83	69.90
11.59	17,469.81	5.87	70.43

V_{des} (ft/s)	W (lb)	D_{50} (ft)	D_{50} (in)
11.65	18,004.56	5.93	71.15
11.69	18,414.52	5.97	71.68
11.75	18,973.20	6.03	72.40
11.80	19,401.42	6.08	72.94
11.86	19,984.88	6.14	73.66
11.90	20,432.00	6.18	74.21
11.96	21,041.11	6.24	74.94
12.00	21,507.81	6.29	75.49
12.06	22,143.46	6.35	76.23
12.10	22,630.41	6.40	76.78
12.16	23,293.53	6.46	77.52
12.21	23,801.42	6.51	78.08
12.25	24,318.51	6.55	78.64
12.31	25,022.50	6.62	79.40
12.35	25,561.57	6.66	79.96
12.40	26,110.27	6.71	80.53
12.44	26,668.76	6.76	81.10
12.50	27,428.87	6.82	81.86
12.54	28,010.72	6.87	82.44
12.59	28,602.82	6.92	83.02
12.63	29,205.32	6.97	83.59
12.69	30,025.06	7.03	84.37
12.73	30,652.38	7.08	84.95
12.78	31,290.58	7.13	85.54
12.82	31,939.81	7.18	86.13
12.86	32,600.23	7.23	86.71
12.91	33,272.00	7.28	87.31

TABLE D.4. ASCE Man-110 (2006) Median Riprap Size Results

V_{des} (ft/s)	W (lb)	D_{50} (ft)	D_{50} (in)
4.10	0.17	0.12	1.50
4.15	0.18	0.13	1.53
4.54	0.31	0.15	1.83
4.32	0.23	0.14	1.66
4.18	0.19	0.13	1.55
3.94	0.13	0.12	1.38
4.02	0.15	0.12	1.43
4.15	0.18	0.13	1.53
4.15	0.18	0.13	1.53
4.15	0.18	0.13	1.53
4.32	0.23	0.14	1.66
4.48	0.29	0.15	1.79
4.64	0.35	0.16	1.92
4.80	0.43	0.17	2.05
4.96	0.53	0.18	2.19
5.10	0.62	0.19	2.31
5.24	0.73	0.20	2.44
5.36	0.83	0.21	2.55
5.43	0.90	0.22	2.63
5.55	1.03	0.23	2.74
5.69	1.20	0.24	2.89
5.83	1.38	0.25	3.02
5.97	1.60	0.26	3.17
6.10	1.82	0.28	3.31
6.22	2.04	0.29	3.44

V_{des} (ft/s)	W (lb)	D_{50} (ft)	D_{50} (in)
6.34	2.28	0.30	3.57
6.45	2.54	0.31	3.71
6.57	2.83	0.32	3.84
6.69	3.15	0.33	3.98
6.79	3.45	0.34	4.10
6.89	3.77	0.35	4.23
6.99	4.12	0.36	4.35
7.10	4.50	0.37	4.48
7.20	4.90	0.38	4.61
7.30	5.33	0.40	4.74
7.39	5.73	0.40	4.86
7.49	6.22	0.42	4.99
7.58	6.67	0.43	5.11
7.68	7.23	0.44	5.25
7.77	7.74	0.45	5.37
7.85	8.28	0.46	5.49
7.94	8.84	0.47	5.61
8.03	9.45	0.48	5.74
8.12	10.08	0.49	5.86
8.21	10.75	0.50	5.99
8.29	11.46	0.51	6.12
8.38	12.21	0.52	6.25
8.45	12.86	0.53	6.36
8.54	13.68	0.54	6.49
8.61	14.40	0.55	6.60

V_{des} (ft/s)	W (lb)	D_{50} (ft)	D_{50} (in)
8.70	15.30	0.56	6.74
8.76	15.92	0.57	6.83
8.83	16.74	0.58	6.94
8.92	17.76	0.59	7.08
8.99	18.65	0.60	7.20
9.07	19.57	0.61	7.32
9.14	20.54	0.62	7.43
9.21	21.54	0.63	7.55
9.29	22.59	0.64	7.67
9.36	23.67	0.65	7.79
9.43	24.80	0.66	7.92
9.49	25.74	0.67	8.01
9.56	26.95	0.68	8.14
9.64	28.21	0.69	8.26
9.69	29.25	0.70	8.36
9.77	30.60	0.71	8.49
9.84	31.99	0.72	8.62
9.90	33.15	0.73	8.72
9.97	34.64	0.74	8.85
10.03	35.88	0.75	8.95
10.09	37.15	0.75	9.06
10.16	38.79	0.77	9.19
10.22	40.15	0.77	9.30
10.28	41.55	0.78	9.40

Table D.4 – Continued

V_{des} (<i>ft/s</i>)	W (lb)	D_{50} (<i>ft</i>)	D_{50} (<i>in</i>)	V_{des} (<i>ft/s</i>)	W (lb)	D_{50} (<i>ft</i>)	D_{50} (<i>in</i>)
10.35	43.35	0.79	9.54	11.75	92.87	1.02	12.29
10.41	44.84	0.80	9.64	11.80	94.97	1.03	12.38
10.47	46.37	0.81	9.75	11.86	97.82	1.04	12.51
10.53	47.94	0.82	9.86	11.90	100.01	1.05	12.60
10.59	49.56	0.83	9.97	11.96	102.99	1.06	12.72
10.64	51.22	0.84	10.08	12.00	105.28	1.07	12.82
10.70	52.93	0.85	10.19	12.06	108.39	1.08	12.94
10.77	55.14	0.86	10.33	12.10	110.77	1.09	13.04
10.83	56.95	0.87	10.44	12.16	114.02	1.10	13.16
10.88	58.35	0.88	10.53	12.21	116.50	1.10	13.26
10.94	60.25	0.89	10.64	12.25	119.03	1.11	13.35
10.99	62.21	0.90	10.76	12.31	122.48	1.12	13.48
11.05	64.22	0.91	10.87	12.35	125.12	1.13	13.58
11.11	66.28	0.92	10.99	12.40	127.81	1.14	13.67
11.17	68.40	0.93	11.10	12.44	130.54	1.15	13.77
11.21	70.03	0.93	11.19	12.50	134.26	1.16	13.90
11.27	72.24	0.94	11.31	12.54	137.11	1.17	14.00
11.33	74.52	0.95	11.42	12.59	140.01	1.17	14.10
11.39	76.85	0.96	11.54	12.63	142.95	1.18	14.19
11.43	78.65	0.97	11.63	12.69	146.97	1.19	14.32
11.49	81.09	0.98	11.75	12.73	150.04	1.20	14.42
11.55	83.59	0.99	11.87	12.78	153.16	1.21	14.52
11.59	85.51	1.00	11.96	12.82	156.34	1.22	14.62
11.65	88.13	1.01	12.08	12.86	159.57	1.23	14.72
11.69	90.14	1.01	12.17	12.91	162.86	1.24	14.82

TABLE D.5. USBR EM-25 (1984) Median Riprap Size Results

V_{des} (<i>ft/s</i>)	D_{50} (<i>ft</i>)	D_{50} (<i>in</i>)	V_{des} (<i>ft/s</i>)	D_{50} (<i>ft</i>)	D_{50} (<i>in</i>)	V_{des} (<i>ft/s</i>)	D_{50} (<i>ft</i>)	D_{50} (<i>in</i>)
4.10	0.22	2.68	6.34	0.55	6.57	8.70	1.05	12.62
4.15	0.23	2.74	6.45	0.57	6.82	8.76	1.07	12.80
4.54	0.28	3.31	6.57	0.59	7.07	8.83	1.08	13.02
4.32	0.25	2.99	6.69	0.61	7.34	8.92	1.11	13.28
4.18	0.23	2.78	6.79	0.63	7.57	8.99	1.13	13.51
3.94	0.21	2.47	6.89	0.65	7.81	9.07	1.14	13.74
4.02	0.21	2.57	6.99	0.67	8.05	9.14	1.16	13.97
4.15	0.23	2.74	7.10	0.69	8.29	9.21	1.18	14.20
4.15	0.23	2.74	7.20	0.71	8.54	9.29	1.20	14.43
4.15	0.23	2.74	7.30	0.73	8.79	9.36	1.22	14.66
4.32	0.25	2.99	7.39	0.75	9.01	9.43	1.24	14.90
4.48	0.27	3.22	7.49	0.77	9.27	9.49	1.26	15.09
4.64	0.29	3.46	7.58	0.79	9.49	9.56	1.28	15.33
4.80	0.31	3.71	7.68	0.81	9.76	9.64	1.30	15.57
4.96	0.33	3.97	7.77	0.83	9.99	9.69	1.31	15.77
5.10	0.35	4.19	7.85	0.85	10.22	9.77	1.33	16.01
5.24	0.37	4.44	7.94	0.87	10.46	9.84	1.36	16.26
5.36	0.39	4.65	8.03	0.89	10.70	9.90	1.37	16.46
5.43	0.40	4.78	8.12	0.91	10.94	9.97	1.39	16.71
5.55	0.42	4.99	8.21	0.93	11.18	10.03	1.41	16.91
5.69	0.44	5.27	8.29	0.95	11.43	10.09	1.43	17.12
5.83	0.46	5.52	8.38	0.97	11.68	10.16	1.45	17.37
5.97	0.48	5.81	8.45	0.99	11.89	10.22	1.46	17.58
6.10	0.51	6.08	8.54	1.01	12.15	10.28	1.48	17.79
6.22	0.53	6.32	8.61	1.03	12.36	10.35	1.50	18.05

Table D.5 – Continued

V_{des} (<i>ft/s</i>)	D_{50} (<i>ft</i>)	D_{50} (<i>in</i>)
10.41	1.52	18.26
10.47	1.54	18.47
10.53	1.56	18.68
10.59	1.57	18.90
10.64	1.59	19.11
10.70	1.61	19.33
10.77	1.63	19.60
10.83	1.65	19.82
10.88	1.67	19.99
10.94	1.68	20.21
10.99	1.70	20.43
11.05	1.72	20.66
11.11	1.74	20.88
11.17	1.76	21.11
11.21	1.77	21.28
11.27	1.79	21.51
11.33	1.81	21.74
11.39	1.83	21.97
11.43	1.85	22.14
11.49	1.86	22.38
11.55	1.88	22.61
11.59	1.90	22.79
11.65	1.92	23.03
11.69	1.93	23.21
11.75	1.95	23.44

V_{des} (<i>ft/s</i>)	D_{50} (<i>ft</i>)	D_{50} (<i>in</i>)
11.80	1.97	23.63
11.86	1.99	23.87
11.90	2.00	24.05
11.96	2.02	24.29
12.00	2.04	24.48
12.06	2.06	24.72
12.10	2.08	24.91
12.16	2.10	25.16
12.21	2.11	25.34
12.25	2.13	25.53
12.31	2.15	25.78
12.35	2.16	25.97
12.40	2.18	26.16
12.44	2.20	26.35
12.50	2.22	26.61
12.54	2.23	26.80
12.59	2.25	26.99
12.63	2.27	27.19
12.69	2.29	27.45
12.73	2.30	27.64
12.78	2.32	27.84
12.82	2.34	28.04
12.86	2.35	28.23
12.91	2.37	28.43

TABLE D.6. USGS Vol. 2 (1986) Median Riprap Size Results

V_{des} (ft/s)	D_{50} (ft)	D_{50} (in)	V_{des} (ft/s)	D_{50} (ft)	D_{50} (in)	V_{des} (ft/s)	D_{50} (ft)	D_{50} (in)
4.10	0.31	3.76	6.34	0.90	10.86	8.70	1.96	23.54
4.15	0.32	3.86	6.45	0.95	11.35	8.76	1.99	23.93
4.54	0.40	4.81	6.57	0.99	11.86	8.83	2.03	24.42
4.32	0.36	4.27	6.69	1.03	12.38	8.92	2.08	25.01
4.18	0.33	3.92	6.79	1.07	12.85	8.99	2.13	25.51
3.94	0.28	3.41	6.89	1.11	13.32	9.07	2.17	26.02
4.02	0.30	3.57	6.99	1.15	13.81	9.14	2.21	26.54
4.15	0.32	3.86	7.10	1.19	14.31	9.21	2.25	27.06
4.15	0.32	3.86	7.20	1.23	14.82	9.29	2.30	27.58
4.15	0.32	3.86	7.30	1.28	15.34	9.36	2.34	28.11
4.32	0.36	4.27	7.39	1.32	15.79	9.43	2.39	28.65
4.48	0.39	4.66	7.49	1.36	16.33	9.49	2.42	29.09
4.64	0.42	5.08	7.58	1.40	16.80	9.56	2.47	29.64
4.80	0.46	5.52	7.68	1.45	17.35	9.64	2.52	30.19
4.96	0.50	5.98	7.77	1.49	17.84	9.69	2.55	30.64
5.10	0.53	6.38	7.85	1.53	18.34	9.77	2.60	31.21
5.24	0.57	6.83	7.94	1.57	18.84	9.84	2.65	31.78
5.36	0.60	7.21	8.03	1.61	19.35	9.90	2.69	32.24
5.43	0.62	7.45	8.12	1.66	19.87	9.97	2.74	32.82
5.55	0.65	7.85	8.21	1.70	20.40	10.03	2.77	33.29
5.69	0.70	8.36	8.29	1.74	20.93	10.09	2.81	33.77
5.83	0.74	8.84	8.38	1.79	21.48	10.16	2.86	34.37
5.97	0.78	9.39	8.45	1.83	21.94	10.22	2.90	34.85
6.10	0.83	9.91	8.54	1.87	22.49	10.28	2.95	35.34
6.22	0.86	10.37	8.61	1.91	22.97	10.35	3.00	35.96

Table D.6 – Continued

V_{des} (<i>ft/s</i>)	D_{50} (<i>ft</i>)	D_{50} (<i>in</i>)
10.41	3.04	36.45
10.47	3.08	36.95
10.53	3.12	37.46
10.59	3.16	37.97
10.64	3.21	38.48
10.70	3.25	39.00
10.77	3.30	39.65
10.83	3.35	40.18
10.88	3.38	40.58
10.94	3.43	41.11
10.99	3.47	41.65
11.05	3.52	42.19
11.11	3.56	42.73
11.17	3.61	43.28
11.21	3.64	43.70
11.27	3.69	44.26
11.33	3.73	44.82
11.39	3.78	45.39
11.43	3.82	45.81
11.49	3.87	46.39
11.55	3.91	46.96
11.59	3.95	47.40
11.65	4.00	47.98
11.69	4.04	48.42
11.75	4.08	49.02

V_{des} (<i>ft/s</i>)	D_{50} (<i>ft</i>)	D_{50} (<i>in</i>)
11.80	4.12	49.46
11.86	4.17	50.06
11.90	4.21	50.52
11.96	4.26	51.12
12.00	4.30	51.58
12.06	4.35	52.20
12.10	4.39	52.66
12.16	4.44	53.28
12.21	4.48	53.75
12.25	4.52	54.22
12.31	4.57	54.86
12.35	4.61	55.33
12.40	4.65	55.81
12.44	4.69	56.30
12.50	4.75	56.94
12.54	4.79	57.43
12.59	4.83	57.92
12.63	4.87	58.41
12.69	4.92	59.08
12.73	4.96	59.57
12.78	5.01	60.08
12.82	5.05	60.58
12.86	5.09	61.09
12.91	5.13	61.60

TABLE D.7. Isbash (1936) Median Riprap Size Results

V_{des} (ft/s)	R_c/W (ft/ft)	D_{50} (ft)	D_{50} (in)	V_{des} (ft/s)	R_c/W (ft/ft)	D_{50} (ft)	D_{50} (in)	V_{des} (ft/s)	R_c/W (ft/ft)	D_{50} (ft)	D_{50} (in)
4.10	8.86	0.11	1.32	6.34	0.96	0.26	3.16	8.70	0.96	0.50	5.96
4.15	5.05	0.11	1.35	6.45	0.96	0.27	3.28	8.76	0.96	0.50	6.04
4.54	3.65	0.14	1.62	6.57	0.96	0.28	3.40	8.83	0.96	0.51	6.14
4.32	2.19	0.12	1.47	6.69	0.96	0.29	3.52	8.92	0.96	0.52	6.26
4.18	1.66	0.11	1.37	6.79	0.96	0.30	3.63	8.99	0.96	0.53	6.37
3.94	1.55	0.10	1.22	6.89	0.96	0.31	3.74	9.07	0.96	0.54	6.47
4.02	1.49	0.11	1.27	6.99	0.96	0.32	3.85	9.14	0.96	0.55	6.57
4.15	1.41	0.11	1.35	7.10	0.96	0.33	3.96	9.21	0.96	0.56	6.68
4.15	1.41	0.11	1.35	7.20	0.96	0.34	4.08	9.29	0.96	0.57	6.79
4.15	1.40	0.11	1.35	7.30	0.96	0.35	4.19	9.36	0.96	0.57	6.89
4.32	1.38	0.12	1.47	7.39	0.96	0.36	4.30	9.43	0.96	0.58	7.00
4.48	1.33	0.13	1.58	7.49	0.96	0.37	4.41	9.49	0.96	0.59	7.09
4.64	1.31	0.14	1.70	7.58	0.96	0.38	4.52	9.56	0.96	0.60	7.20
4.80	1.30	0.15	1.82	7.68	0.96	0.39	4.64	9.64	0.96	0.61	7.31
4.96	1.27	0.16	1.94	7.77	0.96	0.40	4.75	9.69	0.96	0.62	7.40
5.10	1.23	0.17	2.04	7.85	0.96	0.40	4.86	9.77	0.96	0.63	7.51
5.24	1.18	0.18	2.16	7.94	0.96	0.41	4.96	9.84	0.96	0.64	7.62
5.36	1.13	0.19	2.26	8.03	0.96	0.42	5.07	9.90	0.96	0.64	7.71
5.43	1.10	0.19	2.32	8.12	0.96	0.43	5.19	9.97	0.96	0.65	7.83
5.55	1.07	0.20	2.42	8.21	0.96	0.44	5.30	10.03	0.96	0.66	7.92
5.69	1.06	0.21	2.55	8.29	0.96	0.45	5.41	10.09	0.96	0.67	8.01
5.83	1.01	0.22	2.67	8.38	0.96	0.46	5.53	10.16	0.96	0.68	8.13
5.97	0.96	0.23	2.81	8.45	0.96	0.47	5.62	10.22	0.96	0.69	8.22
6.10	0.96	0.24	2.93	8.54	0.96	0.48	5.74	10.28	0.96	0.69	8.31
6.22	0.96	0.25	3.04	8.61	0.96	0.49	5.84	10.35	0.96	0.70	8.43

Table D.7 – Continued

V_{des} (ft/s)	R_c/W (ft/ft)	D_{50} (ft)	D_{50} (in)
10.41	0.96	0.71	8.53
10.47	0.96	0.72	8.62
10.53	0.96	0.73	8.72
10.59	0.96	0.73	8.82
10.64	0.96	0.74	8.92
10.70	0.96	0.75	9.01
10.77	0.96	0.76	9.14
10.83	0.96	0.77	9.24
10.88	0.96	0.78	9.31
10.94	0.96	0.78	9.41
10.99	0.96	0.79	9.51
11.05	0.96	0.80	9.61
11.11	0.96	0.81	9.72
11.17	0.96	0.82	9.82
11.21	0.96	0.82	9.89
11.27	0.96	0.83	10.00
11.33	0.96	0.84	10.10
11.39	0.96	0.85	10.21
11.43	0.96	0.86	10.28
11.49	0.96	0.87	10.39
11.55	0.96	0.87	10.50
11.59	0.96	0.88	10.58
11.65	0.96	0.89	10.68
11.69	0.96	0.90	10.76
11.75	0.96	0.91	10.87

V_{des} (ft/s)	R_c/W (ft/ft)	D_{50} (ft)	D_{50} (in)
11.80	0.96	0.91	10.95
11.86	0.96	0.92	11.06
11.90	0.96	0.93	11.14
11.96	0.96	0.94	11.25
12.00	0.96	0.94	11.33
12.06	0.96	0.95	11.45
12.10	0.96	0.96	11.53
12.16	0.96	0.97	11.64
12.21	0.96	0.98	11.72
12.25	0.96	0.98	11.81
12.31	0.96	0.99	11.92
12.35	0.96	1.00	12.01
12.40	0.96	1.01	12.09
12.44	0.96	1.01	12.18
12.50	0.96	1.02	12.29
12.54	0.96	1.03	12.38
12.59	0.96	1.04	12.46
12.63	0.96	1.05	12.55
12.69	0.96	1.06	12.67
12.73	0.96	1.06	12.76
12.78	0.96	1.07	12.84
12.82	0.96	1.08	12.93
12.86	0.96	1.09	13.02
12.91	0.96	1.09	13.11